NASA TECHNICAL NOTE

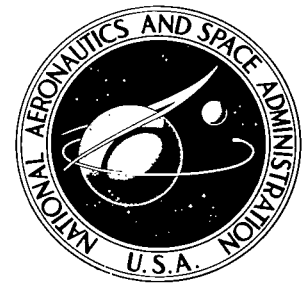

NASA TN D-6375

NASA TN D-6375

DYNAMIC RESPONSES OF RAILROAD CAR MODELS TO VERTICAL AND LATERAL RAIL INPUTS

by John L. Sewall, Russell V. Parrish, and Barbara J. Durling

Langley Research Center
Hampton, Va. 23365

NATIONAL AERONAUTICS AND SPACE ADMINISTRATION • WASHINGTON, D. C. • NOVEMBER 1971

Copy ltd 24 May 76 DM

ERRATA

NASA Technical Note D-6375

DYNAMIC RESPONSES OF RAILROAD CAR MODELS
TO VERTICAL AND LATERAL RAIL INPUTS

By John L. Sewall, Russell V. Parrish,
and Barbara J. Durling
November 1971

Page 9: The second of equations (4) should read

$$\omega[C]\{\dot{q}_1\} + \left[[K] - \omega^2[M]\right]\{q_2\} = \omega\{Q_2\}$$

Page 31: The last line of equation (A7) should read

$$+\frac{1}{2}\frac{g_{cv}}{\omega}(EI)_v \int_0^L \left[\dot{a}(t)\frac{d^2W(x)}{dx^2}\right]^2 dx$$

Issued April 1976

1. Report No. NASA TN D-6375	2. Government Accession No.	3. Recipient's Catalog No.
4. Title and Subtitle DYNAMIC RESPONSES OF RAILROAD CAR MODELS TO VERTICAL AND LATERAL RAIL INPUTS		5. Report Date November 1971 6. Performing Organization Code
7. Author(s) John L. Sewall, Russell V. Parrish, and Barbara J. Durling		8. Performing Organization Report No. L-7283
9. Performing Organization Name and Address NASA Langley Research Center Hampton, Va. 23365		10. Work Unit No. 136-63-02-02 11. Contract or Grant No.
12. Sponsoring Agency Name and Address National Aeronautics and Space Administration Washington, D.C. 20546		13. Type of Report and Period Covered Technical Note 14. Sponsoring Agency Code
15. Supplementary Notes		

16. Abstract

Simplified dynamic models were applied in a study of vibration in a high-speed railroad car. The mathematical models used were a four-degree-of-freedom model for vertical responses to vertical rail inputs and a ten-degree-of-freedom model for lateral responses to lateral or rolling (cross-level) inputs from the rails. Elastic properties of the passenger car body were represented by bending and torsion of a uniform beam. Rail-to-car (truck) suspensions were modeled as spring-mass-dashpot oscillators. Lateral spring nonlinearities approximating certain complicated truck mechanisms were introduced. The models were excited by displacement and, in some cases, velocity inputs from the rails by both deterministic (including sinusoidal) and random input functions. Results were obtained both in the frequency and time domains.

Solutions in the time domain for the lateral model were obtained for a wide variety of transient and random inputs generated on-line by an analog computer. Variations in one of the damping properties of the lateral car suspension gave large fluctuations in response over a range of car speeds for a given input. This damping coefficient was significant in reducing lateral car responses that were higher for nonlinear springs than for linear springs for three different inputs. Results showed that knowledge of car stiffness properties is needed in order to locate system resonances which need to be avoided.

17. Key Words (Suggested by Author(s)) Rail car dynamic responses Real-time simulation Optimization of dynamic response Transient dynamic responses	18. Distribution Statement Unclassified – Unlimited

19. Security Classif. (of this report) Unclassified	20. Security Classif. (of this page) Unclassified	21. No. of Pages 97	22. Price* $3.00

*For sale by the National Technical Information Service, Springfield, Virginia 22151

DYNAMIC RESPONSES OF RAILROAD CAR MODELS TO VERTICAL AND LATERAL RAIL INPUTS

By John L. Sewall, Russell V. Parrish,
and Barbara J. Durling
Langley Research Center

SUMMARY

Simplified dynamic models were applied in a study of vibration in a high-speed railroad car. The mathematical models used were a four-degree-of-freedom model for vertical responses to vertical rail inputs and a ten-degree-of-freedom model for lateral responses to lateral or rolling (cross-level) inputs from the rails. Elastic properties of the passenger car body were represented by bending and torsion of a uniform beam. Rail-to-car (truck) suspensions were modeled as spring-mass-dashpot oscillators. Lateral spring nonlinearities approximating certain complicated truck mechanisms were introduced. The models were excited by displacement and, in some cases, velocity inputs from the rails by both deterministic (including sinusoidal) and random input functions. Results were obtained both in the frequency and time domains.

Solutions in the time domain for the lateral model were obtained for a wide variety of transient and random inputs generated on-line by an analog computer. Variations in one of the damping properties of the lateral car suspension gave large fluctuations in response over a range of car speeds for a given input. This damping coefficient was significant in reducing lateral car responses that were higher for nonlinear springs than for linear springs for three different inputs. Results showed that knowledge of car stiffness properties is needed in order to locate system resonances which need to be avoided.

INTRODUCTION

The recent introduction of high-speed rail passenger service between metropolitan areas has stimulated considerable interest in the effects of vibration on passenger comfort. Vibrations are caused by track irregularities, and reduction of these vibrations at high speeds is a particularly difficult task.

References 1 to 5 report some of the analytical research directed toward understanding the parameters influencing the generation and transmission of vibrations in rail systems. In all these studies, significant motions and structural characteristics in highly

complicated suspension mechanisms are represented by simple spring-mass-damper models. In reference 1, accelerations and forces transmitted from the rails were studied for ranges of spring constants and damping coefficients of a three-degree-of-freedom model of vertical motion that included railbed flexibility. Lateral accelerations and forces were studied for a seven-degree-of-freedom model that was also used to explore yaw stability. Reference 2 is a study of the responses of a simplified model of an auto ferry transport to transient inputs. In reference 3, a four-degree-of-freedom model is utilized to show the advantages of a new suspension design over a conventional design in reducing accelerations transmitted to the car. Reference 4 is a vibration-minimization study of a three-degree-of-freedom model of an electrically powered railroad car subject to vertical sinusoidal and random inputs from the rails. In reference 5 a four-degree-of-freedom vertical model and a ten-degree-of-freedom lateral model were used to examine a wide variety of parameter variations, including the effects of car bending stiffness and spring nonlinearity on car response.

Topics not sufficiently considered in previous studies are lateral responses to both transient and random inputs, optimization that includes the effects of truck-suspension (equalizer) damping and stiffness, and damping effects in models which include spring nonlinearities. None of these studies (including the present one) allows for rigid-body pitch motion of the car; consequently out-of-phase vertical inputs to front and rear suspensions cannot be considered.

The objectives of the present investigation were (1) to examine the relation between car spring and damping parameters and car responses when the car is subjected to simulated rail irregularities including sinusoidal and various transient and random inputs, and (2) to demonstrate a method of minimizing car accelerations by appropriate choices of spring and damping parameters for the vertical model. The minimization is more concerned with damping than with stiffness because damping properties are assumed to be more easily adjusted in an actual rail car than stiffness properties.

The linear equations of motion were solved by digital computer programs for the sinusoidal inputs to both models and for one random input to the vertical model. To include nonlinearities in the lateral truck suspension system, a real-time simulation (RTS) digital computer program was developed and utilized. This program involved numerical integration of the equations of motion in scaled real time. Both linear and nonlinear acceleration responses to transient deterministic and random inputs were obtained for the lateral model by means of this program.

SYMBOLS

Values are given in both SI and U.S. Customary Units. The measurements and calculations were made in U.S. Customary Units.

A_q	maximum acceleration response at steady state for qth degree of freedom
a(t)	generalized coordinate for vertical car bending
B	lateral distance between bolster springs (see fig. 13(b))
b(t)	generalized coordinate for lateral car bending
$[C]$	damping matrix
c_q	viscous damping constant for qth degree of freedom
D	dissipation energy
d	distance from end of car to center line of trucks (see figs. 1 and 13(a))
E	Young's modulus
f	forcing frequency, $\frac{\omega}{2\pi}$
f_q	frequency of qth degree of freedom, $\frac{\omega_q}{2\pi}$
G	modulus of rigidity
g	acceleration due to gravity
g_c	structural damping coefficient of car in bending or torsion
g_{rms}	root mean square of output spectral density in g units
h_T	vertical distance between car elastic axis and line of action of lateral transformer spring (see fig. 13(a))

h_1 vertical distance from traction-motor center of gravity to line of action of lateral equalizer spring (see fig. 13(b))

h_2 vertical distance from traction-motor center of gravity to line of action of lateral bolster spring (see fig. 13(b))

h_3 vertical distance between car elastic axis and line of action of lateral bolster spring (see fig. 13(b))

h_4 vertical distance of car section center of gravity from car elastic axis, positive for center of gravity above elastic axis (see fig. 13(b))

I flexural moment of inertia of car cross section

I_A mass moment of inertia of traction motor in roll about its center of gravity

I_{EA} mass moment of inertia of car in roll about car elastic axis, per unit length

J torsional constant of car cross section

$[K]$ stiffness matrix

k_q spring constant for qth degree of freedom

L length of car (see figs. 1 and 13(a))

$[M]$ mass matrix

M_A traction-motor mass

M_c car mass, mL

M_g transformer mass

m mass of car per unit length

n_q viscous damping coefficient for qth degree of freedom

Q(t) general displacement forcing function

Q_o amplitude of forcing function

$q(t)$ generalized coordinate

$q_1 = \bar{q}_1 Q_o$, $q_2 = \bar{q}_2 Q_o$ amplitudes of sinusoidal motion in qth degree of freedom in terms of dimensionless quantities $\bar{q}_1$ and $\bar{q}_2$

R lateral distance between equalizer springs (see fig. 13(b))

$S(t)$ vertical displacement forcing function at rails (see fig. 1)

$S_I(f)$ input spectral density of vertical model (see eq. (3))

$S_q(f)$ output spectral density of vertical model (see eqs. (7) and (8))

T kinetic energy

t time

U potential energy

v car speed

$v(x,t)$ lateral bending deformation of car (see eq. (B2))

$W(x)$ car bending-mode-shape value at any x

$w(x,t)$ vertical bending deformation of car (see eq. (A3))

x length along car, measured from rear of car

$Y(t)$ lateral displacement forcing function at rails (see fig. 13(b))

$Y_I(f)$ spectral density of lateral input at rails

$y_A(t)$ generalized coordinate of lateral translation of traction motor

$y_c(t)$ generalized coordinate of lateral rigid-body translation of car (see fig. 13(b))

$y_g(t)$ generalized coordinate of lateral transformer translation

$z_A(t)$ generalized coordinate of vertical translation of traction motor

$z_c(t)$ generalized coordinate of vertical rigid-body translation of car (see fig. 1)

$z_g(t)$ generalized coordinate of vertical transformer translation

α_m, β_m eigenvalue properties of beam in bending (see eqs. (A8) and (A9))

$(\Delta l)_t$ center-to-center distance between axles of a truck suspension system (see eqs. (11) to (14))

$\Delta y(t)$ displacement relation in lateral bolster springs for nonlinear spring behavior (see eqs. (15))

$\delta(t)$ increment of vertical displacement at rails associated with cross-level (or rolling) displacement input (see fig. 13(b))

$\delta_I(f)$ spectral density of cross-level input at rails

$\eta(t)$ generalized coordinate of car in rigid-body yaw

$\theta_A(t)$ generalized coordinate of traction-motor rolling degree of freedom

$\theta_c(x,t)$ rigid-body roll and torsion of car (see eq. (B3))

$\theta_{c0}(t)$ generalized coordinate for rigid-car roll

λ wavelength for wave input

ω angular forcing frequency, $2\pi f$, rad/sec

ω_q angular frequency of qth degree of freedom, $2\pi f_q$, rad/sec

Subscripts:

A identifies properties associated with the traction-motor-equalizer system

B denotes vertical car bending frequency

c	associated with car
cl	identifies structural damping coefficient of car in lateral bending; also, lateral car acceleration (see table III)
cT	identifies structural damping coefficient of car in torsion
cv	identifies structural damping coefficient of car in vertical bending
f	identifies forward trucks
g	associated with transformer
L	identifies energies and car bending stiffness of lateral model (see appendix B)
l	identifies properties of traction-motor-lateral-equalizer system
lB	denotes lateral car bending frequency
lc	identifies properties of lateral bolster spring-damper system
lg	identifies properties of lateral transformer spring-mass system
m	integer associated with mth car bending mode
o	identifies amplitude of forcing function
oT	identifies bolster rigid-body damping coefficients and frequency
q	identifies general degree of freedom
r	identifies rear trucks
s	identifies properties of vertical bolster spring-damper system
T	associated with car torsion

v identifies energies and car bending stiffness of vertical model

α identifies roll stiffness and damping properties of traction motor

Dots over quantities denote differentiation with respect to time. Bars over quantities denote maximum amplitude in acceleration transfer functions.

ANALYSIS OF VERTICAL MOTION

Equations

Mathematical model.- The mathematical model used in the analysis of the vertical motions of the railroad car is shown in figure 1. The model consists of a uniform beam representing the railroad car, a heavy mass M_g attached to the center of the car by a spring and damper (this mass represents an electrical transformer used in powering the railroad car), and two masses M_A attached by springs and dampers to the car and to a vibrating base representing the rails. The masses M_A represent the flexibly mounted sections of the truck frame and traction motors in the suspension system of the railroad car. For convenience in further discussions, each mass M_A with its attached springs and dampers is referred to as a truck suspension, the mass M_A is called the traction motor, the spring-damper combination between this mass and the car is called the bolster, and the spring-damper combination connecting the traction motor M_A to the rails is called the equalizer. A schematic view of the truck suspension system is shown in figure 2. The wheels, axles, and side frames (supporting the equalizer springs) are considered to be part of the rails, and the connections between the axles and traction motors are not taken into account in the model. In addition to the viscous dampers in the transformer and truck suspensions, structural damping is included in the car. The degrees of freedom considered are car rigid-body displacement, $z_c(t)$; car bending motion, $w(x,t) = a(t)w(x)$; transformer displacement, $z_g(t)$; and traction-motor displacement, $z_A(t)$. The model is symmetric about the middle of the car, and the same rail input is applied simultaneously to both truck suspensions; therefore, both traction motors have the same motion, and only one degree of freedom z_A is required. With different inputs to front and rear trucks, separate degrees of freedom are required to specify the vertical motion of the front and rear traction motors, and rigid-body pitch would also have to be included.

The equations of motion of the mathematical model are derived in appendix A. The matrix equations of motion are of the form:

$$[M]\{\ddot{q}\} + [C]\{\dot{q}\} + [K]\{q\} = \{Q\} + \{\dot{Q}\} \tag{1}$$

where the column matrix $\{q\}$ contains the displacements $a(t)$, $z_c(t)$, $z_g(t)$, and $z_A(t)$. In equation (1) $[M]$ is the mass matrix, $[C]$ is the damping matrix, $[K]$ is the stiffness matrix, $\{Q\}$ is the displacement input, and $\{\dot{Q}\}$ is the velocity input.

Rail inputs.- The time history of the rail input used in this analysis was either sinusoidal or random. The sinusoidal input is

$$\left.\begin{aligned} Q(t) &= S_o \sin \omega t \\ \dot{Q}(t) &= S_o \omega \cos \omega t \end{aligned}\right\} \tag{2}$$

where ω is the input frequency and S_o is the displacement amplitude. The random input is given by the spectral density variation identified as "middle estimate" in figure 8 of reference 4 and is based on measured railroad roughness data. The spectral density for this displacement is

$$\left.\begin{aligned} S_I(f) &= \frac{46.9 \times 10^{-5}}{f^{2.64}} \text{ cm}^2/\text{Hz} \\ &= \frac{7.27 \times 10^{-5}}{f^{2.64}} \text{ in}^2/\text{Hz} \end{aligned}\right\} \tag{3}$$

f being the input frequency in hertz. The root-mean-square (rms) amplitude of this spectral density is 1.113 mm (0.0438 in.) for a frequency range of 0.1 to 10 Hz.

Acceleration transfer functions.- With sinusoidal input (eqs. (2)) and the assumption of sinusoidal motion in the form

$$\{q(t)\} = \{q_1\} \sin \omega t + \{q_2\} \cos \omega t$$

equation (1) leads to the equations:

$$\left.\begin{aligned} \left[[K] - \omega^2[M]\right]\{\bar{q}_1\} - \omega[C]\{\bar{q}_2\} &= \{Q_1\} \\ \omega[C]\{\bar{q}_1\} + \left[[K] - \omega^2[M]\right]\{\bar{q}_2\} &= \omega\{Q_2\} \end{aligned}\right\} \tag{4}$$

The elements of the matrices $[K]$, $[M]$, $[C]$, $\{\bar{q}_1\}$, $\{\bar{q}_2\}$, $\{Q_1\}$, and $\{Q_2\}$ are given in appendix A. Equations (4) are solved for $\{\bar{q}_1\}$ and $\{\bar{q}_2\}$ by using standard digital computer routines. From the solution of equations (4), the amplitude $\{\bar{q}\}$ is determined by use of the relation

$$\bar{q}_j = \sqrt{\bar{q}_{1j}^2 + \bar{q}_{2j}^2} \sin\left(\omega t + \psi_j\right) \tag{5}$$

where $\sqrt{\bar{q}_{1j}^2 + \bar{q}_{2j}^2}$ is the response amplitude and $\psi_j = \tan^{-1}\frac{\bar{q}_{2j}}{\bar{q}_{1j}}$ is the phase angle. In this paper, as in reference 4, no results are presented for the phase angle ψ_j.

On the basis of equation (5), a general expression for the steady-state acceleration response to sinusoidal input, or transfer function, may be written as

$$A_{qj} = \omega^2 Q_o \sqrt{\bar{q}_{1j}^2 + \bar{q}_{2j}^2} \tag{6}$$

The expressions for transfer function at different model locations are given in the following table:

Location	Acceleration transfer function
Car	$\frac{A_c(x)}{gS_o} = \frac{\omega^2}{g}\sqrt{\left[\bar{a}_1 W(x) + \bar{z}_{c1}\right]^2 + \left[\bar{a}_2 W(x) + \bar{z}_{c2}\right]^2}$
Transformer	$\frac{A_g}{gS_o} = \frac{\omega^2}{g}\sqrt{\bar{z}_{g1}^2 + \bar{z}_{g2}^2}$
Traction motors	$\frac{A_A}{gS_o} = \frac{\omega^2}{g}\sqrt{\bar{z}_{A1}^2 + \bar{z}_{A2}^2}$

The two car locations for which acceleration transfer functions were studied were the end of the car (x = 0) and the middle of the car (x = L/2).

Spectral density.- The spectral density of the acceleration response at a given model location is obtained from the transfer function and the spectral density of the input $S_I(f)$ by the equation

$$S_q(f) = \left(\frac{A_q}{gS_o}\right)^2 S_I(f) \tag{7}$$

The root-mean-square value of $S_q(f)$ in g units is obtained from

$$g_{rms} = \left[\int_{f_b}^{f_e} S_q(f)\, df\right]^{1/2} \tag{8}$$

The integration limits f_b and f_e were taken as 0.1 and 10 Hz, respectively, for this study.

Optimization Procedure

Sinusoidal input.- With the sinusoidal input, the objective of the optimization was to minimize the largest value of the acceleration transfer function occurring between 0 Hz and 20 Hz. The procedure used was the same as that used in reference 4. The first step in this procedure is to generate transfer function curves such as shown in figure 3 for a range of values of one of the system parameters. The next step is to plot the value of the transfer function associated with a given peak (determined from curves such as those of fig. 3) as a function of the varying system parameter. For example, figure 3(a) shows that peaks occur at about 1 Hz and 8.3 Hz in the transfer function at the end of the car, and figure 4(a) shows the variation of the transfer function associated with each of these peaks as the transformer frequency is varied. Similarly, parts (b), (c), and (d) of figures 3 and 4 show where the peaks occur for other positions in the model and how the peak values vary with transformer frequency. The frequency range associated with each peak is shown next to each curve in figure 4.

The next step in the optimization is to identify a curve which shows the largest value of transfer function for each value of the varying parameter. Such a curve is called a maximum acceleration function and is indicated for each model location in figure 4 by the segments of the curves joining the circular symbols. A value of the varying parameter that minimized the maximum acceleration function is then chosen. Figure 4 shows that a transformer frequency of 6.5 Hz minimizes the maximum acceleration function at both car locations but not at either the transformer or traction-motor location. In the present study, a value was chosen that minimized the car location accelerations because they were considered more important from the standpoint of passenger comfort.

Finally, with the optimum value of the first system parameter, a second system parameter is varied and the process described is used to determine an optimum value of the second parameter. In the present study, this procedure was repeated through four parameters and constituted an optimizing cycle. The cycle was repeated, as in reference 4, until the value obtained as optimum for a given parameter was the same as the value obtained in the previous optimizing cycle. Fortunately, no more than two optimizing cycles were required in this study. Figures 4 to 7 show the curves used to determine the optimum values of the varied parameters (with $f_A = 4.12$ Hz) and are discussed in the section "Results of Vertical Motion Analysis."

Random input.- The objective of the optimization with the random input was to minimize the value of the root-mean-square (rms) acceleration in the frequency band from 0.1 to 10 Hz. The procedure was to obtain values of rms acceleration for each model location by using equations (4), (7), and (8) for a range of values of a system

parameter. A value of the system parameter was chosen to minimize accelerations at all locations, if possible, and the value chosen was then held constant while a second system parameter was varied. Only a single optimization cycle was required to obtain sufficiently accurate optimum values of the two parameters varied in this study.

Results of Vertical Motion Analysis

Two studies were carried out with the vertical model: (1) an optimization study based on minimum response of the car and (2) a parameter variation study of the effect on acceleration transfer function of two parameters that were not varied in the optimization study. The full scope of both of these studies is indicated in table I. Table I(a) contains the values of the constant parameters and table I(b) indicates the parameters that were varied, along with the value of each parameter used for each figure.

Optimization for sinusoidal input.- The optimization procedure described for the sinusoidal input was used to determine optimum values of the frequency of the transformer and the damping coefficients of the transformer, bolster, and equalizer. The curves used to determine optimum values are shown in figures 4 to 7, and the values of the remaining parameters are given in table I. The optimum transformer frequency was chosen from figure 4 to be 6 Hz. Figure 5 shows that the tranformer damping value of 0.25 minimizes the transfer function for both car locations and, in addition, results in near-minimum values of transfer function for the transformer and traction-motor locations. Figure 6 shows that the transfer function is minimum at the end of the car for a bolster damping coefficient n_S of 0.09 but at the middle of the car for $n_S = 0.14$. The transfer function is sensitive to variations in bolster damping. In this case, n_S was chosen as 0.11. This value is good for the transformer location but not for the traction motor, for which the minimum transfer function is obtained for $n_S \geqq 0.5$. Figure 7 shows that optimum equalizer damping is 0.03 for the end of the car but is 0.31 for the middle of the car. The compromise value of $n_A = 0.1$ was chosen arbitrarily, between the two minimizing values.

Figures 4 to 7 show that it was not possible to choose a value of the varying parameter that minimized the transfer function at all model locations simultaneously. This result was also observed for the three-degree-of-freedom model of vertical car motion studied in reference 4. Because of this result, care must be taken in a real rail car situation that an optimum value of a system parameter chosen to minimize acceleration at, for example, a car location does not result in excessive acceleration at another location, such as the traction motors. The factors to be considered when the accelerations at both car locations cannot be minimized together, such as those shown in figures 6 and 7, are discussed in reference 4.

The results shown in figures 4 to 7 were obtained by using an equalizer spring value that resulted in an equalizer frequency of 4.12 Hz. The study represented by these figures was repeated with an equalizer frequency of 5.53 Hz (a stiffer equalizer spring). The values of the other nonvarying parameters were the same as those shown in table I(a) for figures 4 to 7. The optimizing curves with the equalizer frequency $f_A = 5.53$ Hz were qualitatively very similar to the curves shown in figures 4 to 7; the optimum values of the varied parameters are compared for the two equalizer frequencies in table II. This table shows that the optimum values of only transformer and bolster damping were different for the two equalizer frequency values. Moreover, the transfer function with $f_A = 5.53$ Hz was insensitive enough to variations of transformer damping n_g to insure that a value of $n_g = 0.25$ would be an acceptable value. Figure 6 shows, however, that transfer function is very sensitive to variations of bolster damping n_s; therefore, the difference between $n_s = 0.057$ and $n_s = 0.11$ is significant. These results indicate (as might have been expected) that the value of the equalizer spring is important in determining one of the optimum damping values, bolster damping. In this particular case, the equalizer spring value is not important for the other parameters f_g, n_g, and n_A.

Optimization for random input.- By using the optimization procedure previously described for the random input, optimum values of bolster and equalizer damping coefficients were determined. The results are presented in figures 8 and 9. The values of all other parameters were the same as those for the sinusoidal input study of figures 4 to 7, as shown in table I. The values of transformer frequency and damping were not varied; however, the optimum values from the sinusoidal input study were used. Figures 8 and 9 both show that the rms acceleration, in general, was insensitive to variations of bolster and equalizer damping. Figure 8 shows that a bolster damping coefficient of about 0.3 is a good value for minimizing rms accelerations. In spite of the insensitivity of rms acceleration to variations of bolster damping, the value of $n_s = 0.11$ as determined from the sinusoidal study has rms accelerations at the car location about 30 percent greater than those for $n_s = 0.3$. Therefore, these rms studies indicate that a higher bolster damping value is required to minimize rms accelerations than is required to minimize peak acceleration transfer functions. This result is in agreement with the results for the three-degree-of-freedom model of reference 4, where, with no mass between the rails and the car, it was shown that the optimum suspension damping values were larger for random inputs than for sinusoidal inputs. Figure 9 shows, however, that rms acceleration is so insensitive to variations of equalizer damping (for the particular values used for the other system parameters) that any value between $n_A = 0$ and $n_A = 0.5$ may be chosen without penalty to rms acceleration.

The rms values shown in figures 8 and 9 were obtained from spectral densities of the type shown in figure 10. These particular spectral densities apply to the optimum values of n_S and $n_A = 0.30$ from figure 9 and show a concentration of energy at the low frequency range (around 1 Hz) for the two car locations and the transformer. For the traction motors, the energy concentration occurred in the higher frequency range, near 5 Hz.

Parameter variation.- Car bending frequency f_B and car weight $M_c g$ were held fixed at 8 Hz and 574 kN (129 000 lb), respectively, for the optimization studies, and the structural damping coefficient g_{cv} was taken equal to zero. To determine how these properties might interact with other parameters in the model, including those chosen for optimization, transfer functions were obtained for wide variations of car bending frequency and car weight and for a nonzero structural damping coefficient. Maximum values of the peak acceleration curves (maximum acceleration functions as described in section "Optimization Procedure") and their associated frequencies are plotted for the two car locations as functions of bending frequency in figure 11 for an arbitrary non-optimum configuration. Variations of acceleration transfer functions with car weight are shown in figure 12 and were obtained by varying both car weight and bending frequency, car bending stiffness being assumed to be fixed at a value corresponding to $f_B = 8.0$ Hz and $M_c g = 574$ kN (129 000 lb). The values of all parameters used to generate figures 11 and 12 are shown in table I(b).

Figure 11 shows that the acceleration transfer function with no car damping has a maximum value for both car locations for a car bending frequency value of 3 Hz. The value of transfer function at its maximum is about 8.5 and 3.9 times the value at frequencies above 6 Hz for the end of the car and the middle of the car, respectively. This sensitivity suggests the need for knowing the bending frequency of a given rail car and its possible variations in service so that large values of acceleration can be avoided by proper design of the system. Figure 12 shows that car acceleration transfer functions were relatively insensitive to wide variations in car weight.

Comparison in figure 11 of the solid curves for zero structural damping with the dashed curve for structural damping $(g_{cv} = 0.05)$ shows that a small amount of structural damping causes large decreases of acceleration transfer function within the frequency range of resonance (<6 Hz). However, if, by proper design, this range can be avoided, structural damping becomes of minor importance, as indicated by the virtual coalescence of the curves of figure 11 away from resonance.

ANALYSIS OF LATERAL MOTION

Mathematical Model

Views of the mathematical lateral model and its coordinate system are shown in figure 13. Viscous damping representation is omitted for figure clarity. The motion of the model is governed by equation (1), and the matrix elements for this equation are derived in appendix B in the same manner as that used in appendix A for the vertical model except for differences in certain strain-energy terms due to the nonlinear lateral bolster springs. Car motion is represented by the torsional and lateral bending of a uniform beam. As in the case of the vertical model, linear viscous damping is assumed for the lateral truck and transformer suspensions and structural damping for the car itself. Symmetry about the center of the car is assumed in lateral as well as longitudinal directions.

Degrees of freedom.- The lateral model consists of ten degrees of freedom identified as follows:

Car lateral bending mode, $b(t)$
Car rigid-body lateral translation, $y_c(t)$
Car rigid-body roll, $\theta_{c0}(t)$
Car first torsion mode, $\theta_{c1}(t)$
Car rigid-body yaw, $\eta(t)$
Transformer lateral translation, $y_g(t)$
Lateral translation of rear traction motor, $y_{Ar}(t)$
Lateral translation of forward traction motor, $y_{Af}(t)$
Roll of rear traction motor, $\theta_{Ar}(t)$
Roll of forward traction motor, $\theta_{Af}(t)$

The car is free to twist about a longitudinal elastic axis (designated in fig. 13(b)), and the first torsion mode shape of the car is given by $\cos\frac{\pi x}{L}$. The total bolster spring constant k_S and damping constant c_S for each truck are divided equally between the springs and dampers located symmetrically beneath each side of the car, as shown in figure 13(b). Similarly, the total equalizer spring constant k_A and damping constant c_A in each truck are each divided equally between the springs and dampers connecting the traction motors to the rails. Both rigid-body roll and torsion $\left(\theta_{c0}(t)\right.$ and $\left.\theta_{c1}(t)\right)$ are resisted by the bolster springs and dampers. The spring constant $\frac{k_A}{2}$ and damping constant $\frac{c_A}{2}$ over each rail represent the combined stiffness and damping of separate equalizers actually located near each wheel; that is, there are four equalizers per truck. Traction-motor roll $\left(\theta_{Ar}(t)\right.$ and $\left.\theta_{Af}(t)\right)$ is assumed to be resisted by this spring-damper system. Additional stiffness and damping in the equalizer-traction-motor system are provided by a rolling spring constant k_α and a damping constant c_α at

the traction-motor center of gravity, as shown in figure 13(b). The introduction of this additional stiffness and damping is intended to simulate the complicated linkage and gear mechanisms between the traction-motor and wheel-axle system in an actual rail car truck, as illustrated in figure 2.

Lateral stiffness and damping in the transformer and truck suspensions are given by spring and damping constants that are assumed to approximate lateral shear stiffness and damping in the vertical transformer suspension, the bolsters, and the equalizers. The lateral transformer spring and damping constants are designated by k_{lg} and c_{lg}, the lateral spring and damping constants of the bolster by k_{lc} and c_{lc}, and the lateral equalizer spring and damping constants are denoted by k_l and c_l. The transformer properties are assumed to be linear, and the bolster and equalizer properties are also assumed to be linear between the small solid semicircles in the truck suspension view (fig. 13(b)). These semicircles represent compressible stops or bumpers, each having the nonlinear spring function shown in figure 14. This function is based on measured force-deflection data for an actual truck suspension.

Rail inputs.- The lateral model was excited by lateral and rolling, or rocking, inputs from the rails as indicated by the horizontal and vertical arrows at the bottom of the truck suspension view in figure 13(b). The lateral input is designated $Y_f(t)$ and $Y_r(t)$ at the forward and rear trucks, respectively. The roll input is identified as cross level, as in reference 1, and was generated by the differences $\delta_f(t)$ and $\delta_r(t)$ between unequal vertical inputs applied to each rail as shown in figure 13(b). This difference was always applied as the displacement of the right-hand rail (with the car viewed from the front). In general, these inputs may be written in vector form as

$$\left.\begin{aligned} Q(t) &= \begin{Bmatrix} Y_f(t) \\ Y_r(t) \\ \delta_f(t) \\ \delta_r(t) \end{Bmatrix} \\ \dot{Q}(t) &= \begin{Bmatrix} \dot{Y}_f(t) \\ \dot{Y}_r(t) \\ \dot{\delta}_f(t) \\ \dot{\delta}_r(t) \end{Bmatrix} \end{aligned}\right\} \tag{9}$$

Three classes of input were applied to the lateral model: sinusoidal, transient, and random as indicated in figure 15. The sinusoidal inputs (fig. 15(a)) may be written in the general form:

$$\left.\begin{aligned} Q_f(t) &= Q_{of} \sin \omega t \\ Q_r(t) &= Q_{or} \sin (\omega t + \kappa) \\ \dot{Q}_f(t) &= Q_{of}\omega \cos \omega t \\ \dot{Q}_r(t) &= Q_{or}\omega \cos (\omega t + \kappa) \end{aligned}\right\} \qquad (10)$$

where ω is the input frequency and Q_{of}, Q_{or} = Y_{of}, Y_{or} or δ_{of}, δ_{or} depending on whether the model is excited by lateral or cross-level inputs, respectively. The quantity κ represents the phase angle between forward and rear inputs, and the model was excited with inputs either in phase or out of phase as illustrated in sketch (a). The out-of-phase option allowed for the influence of car torsion and traction-motor rolling effects to be examined.

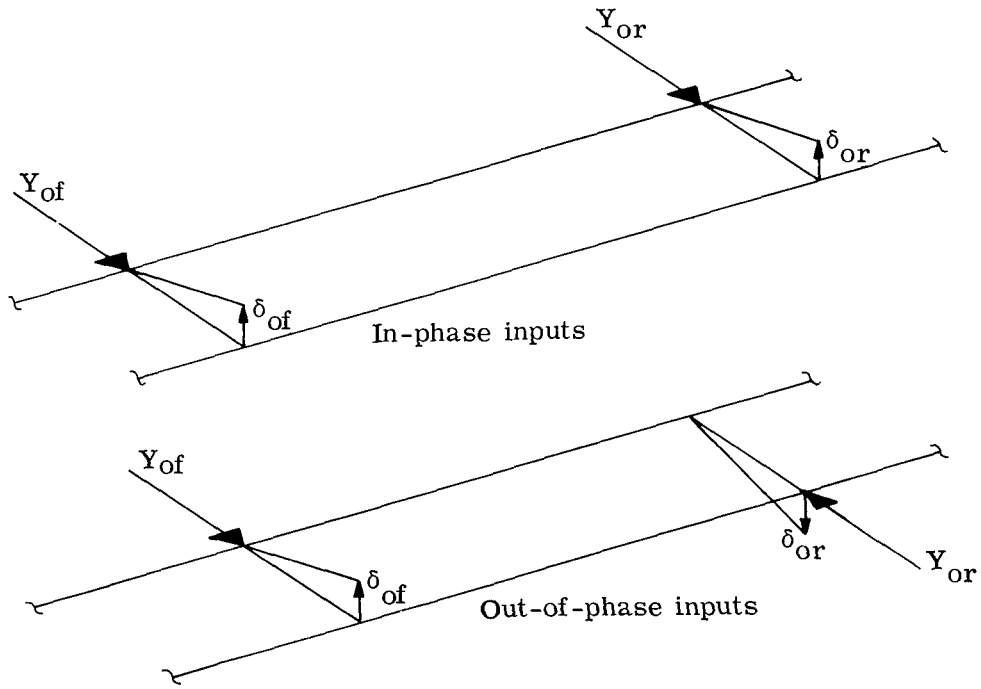

Sketch (a)

The three nonsinusoidal deterministic inputs in figure 15 are transients representing different types of disturbances of finite length λ along the rails. The first of these inputs is a single square pulse (fig. 15(b)) with a constant displacement applied to the front trucks Q_{of} and rear trucks Q_{or} in a sequence of time intervals which introduces car speed v as an additional variable through the simple relations

$$t_1 - t_0 = t_3 - t_2 = \frac{\lambda + (\Delta l)_t}{v} \tag{11a}$$

$$t_2 - t_1 = \frac{L - 2d - (\Delta l)_t - \lambda}{v} \tag{11b}$$

where $t_1 - t_0$ is the time interval required for the forward truck to roll over the disturbance, $t_2 - t_1$ is the time between when the front truck leaves the disturbance and the rear truck encounters it, and $t_3 - t_2$ is the time it takes for the rear truck to roll over the distrubance. If $L - 2d - (\Delta l)_t$ is less than λ, corresponding to a long disturbance, $t_2 - t_1$ becomes negative and indicates that the rear truck encounters the disturbance before the front truck leaves it. The distance $(\Delta l)_t$ is the center-to-center distance between the axles of a truck. The velocity inputs $\dot{Q}_f(t)$ and $\dot{Q}_r(t)$ are assumed to be zero. Lateral or cross-level inputs were applied in the directions indicated in the foregoing in-phase sketch, and the only phase lag of the rear truck behind the forward truck was due to car speed, in accordance with equations (11).

The second transient input is the square pulse train (fig. 15(c)) which is intended to reproduce the effect of rail joints as illustrated in sketch (b):

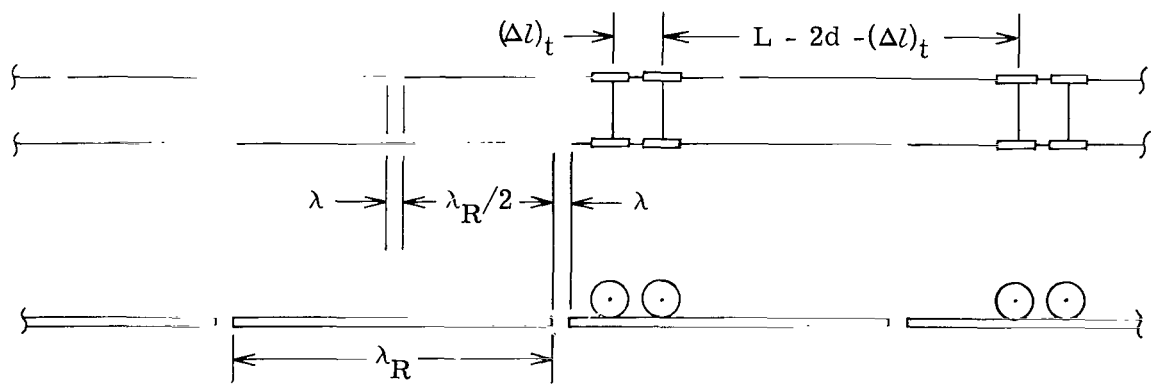

Sketch (b)

The length λ_R is the distance between joints, and λ is the gap between the ends of the rail joints. In the present paper, λ was chosen as 2.54 cm (1 in.) and λ_R as

11.9 m (468 in. or 39 ft). This input is treated as a succession of square pulses applied to one rail (the right-hand one for the front view of the car, consistent with the foregoing in-phase sketch). The displacement inputs to each truck are constant and the velocity inputs are assumed to be zero, as for the square pulse. In addition to equations (11), two other time-distance relations are involved, namely

$$t_5 - t_4 = \frac{\lambda + (\Delta l)_t}{v} \tag{12a}$$

and

$$t_5 - t_1 = \frac{\frac{\lambda_R}{2} + \lambda}{v} \tag{12b}$$

where $t_5 - t_4$ is the time required for the forward truck to roll over the disturbance due to the gap in the other (left hand) rail, and $t_5 - t_1$ is the time required for a truck to traverse the distance between gaps which occur on opposite rails.

The third transient input is a single-wave pulse (fig. 15(d)) which is intended to simulate the effects of a lateral deviation of the track from a straight course or the bank on a curve, depending on whether the inputs are lateral or cross level. This input is governed by trigonometric relations of a form similar to those used in reference 2. For the forward truck, the displacement input is

$$Q_f(t) = \frac{Q_{of}}{2}\left[1 - \cos\frac{2\pi v(t - t_0)}{\lambda + (\Delta l)_t}\right] \tag{13a}$$

and for the rear truck

$$Q_r(t) = \frac{Q_{or}}{2}\left[1 - \cos\frac{2\pi v(t - t_2)}{\lambda + (\Delta l)_t}\right] \tag{13b}$$

The velocity input for this case is

$$\dot{Q}_f(t) = \frac{Q_{of}\pi v}{\lambda + (\Delta l)_t}\sin\frac{2\pi v(t - t_0)}{\lambda + (\Delta l)_t} \tag{14a}$$

$$\dot{Q}_r(t) = \frac{Q_{or}\pi v}{\lambda + (\Delta l)_t}\sin\frac{2\pi v(t - t_2)}{\lambda + (\Delta l)_t} \tag{14b}$$

Equations (11) apply for this input as well as for the square pulse. In the application of equations (13) and (14), λ was varied over a wide enough range to insure that $L - 2d - (\Delta l)_t - \lambda$ was both positive and negative.

Random inputs to the lateral model included the functions illustrated in figures 15(e) to 15(g). Spectral densities identified as 1 and 2 in figure 15(e) correspond to rms amplitudes of 5.08 cm (2 in.) and 2.54 cm (1 in.), respectively. Spectral density 3 is based on an experimental measurement of random vertical displacements along a 3.2-km (2-mile) section of test track in the eastern United States, and the rms amplitude was 1.524 mm (0.06 in.) for a vehicle speed of 49.2 m/sec (110 mph). This input was arbitrarily applied to the lateral model with a 2.54-cm (1 in.) rms lateral amplitude. Figure 15(f) illustrates the square-pulse train input with random amplitudes. Figure 15(g) shows a time history of a combination of this random-pulse train input with spectral density 4 in figure 15(e) for a 2.54-cm (1 in.) rms amplitude. This input was also applied arbitrarily as lateral input to the lateral model. Spectral density and rms inputs are denoted by $Y_I(f)$ and Y_{rms} for the lateral input and $\delta_I(f)$ and δ_{rms} for the cross-level input. All these random inputs were applied simultaneously to front and rear trucks. Velocity random inputs were neglected.

Outputs.- Responses of the lateral model were obtained in the forms of acceleration transfer functions for the sinusoidal inputs, absolute values of maximum accelerations in g units for the transient inputs, and acceleration spectral densities and rms values for the random inputs. Lateral acceleration responses were calculated in the car at various stations distributed along the longitudinal center line of the car and also for the transformer and traction motors. Vertical acceleration responses were determined in the car just over the bolsters and in the traction motors over the equalizers. Acceleration transfer functions for the sinusoidal input were obtained from equations (4) to (6) as for the vertical model, and particular forms of equation (6) are listed in table III for the lateral model.

Solutions of equations of motion.- Equations (4) and the transfer functions listed in table III were programed on the Control Data 6600 computer system at the Langley Research Center, as were the corresponding equations for the vertical model. This program is restricted to linear spring elements. The solutions of equation (1) for the transient and random inputs in figure 15 were programed, along with equations (11) to (14), for another Langley computer facility, discussed in the following section, that was also able to handle the nonlinear spring characteristics shown in figure 14.

Scaled Real-Time Simulation

The presence of the nonlinear springs and the wide selection of inputs previously described prompted application of another method of solving equation (1) for the lateral model. This method involved the numerical integration of this equation in time by use of the real-time simulation (RTS) capabilities of the Langley central digital data recording facility. In this approach, the ten simultaneous equations represented by equation (1)

were integrated in the time domain on the Control Data 6600 computer system, and solutions were fed through digital-to-analog converters (DAC) to give time histories of displacements, velocities, and accelerations in various parts of the model. To insure sufficiently accurate integrations, the independent variable time had to be slowed, or scaled, during the computation. A time interval of 1.5625 msec was used in a second-order Runge-Kutta integration scheme. Results from this program for sinusoidal inputs were checked with those obtained from the digital transfer-function program. The sinusoidal inputs of equations (10) could be applied in the RTS program for an arbitrary phase angle κ, whereas the digital solution was programed only for solutions with κ equal to integral multiples of π corresponding to in-phase and out-of-phase inputs to the front and rear trucks, respectively.

An important feature of the RTS approach is the on-line random input capability represented in the flow chart of figure 16. In this arrangement, band-limited white noise, which was generated by an analog computer, could be introduced directly through a cut-off filter, or through a desired shaping filter, into the RTS computer program for solving equation (1). Outputs of this program and the random input were both fed on-line into a time series analysis digital program (TSA), in which statistical properties of input and output were calculated. Spectral density and rms value were the two properties of interest in this investigation. By appropriate choices of shaping filters, reasonable approximations to the spectral-density shapes for inputs 3 and 4 in figure 15(e) could be generated for any desired input amplitude.

Real-time simulation system.- The real-time simulation (RTS) system used to solve the ten equations of motion provides console control combined with digital accuracy and convenience. (See ref. 6.) The ten second-order derivatives in equation (1) were formed and numerically integrated twice during each machine iteration to yield the velocities and displacements. These operations are indicated on the flow chart of figure 17. During most of this study, 32 iterations per second (20-to-1 slow) was the normal iteration rate, whereas 64 iterations per second (10-to-1 slow) were used whenever possible.

Random studies.- An Electronic Associated, Incorporated (EAI) 231-R analog computer was programed with appropriate filters and a mean and rms control circuit to produce desired random inputs to the mathematical model from an analog Gaussian noise generator. This equipment is represented by the random-input (or noise generator) box in the flow chart of figure 16. Outputs from the mathematical model were directed to an on-line TSA program located at a separate control point of the RTS system. This program computes mean values, standard deviations, chi-square tests for normality, histograms, autocorrelation functions, and power spectral density functions (PSD) for its input channels. These statistical properties are discussed in detail in reference 7. A

CDC-250 cathode ray tube (CRT) was used to display linear or log-log plots of the PSD values generated by the TSA program. Control stations such as those used for solving the equations of motion, operation of the TSA program, and operation of the CRT are shown in figure 18. Also shown are a CRT console and the time-history recorders, each capable of displaying 8 different displacements, velocities, or accelerations.

Visual car display.- An oscilloscope display showing a front cutaway view of the car at the forward truck was driven by a program on the GPS 10 000 iterative analog computer. As indicated in figure 16, this analog program transformed DAC outputs from the mathematical-model solution into signals for the scope display. This display was of small analytical value because of the 20-to-1 or 10-to-1 time scales but was useful for demonstration purposes.

Results of Lateral Motion Analysis

The presence of eight spring elements and eight dampers in the lateral model requires the use of a computerized algorithm for minimizing vibration levels in the system. The trial-and-error cycling approach utilized in a limited optimization of the vertical model, with eight system elements at most, was considered to be impractical for the lateral model. Instead, the analytical tools previously described were exploited to obtain trends of acceleration responses to inputs involving realistic ingredients for lateral and cross-level rail disturbances. Parameter variations included realistic rail car values, and the widest variations were made for the sinusoidal inputs utilizing the transfer-function digital program. The RTS capabilities were employed to explore (1) relations between car speed and damping coefficients in the truck suspension and (2) nonlinear spring effects for the transient and random inputs. Some effects of input wavelength were also considered. The full scope of this study is given in tables IV and V. The fixed properties are listed in table IV, and the values of the variable properties and inputs in each of the figures are presented in table V. Inputs in table V are identified according to the appropriate parts of figure 15.

Results for sinusoidal input.- Typical acceleration transfer functions for various stations in the lateral model are shown in figure 19. With all damping coefficients reduced to 0.001 and the car structural damping coefficients set equal to zero, peak acceleration responses occurred near the uncoupled frequencies of the system. The existence of only a few peaks in figure 19 is attributed to the moderate to high damping levels indicated by the values listed in table V for this figure. A dominant peak at 0.44 Hz occurred frequently in the car and transformer responses as shown in figures 19(a) and 19(b). The response was sensitive to the magnitude of the lateral bolster damping coefficient n_{lc}. Other parts of the model experienced dominant peak

accelerations at higher frequencies for the cases considered, as is evident, for example, in figures 19(c) to 19(e).

All ten degrees of freedom were retained in nearly all the studies; however, the effects of deleting traction-motor rolling degrees of freedom $\left(\theta_{Ar}(t) \text{ and } \theta_{Af}(t)\right)$ and of changing traction-motor stiffnesses $\left(k_{\alpha r} \text{ and } k_{\alpha f}\right)$ were given limited attention. The effects of these parameter variations are compared in the transfer-function plots of figures 20 and 21. Figures 20(a) and 20(b) show only a 7-percent reduction in maximum lateral car accelerations to lateral in-phase inputs because of the complete elimination of these rolling degrees of freedom and about 4-percent reduction with traction-motor rolling stiffnesses increased from $k_{\alpha r} = k_{\alpha f} = 26.8$ to 101.5 MN-m/rad (corresponding to 2.375×10^8 to 9.00×10^8 in-lb/rad and to a frequency increase from $f_\alpha = 18$ Hz to 35 Hz). Somewhat larger effects on the vertical bolster responses are evident in figure 20(e). Figure 21 shows still larger effects of traction-motor rolling stiffness on maximum acceleration responses to cross-level out-of-phase inputs. Lateral end-of-car response (fig. 21(a)) and the vertical response over the bolster (fig. 21(c)) are each reduced by about two-thirds with f_α increased from 18 to 35 Hz; however, these maximum responses occurred close to 18 Hz, and at lower frequencies within the range of interest of this study, these effects are seen to be much smaller. In general, changes in car accelerations due to these variations in traction-motor stiffness and rolling degrees of freedom in figures 20 and 21 are considered to be small by comparison with the effects of other parameters in the model.

Maximum values of peak acceleration curves are shown as functions of frequency (that is, spring) and damping parameters in figures 22 to 29 for sinusoidal inputs. Frequencies associated with these peak accelerations are identified at points along the curves. Figure 22 reveals a resonant region of significantly increased lateral car accelerations due to lateral car bending frequencies (eq. (B16a)) falling within range of other frequencies of the model. These trends are similar to those observed in figure 11 because of vertical bending frequencies. The great reduction in lateral car accelerations due to car structural damping in this resonant region is similar to that observed in figure 11 for the vertical model. Likewise, with lateral car bending frequencies well removed from the other frequencies of the system, lateral car accelerations were greatly reduced and were insensitive to variations in structural damping, as were vertical car accelerations in figure 11. For a lateral bending frequency of 8 Hz, the maximum transfer function was about 0.25 g per inch at both the end and middle of the car and occurred at a frequency of 0.44 Hz. The results in figure 22 were obtained with lateral in-phase inputs from the rails.

Maximum lateral car acceleration responses to out-of-phase lateral and cross-level inputs are plotted as functions of car torsional frequency in figure 23. Lateral

responses in figure 23(a) are seen to be constant over a wide range of torsional frequencies and significantly reduced with f_T less than about 5 Hz. The effect of cross-level inputs in figure 23(b) is somewhat reversed, maximum acceleration responses increasing as f_T is moved beyond the range of other system frequencies. It may also be observed that the lateral car responses to lateral inputs were higher than the lateral car responses to cross-level inputs, and this result is a general one of this study not only for the sinusoidal inputs but for the other inputs as well. Higher car responses to lateral than to cross-level inputs were also obtained in reference 1. The large variations in response shown in figures 22 and 23 indicate the need for accounting for car lateral bending and torsional stiffnesses in analyzing car vibrations. Comparison of the trends in figure 23, particularly figure 23(b), with those in figure 22 suggests that torsional stiffness plays a smaller role than bending stiffnesses in car vibrations.

Variations in acceleration transfer functions with car weight are shown in figure 24 for out-of-phase inputs. These variations were obtained by varying car weight, rolling moment of inertia, lateral bending frequency, and torsional frequency with car bending and torsional stiffness assumed to be fixed at values corresponding to $f_{\ell B} = 8.0$ Hz, $f_T = 15.0$ Hz, $M_c g = 574$ kN (129 000 lb), and $I_{EA} = 3090$ kg-m (695 lb-sec^2). Although the trends differ from those shown for the vertical model in figure 12, the effects of a wide variation in car weight on lateral car transfer functions are small, as these effects were for the vertical car transfer functions.

The flexibly mounted transformer beneath the middle of the car acted as a vibration absorber for reducing lateral car accelerations in an analogous manner to its role in reducing vertical car accelerations in the vertical model. The peak responses in figures 25 and 26 show reductions that were obtained for a wide range of transformer frequencies and damping coefficients with all other parameters held constant at the values listed in tables IV and V.

A vibration-absorber role can also be assumed for the lateral truck suspension. However, the present trend study was limited to the effects of damping with fixed spring parameters. Thus, with fixed lateral bolster and equalizer frequencies, lateral bolster and equalizer damping coefficients were varied and reductions in peak acceleration curves obtained as in figures 27 and 28. The results in figure 27 show relative minimum lateral car accelerations at different car locations for different bolster damping coefficients due to lateral in- and out-of-phase inputs. In this case, structural damping has the effect of widening these differences in the bolster damping values for minimum acceleration responses. Similar results are shown in figure 28 for the equalizer damping variation, except for the effect of structural damping which is not included. Figure 29 shows the relative minimum of peak lateral car accelerations at different values of bolster roll damping coefficient for in-phase and out-of-phase cross-level inputs. With car torsional structural damping included, out-of-phase responses were sharply reduced

with a minimum lateral response indicated at $n_{oT} = 0$. This reduction in response due to structural damping is consistent with that shown in figure 23. These results indicate the joint influence of both car and suspension damping on lateral car acceleration responses.

Results for transient and random inputs.- In utilizing RTS capabilities to examine linear car responses to various transient deterministic and random inputs, the main variables of interest were car speed v, input disturbance length λ, and lateral bolster damping coefficient n_{lc}. Some effects of bolster roll damping coefficient n_{oT} were also explored. Most of the results are presented in plots of peak lateral car acceleration responses as functions of car speed, as shown in figures 30 to 35. Some variations of peak responses with car length are shown in figure 36 for the square-pulse train input of figure 15(c).

These results show wide differences in peak lateral car responses due to changes in input and changes in car speed for individual inputs. Lateral inputs generally produced higher lateral car responses than did cross-level inputs, as was noted in figure 23 for sinusoidal inputs. Mid-car responses were lower than end-of-car responses for transient deterministic inputs (figs. 30 to 33) and for the combined random input (fig. 35). In some cases, such as those illustrated in figure 36, minimum car responses along the length of the car occurred at about 25 percent and 75 percent of the car length. Moreover, the spread between front and rear responses of the car was considerably larger for the wave-pulse inputs than for the other inputs. Figures 32 and 33 show responses at the rear of the car that are significantly higher than those at the front of the car. Sample time histories in figures 30 and 32 further illustrate differences in the character of the car responses for square-pulse and wave-pulse inputs for two widely different disturbance lengths. Initial accelerations due to a pulse input for $\lambda = 0.305$ m (12 in.) in figure 30 were more erratic than those due to a wave input for $\lambda = 76.2$ m (3000 in.) in figure 32. Peak accelerations were about 0.047g for both time histories.

Other indications of how dependent these results were on the nature of the input are afforded in comparisons of rms accelerations in table VI for two different random inputs, and in comparisons of acceleration responses for deterministic and random pulse train inputs in figure 34. The table compares rms lateral responses for the test track input, corresponding to input spectral density 3 in figure 15(e), and the combined input of figure 15(g) for a 2.54 cm (1 in.) rms amplitude. The results are taken from figures 35 and 37 for the same car speed 49.3 m/sec (110 mph) and lateral bolster damping coefficient $\left(n_{lc} = 0.11\right)$. Responses to the test track input are seen to be 22.5 to 39 percent higher than responses to the combined input, and mid-car responses are higher than responses at the truck locations in contrast to the combined-input responses. In figure 34, n_{lc} was 0.057, and the lateral-input amplitudes were 2.54 cm (1 in.) for the

deterministic pulse train input and 2.54 cm (1 in.) rms for the random pulse train input. As the figure shows, lateral responses due to random input were larger than those due to deterministic transient input, and differences in lateral responses between the trucks and the middle of the car were greater for the random than for the deterministic transient inputs. The lateral responses to random pulse train inputs (λ = 2.54 cm (1.0 in.)) followed about the same trends and were about the same magnitudes as the lateral responses to the deterministic pulse inputs (λ = 0.305 m (12 in.)) in figure 30. However, rms accelerations at rear and forward truck locations tend to be more nearly equal in figure 34 than do the corresponding peak accelerations in figure 30; thus, the effects of input variation on car response are also apparent in this comparison. These results further support the recommendations in references 1 and 4 which point out the need for obtaining measured input spectra for studies of this kind.

Effects of wavelength λ were explored for the wave-pulse inputs, and figure 33 shows the variation of peak lateral car accelerations with car speed for two different values of λ, both less than that of figure 32. Comparison of the results in these two figures indicates that lowering λ from 76.2 m (3000 in.) to 19.05 m (750 in.) substantially reduced the speed range bounding the wide spread in end-of-car acceleration responses to lateral inputs. The much smaller lateral response to cross-level inputs behaved in a manner somewhat similar to that of the lateral-input responses; however, the spread in end responses still extended over about the same speed range regardless of λ value, and cross-level responses for λ = 38.1 m (1500 in.) are shown in figure 33 to be nearly indistinguishable from those for λ = 19.05 m (750 in.).

In addition to the effects of input variations and disturbance length, variation of damping in the lateral bolster (n_{lc}) also caused large fluctuations in lateral car acceleration response. For example, localized increases in response were observed at particular car speeds for the deterministic pulse train and combined random inputs in figures 31 and 35; however, the effects of this damping are reversed. That is, increased damping for the deterministic input tended to increase responses near 53.7 m/sec (120 mph, fig. 31), whereas increased damping for the random input not only gave reduced responses but also caused them to be largely invariant over the speed range (fig. 35). It should be noted that car speed variations for the combined random input of figure 35 are due solely to the pulse train part of the input. By contrast with these effects, the wave-pulse input caused steep increases in lateral car peak responses to maximum values near 44.7 m/sec (100 mph) and slight decreases at higher speeds (fig. 32). Within the 35.8 to 44.7 m/sec (80 to 100 mph) speed range, increased lateral bolster damping coefficients were more effective in reducing lateral car acceleration responses than at other speeds. These damping effects clearly indicate that no fixed damping value would reduce lateral car accelerations at all speeds or at all locations in the car for any of the inputs considered.

Effects of bolster roll damping on lateral car acceleration responses were much smaller for cross-level inputs than the effects of lateral bolster damping were for lateral inputs. An indication of these effects may be seen in figure 30 where responses for $n_{oT} = 0.30$ are higher than those for $n_{oT} = 0.20$ at nearly all car responses from 17.88 to 71.52 m/sec (40 to 160 mph). Other results (not included) show still higher responses for $n_{oT} = 0.40$. As observed for the lateral bolster damping effect, the effect of bolster roll damping was also very much a function of car speed.

Nonlinear spring behavior.- All the results presented thus far are based on linear spring characteristics in the model. In addition to its application to the simulation of various rail irregularity inputs, the RTS method was also used to explore the effects of spring nonlinearity in the lateral bolster suspensions. The nonlinear spring characteristics shown in figure 14 were assumed for this purpose, and the deflections in the abscissa of the figure are related to the degrees of freedom in the model through the equations*

$$\Delta y_r(t) = -b(t)\, W(d) - y_c(t) + \left(\frac{L}{2} - d\right) \eta(t) + y_{Ar}(t) - h_{2r}\, \theta_{Ar}(t) - h_3 \left[\theta_{c0}(t) + \theta_{c1}(t) \cos \frac{\pi d}{L}\right] \tag{15a}$$

$$\Delta y_f(t) = -b(t)\, W(L - d) - y_c(t) - \left(\frac{L}{2} - d\right) \eta(t) + y_{Af}(t) - h_{2f}\, \theta_{Af}(t) - h_3 \left[\theta_{c0}(t) + \theta_{c1}(t) \cos \frac{\pi(L - d)}{L}\right] \tag{15b}$$

Through these equations, nonlinear behavior in the bumpers directly below the car is felt in the car and the traction-motor suspension.

With the nonlinear spring characteristics allowed for in equation (1), acceleration responses to sinusoidal inputs failed to reach a steady-state condition but varied in amplitude for a finite number of cycles of oscillation in repeated sequences in time. This response behavior ceased after termination of the sinusoidal forcing function. With band-limited lateral white-noise amplitude of 2.54 cm (1 in.) rms input (no. 2 in fig. 15(e))

*Additional relations are included in reference 5 for an assumed nonlinearity in the lateral equalizer springs. However, these relations (eqs. (6) of ref. 5) have been found to be incorrect because of the omission of lateral inputs from the right sides of the equations. Consequently, the "nonlinear" curves in figure 11 of reference 5 are incorrect and have been omitted from figure 37 of the present paper. In addition, the terms $-h_{2r}\theta_{Ar}(t)$ and $-h_{2f}\theta_{Af}(t)$ in equations (15) were erroneously omitted from equations (5) of reference 5 but were included in calculations for the nonlinear spectral density in figure 7 of this reference.

to equation (1), output spectral densities and rms values, such as those shown in figure 38, were obtained and are seen to be considerably higher for the nonlinear case than for the linear case. Figure 38 also shows large reductions in responses due to increasing lateral bolster damping from $n_{lc} = 0.057$ to 0.11.

Similar effects of the nonlinear springs were observed in lateral acceleration responses along the length of the car due to wave pulse inputs as shown in figure 39. Here the input wavelength λ was 9.52 m (375 in.), and the car speed 35.8 m/sec (80 mph). The solid curve identified as "linear" applies to lateral acceleration responses for which k_{lc} was linear and is included for comparison with the other curves for which k_{lc} was nonlinear. As may be seen, increasing n_{lc} from 0.057 to 0.30 resulted in drastically reduced responses, as in figure 38 for the random input. With $n_{lc} = 0.30$, the responses were reduced to the levels of the linear responses over the length of the car.

It thus appears that higher car accelerations can be obtained with nonlinear springs than with linear springs in the model and that this result is not likely to change when the input changes. It is also evident that a moderate amount of damping can be very effective in reducing nonlinear acceleration responses.

CONCLUDING REMARKS

Simplified vertical and lateral dynamic models of a high-speed rail passenger car have been developed and studied to obtain dynamic response information which is relevant to the problem of passenger comfort. Vertical responses of the car to vertical inputs from the rails have been obtained in a four-degree-of-freedom model, and lateral responses to lateral and rolling (cross-level) rail inputs have been obtained in a ten-degree-of-freedom model. Elastic properties of the passenger car body were represented by the bending and torsion of a uniform beam, and the rail-to-car (truck) suspension systems were modeled as simple spring-mass-dashpot oscillators. Lateral spring nonlinearities approximating certain complicated truck mechanisms were introduced and their effects on car response were explored. The models have been excited by displacement and, in some cases, velocity inputs from the rails, and a wide variety of deterministic (including sinusoidal) and random input functions have been used. Results were obtained in the form of acceleration responses in various parts of the models, particular attention being given to car responses. From this study, the following observations are made.

A trial-and-error optimization procedure for minimizing acceleration responses in the car has been shown to be feasible for a dynamic system with a few spring and damping elements. This feasibility was demonstrated for the vertical model, in which a

systematic variation of stiffness and damping properties showed that larger optimum car suspension damping was required for random than for sinusoidal inputs and that it was not possible to choose values of system parameters that simultaneously minimized accelerations in the car and in other parts of the model. The lateral model contained too many spring and damping elements for a practicable optimization by this approach and would require instead the application of a computer algorithm.

The stiffness of the equalizer in the truck suspension was found to be important in determining optimum damping in the vertical car suspension (bolster) but was not important for the optimum equalizer damping nor the optimum stiffness and damping of a simulated transformer mounting beneath the middle of the car.

Knowledge of car stiffness and weight properties is needed so that with proper design its natural frequencies are sufficiently removed from other frequencies in the system to avoid resonances characterized by high car acceleration responses. Torsional stiffness properties appeared to be less important than either vertical or lateral bending stiffness. Structural damping in the car was shown to be important at car bending and torsional frequencies within range of other frequencies in the system. However, car responses at car frequencies well removed from this resonant region were insensitive to variations in car structural damping. Car responses were also shown to be relatively insensitive to wide variations in car weight.

Car acceleration responses to sinusoidal input (transfer functions) were shown to be sensitive to variations in vertical and lateral bolster damping and relatively insensitive to variations in transformer stiffness (frequency) and damping.

Rolling stiffness and displacement of the traction motor in the truck suspension were shown to have minor effects on car acceleration responses in the lateral model.

Results of the study for the lateral model indicate that the real-time simulation (RTS) method could be used in preliminary design and troubleshooting of rail car configurations. Wide differences in lateral car response were shown for different car speeds and the various transient and random inputs that were available with this method, and results further showed that no fixed value of lateral bolster damping would reduce lateral car accelerations at all car speeds or in all car locations.

Lateral car acceleration responses were higher for nonlinear than for linear springs for two different inputs, and these responses are shown to be particularly sensitive to variations in lateral bolster damping.

Langley Research Center,
National Aeronautics and Space Administration,
Hampton, Va., June 30, 1971.

APPENDIX A

DERIVATION OF EQUATIONS OF MOTION FOR VERTICAL MODEL

This appendix presents the derivation of the matrix elements of equations (1) and (4) for the vertical model. These equations were obtained from Lagrange's equation in the form

$$\frac{d}{dt}\left(\frac{\partial T}{\partial \dot{q}_j}\right) + \frac{\partial D}{\partial \dot{q}_j} + \frac{\partial U}{\partial q_j} = 0 \tag{A1}$$

where T is the kinetic energy which is assumed here to be a homogeneous quadratic function of the velocities, D is the dissipation energy, U is the potential energy, and q_j is a generalized coordinate. These energies are given in terms of the degrees of freedom of the mathematical model of figure 1. Pitching and rolling motions of the car are neglected, and small displacements are assumed throughout the model, consistent with linear theory. Performance of the indicated operations in equation (A1) for each degree of freedom leads to a set of simultaneous equations of motion represented by the general matrix equation (4).

Energies of the Vertical Model

Kinetic energy.- The kinetic energy of the four-degree-of-freedom model in figure 1 is given by

$$T_V = \frac{m}{2}\int_0^L \left[\dot{w}(x,t) + \dot{z}_c(t)\right]^2 dx + \frac{1}{2}M_g\left[\dot{z}_g(t)\right]^2 + M_A\left[\dot{z}_A(t)\right]^2 \tag{A2}$$

where m is the mass of the car per unit length L, M_g is the mass of the transformer, and M_A is the mass of the traction motor in each truck. The bending deformation of the car is given by

$$w(x,t) = a(t)\, W(x) \tag{A3}$$

where $a(t)$ is the generalized coordinate having the units of displacement and $W(x)$ is the mode shape. The vertical traction-motor displacement z_A is the same for both forward and rear trucks.

Potential energy.- The potential energy of the vertical model is

$$U_V = \frac{(EI)_V}{2}\int_0^L \left[\frac{\partial^2 w(x,t)}{\partial x^2}\right]^2 dx + \frac{k_S}{2}\left\{\left[z(d,t) - z_A(t)\right]^2 + \left[z(L-d,t) - z_A(t)\right]^2\right\}$$

$$+ \frac{k_g}{2}\left[z\left(\frac{L}{2},t\right) - z_g(t)\right]^2 + k_A\left[z_A(t) - S(t)\right]^2 \tag{A4}$$

where $(EI)_V$ is the bending stiffness of the car in the vertical direction, $z(d,t)$ is the vertical displacement of the rear trucks, $z(L-d,t)$ the vertical displacement of the forward trucks, $z\left(\frac{L}{2},t\right)$ is the vertical displacement of the middle of the car, and $S(t)$ is the displacement input from the rail to both trucks. The truck and mid-car displacements are related to the four degrees of freedom by

$$\left.\begin{aligned} z(d,t) &= w(d,t) + z_c(t) = a(t)\,W(d) + z_c(t) \\ z(L-d,t) &= w(L-d,t) + z_c(t) = a(t)\,W(L-d) + z_c(t) \\ z\left(\frac{L}{2},t\right) &= w\left(\frac{L}{2},t\right) + z_c(t) = a(t)\,W\left(\frac{L}{2}\right) + z_c(t) \end{aligned}\right\} \tag{A5}$$

Substitution of equations (A5) into equation (A4) gives

$$U_V = \frac{(EI)_V}{2}\int_0^L \left[a(t)\frac{d^2W(x)}{dx^2}\right]^2 dx + \frac{k_S}{2}\left\{\left[a(t)\,W(d) + z_c(t) - z_A(t)\right]^2\right.$$

$$\left. + \left[a(t)\,W(L-d) + z_c(t) - z_A(t)\right]^2\right\}$$

$$+ \frac{k_g}{2}\left[a(t)\,W\left(\frac{L}{2}\right) + z_c(t) - z_g(t)\right]^2 + k_A\left[z_A(t) - S(t)\right]^2 \tag{A6}$$

Dissipation energy.- The dissipation energy is given in terms of viscous and structural damping constants by

$$D_V = \frac{c_S}{2}\left\{\left[\dot{a}(t)\,W(d) + \dot{z}_c(t) - \dot{z}_A(t)\right]^2 + \left[\dot{a}(t)\,W(L-d) + \dot{z}_c(t) - \dot{z}_A(t)\right]^2\right\}$$

$$+ \frac{c_g}{2}\left[\dot{a}(t)\,W\left(\frac{L}{2}\right) + \dot{z}_c(t) - \dot{z}_g(t)\right]^2 + c_A\left[\dot{z}_A(t) - \dot{S}(t)\right]^2$$

$$+ \frac{1}{2}\frac{g_{cv}}{\omega}(EI)_V\int_0^L \left[\dot{a}(t)\frac{d^2W(x)}{dx^2}\right]^2 dx \tag{A7}$$

where g_{cv} is the structural damping coefficient of the car in vertical bending. By following the approach of reference 8, structural damping is introduced in equation (A7) with its magnitude proportional to the elastic restoring forces in the car and in phase with the velocities of oscillation of the car. The presence of the frequency ω in the denominator of the last term of equation (A7) limits the use of the structural damping concept to systems with sinusoidal motions. In this investigation, structural damping was included only in the acceleration transfer-function computer program for equations (4).

Car Bending Mode

The bending mode shape of the car in equation (A3) is taken as the bending mode of a uniform free-free beam and is given by

$$W(x) \equiv W_m(x) = \cosh \beta_m x + \cos \beta_m x - \alpha_m(\sinh \beta_m x + \sin \beta_m x) \tag{A8}$$

where β_m and α_m are obtained from the equations

$$\left.\begin{aligned} &\cosh \beta_m L \cos \beta_m L = 1 \\ &\alpha_m = \frac{\cosh \beta_m L - \cos \beta_m L}{\sinh \beta_m L - \sin \beta_m L} \end{aligned}\right\} \tag{A9}$$

for $m = 1, 2, \ldots$ Solutions of equations (A9) are given in various places in the literature. (See, for example, ref. 9.) Since it was assumed that the motion of the car could be adequately represented by using only the fundamental mode, it was sufficient to consider $m = 1$, for which $\beta_1 L = 4.730$ and $\alpha_1 = 0.9825$. This assumption is essentially the same as that made in reference 4, except for the different approximation made for the mode shape. Mode-shape values for different stations along the car are given in table VII.

Matrix Elements of the Mathematical Vertical Model

The elements of the matrices $[M]$, $[C]$, and $[K]$ of equations (4) were obtained by carrying out the operations indicated in Lagrange's equation (A1) for each degree of freedom in the model and these elements are listed in tables VIII and IX. All matrix elements of equations (4) were obtained by dividing through each of the equations by the car mass M_c and the sinusoidal input amplitude S_o. The elements of $\{\bar{q}_1\}$, $\{\bar{q}_2\}$, $\{Q_1\}$, and $\{Q_2\}$ are as follows:

$$
\left.
\begin{aligned}
\{\bar{q}_1\} &= \begin{Bmatrix} \frac{a_1}{S_o} \\ \frac{z_{c1}}{S_o} \\ \frac{z_{g1}}{S_o} \\ \frac{z_{A1}}{S_o} \end{Bmatrix} \\
\{\bar{q}_2\} &= \begin{Bmatrix} \frac{a_2}{S_o} \\ \frac{z_{c2}}{S_o} \\ \frac{z_{g2}}{S_o} \\ \frac{z_{A2}}{S_o} \end{Bmatrix} \\
\{Q_1\} &= \begin{Bmatrix} 0 \\ 0 \\ 0 \\ 2\frac{M_A}{M_c}\omega_A{}^2 \end{Bmatrix} \\
\{Q_2\} &= \begin{Bmatrix} 0 \\ 0 \\ 0 \\ 4n_A\,\omega_A\,\frac{M_A}{M_c} \end{Bmatrix}
\end{aligned}
\right\} \qquad \text{(A10)}
$$

In the matrix elements, the natural frequencies of various parts of the model considered separately (ω_B, ω_s, ω_g, and ω_A), and the dimensionless viscous damping coefficients, are related to the spring mass and damping constants by

First vertical bending frequency of car:

$$\omega_B = (\beta_1 L)^2 \sqrt{\frac{(EI)_v}{M_c L^3}} \tag{A11a}$$

Bolster rigid-body vertical translation frequency:

$$\omega_s = \sqrt{\frac{2k_s}{M_c}} \tag{A11b}$$

Transformer frequency:

$$\omega_g = \sqrt{\frac{k_g}{M_g}} \tag{A11c}$$

Equalizer spring-traction-motor frequency:

$$\omega_A = \sqrt{\frac{k_A}{M_A}} \tag{A11d}$$

Bolster damping coefficient (for both trucks):

$$n_s = \frac{c_s}{M_c \omega_s} \tag{A11e}$$

Damping coefficient for the transformer suspension:

$$n_g = \frac{c_g}{2M_g \omega_g} \tag{A11f}$$

Damping coefficient of equalizer suspension in each truck:

$$n_A = \frac{c_A}{2M_A \omega_A} \tag{A11g}$$

where $M_c = mL$ is the mass of the rail car. The equation for ω_B is a reduced form of the equation

$$\omega_B = \sqrt{\frac{(EI)_v \int_0^L \left(\frac{d^2 W_m}{dx^2}\right)^2 dx}{m \int_0^L W_m{}^2 dx}} \tag{A12}$$

Using equation (A8) for $W_m(x)$ leads to $\int_0^L W_m{}^2(x)\,dx = L$ and $\int_0^L \left[\frac{d^2W_m(x)}{dx^2}\right]^2 dx = \beta_m{}^4 L$. Substitution into equation (A12) of these values of the integrals leads to equation (A11a). It should also be noted that in the derivation of equations (4), there is an off-diagonal element $M_{12} = m\int_0^L W_m(x)\,dx$. However, by virtue of conservation of momentum in a free-free beam, this integral vanishes, and the mass matrix reduces to a diagonal matrix. Evaluation of the three foregoing integrals is found in reference 10.

APPENDIX B

DERIVATION OF EQUATIONS OF MOTION FOR LATERAL MODEL

This appendix presents the derivation of equations (1) and (4) for the lateral model. These equations were obtained in the same manner as those for the vertical model, beginning with Lagrange's equation (eq. (A1)). The derivation of equation (1) also involved the introduction of terms into the potential energy to allow for the presence of nonlinear lateral bolster springs, and these terms were different from those corresponding to the linear lateral bolster springs. The lateral model is further assumed to be uncoupled from the vertical model.

Energies of Lateral Model

Kinetic energy.- The kinetic energy of the ten-degree-of-freedom model shown in figure 13 is:

$$T_L = \frac{m}{2}\int_0^L \left[\dot{v}(x,t) + \dot{y}_c(t) - h_4\dot{\theta}_c(x,t) - \left(\frac{L}{2} - x\right)\dot{\eta}(t)\right]^2 dx$$

$$+ \frac{I_c}{2}\int_0^L \left[\dot{\theta}_c(x,t)\right]^2 dx + \frac{1}{2}M_g\left[\dot{y}_g(t)\right]^2 + \frac{1}{2}M_A\left[\dot{y}_{Ar}(t)\right]^2$$

$$+ \frac{1}{2}M_{Af}\left[\dot{y}_{Af}(t)\right]^2 + \frac{1}{2}I_{Ar}\left[\dot{\theta}_{Ar}(t)\right]^2 + \frac{1}{2}I_{Af}\left[\dot{\theta}_{Af}(t)\right]^2 \qquad \text{(B1)}$$

where I_c is the mass moment of inertia of the car cross section in roll about the section center of gravity. The lateral bending deformation of the car is given by

$$v(x,t) = b(t)\, W(x) \qquad \text{(B2)}$$

with $b(t)$ the generalized coordinate for the car and $W(x)$ the bending mode shape given by equations (A8) and (A9). Rigid-body roll and torsion of the car are contained in the following expression for $\theta_c(x,t)$:

$$\theta_c(x,t) = \theta_{c0}(t) + \theta_{c1}(t)\cos\frac{\pi x}{L} \qquad \text{(B3)}$$

Potential energy.- The general expression for the potential energy of the lateral model with linear springs may be written as

$$U_L = \frac{(EI)_L}{2}\int_0^L \left[\frac{\partial^2 v(x,t)}{\partial x^2}\right]^2 dx + \frac{GJ}{2}\int_0^L \left[\frac{\partial \theta_c(x,t)}{\partial x}\right]^2 dx$$

$$+ \frac{k_{\ell cr}}{2}\left[y_{Ar}(t) - y(d,t) - h_{2r}\theta_{Ar}(t) - h_3\theta_c(d,t)\right]^2$$

$$+ \frac{k_{\ell cf}}{2}\left[y_{Af}(t) - y(L-d,t) - h_{2f}\theta_{Af}(t) - h_3\theta_c(L-d,t)\right]^2$$

$$+ \frac{k_{\ell g}}{2}\left[y_g(t) - y\left(\frac{L}{2},t\right) - h_T\theta_c\left(\frac{L}{2},t\right)\right]^2$$

$$+ \frac{k_S}{4}\left\{\left[\frac{B}{2}\theta_c(d,t) - \frac{B}{2}\theta_{Ar}(t)\right]^2 + \left[-\frac{B}{2}\theta_c(d,t) + \frac{B}{2}\theta_{Ar}(t)\right]^2\right.$$

$$\left. + \left[\frac{B}{2}\theta_c(L-d,t) - \frac{B}{2}\theta_{Af}(t)\right]^2 + \left[-\frac{B}{2}\theta_c(L-d,t) + \frac{B}{2}\theta_{Af}(t)\right]^2\right\}$$

$$+ \frac{k_{Ar}}{4}\left\{\left[\frac{R}{2}\theta_{Ar}(t) - S_r(t) - \delta_r(t)\right]^2 + \left[-\frac{R}{2}\theta_{Ar}(t) - S_r(t)\right]^2\right\}$$

$$+ \frac{k_{Af}}{4}\left\{\left[\frac{R}{2}\theta_{Af}(t) - S_f(t) - \delta_f(t)\right]^2 + \left[-\frac{R}{2}\theta_{Af}(t) - S_f(t)\right]^2\right\}$$

$$+ \frac{k_{\ell r}}{2}\left[y_{Ar}(t) + h_{1r}\theta_{Ar}(t) - Y_r(t)\right]^2 + \frac{k_{\ell f}}{2}\left[y_{Af}(t) + h_{1f}\theta_{Af}(t) - Y_f(t)\right]^2$$

$$+ \frac{k_{\alpha r}}{2}\theta_{Ar}^2(t) + \frac{k_{\alpha f}}{2}\theta_{Af}^2(t) \qquad \text{(B4)}$$

The lateral and torsional displacements of the car at the trucks and the middle of the car are given by

$$\left.\begin{aligned}
&y(d,t) = v(d,t) + y_c(t) - \left(\frac{L}{2} - d\right)\eta(t) = b(t)\,W(d) + y_c(t) - \left(\frac{L}{2} - d\right)\eta(t)\\
&y(L-d,t) = v(L-d,t) + y_c(t) + \left(\frac{L}{2} - d\right)\eta(t) = b(t)\,W(L-d) + y_c(t) + \left(\frac{L}{2} - d\right)\eta(t)\\
&y\left(\frac{L}{2},t\right) = v\left(\frac{L}{2},t\right) + y_c(t) = b(t)\,W\left(\frac{L}{2}\right) + y_c(t)\\
&\theta_c(d,t) = \theta_{c0}(t) + \theta_{c1}(t)\cos\frac{\pi d}{L}\\
&\theta_c(L-d,t) = \theta_{c0}(t) + \theta_{c1}(t)\cos\frac{\pi(L-d)}{L}\\
&\theta_c\left(\frac{L}{2},t\right) = \theta_{c0}(t)
\end{aligned}\right\} \qquad \text{(B5)}$$

Substitution of equations (B2), (B3), and (B5) into equation (B4) gives the following expression for potential energy as a function of the generalized coordinates:

$$\begin{aligned}
U_L = {}& \frac{(EI)_L}{2}\int_0^L \left[b(t)\frac{d^2W(x)}{dx^2}\right]^2 dx + \frac{GJ}{2}\int_0^L \left[-\theta_{c1}(t)\frac{\pi}{L}\sin\frac{\pi x}{L}\right]^2 dx\\
&+ \frac{k_{lcr}}{2}\left[y_{Ar}(t) - b(t)\,W(d) - y_c(t) + \left(\frac{L}{2} - d\right)\eta(t) - h_{2r}\theta_{Ar}(t) - h_3\left(\theta_{c0}(t) + \theta_{c1}(t)\cos\frac{\pi d}{L}\right)\right]^2\\
&+ \frac{k_{lcf}}{2}\left\{y_{Af}(t) - b(t)\,W(L-d) - y_c(t) - \left(\frac{L}{2} - d\right)\eta(t) - h_{2f}\theta_{Af}(t) - h_3\left[\theta_{c0}(t) + \theta_{c1}(t)\cos\frac{\pi(L-d)}{L}\right]\right\}^2\\
&+ \frac{k_{lg}}{2}\left[y_g(t) - b(t)\,W\left(\frac{L}{2}\right) - y_c(t) - h_T\theta_{c0}(t)\right]^2\\
&+ \frac{k_s B^2}{8}\left\{\left[\theta_{c0}(t) + \theta_{c1}(t)\cos\frac{\pi d}{L} - \theta_{Ar}(t)\right]^2 + \left[\theta_{c0}(t) + \theta_{c1}(t)\cos\frac{\pi(L-d)}{L} - \theta_{Af}(t)\right]^2\right\}\\
&+ \frac{k_{Ar}}{4}\left\{\left[\frac{R}{2}\theta_{Ar}(t) - S_r(t) - \delta_r(t)\right]^2 + \left[\frac{R}{2}\theta_{Ar}(t) + S_r(t)\right]^2\right\}\\
&+ \frac{k_{Af}}{4}\left\{\left[\frac{R}{2}\theta_{Af}(t) - S_f(t) - \delta_f(t)\right]^2 + \left[\frac{R}{2}\theta_{Af}(t) + S_f(t)\right]^2\right\}\\
&+ \frac{k_{lr}}{2}\left[y_{Ar}(t) + h_{1r}\theta_{Ar}(t) - Y_r(t)\right]^2 + \frac{k_{lf}}{2}\left[y_{Af}(t) + h_{1f}\theta_{Af}(t) - Y_f(t)\right]^2 + \frac{k_{\alpha r}}{2}\theta_{Ar}^2(t) + \frac{k_{\alpha f}}{2}\theta_{Af}^2(t)
\end{aligned} \qquad \text{(B6)}$$

With nonlinearities allowed in the lateral bolster springs, k_{lcr} and k_{lcf} are no longer constant, and the potential energy terms associated with these variable spring constants must therefore be replaced. The replacement terms are derived by first defining a variable spring function $k(\xi)$ such that the restoring force is $k(\xi)\,\xi$, where ξ is the spring deformation. The work done by this force moving through a differential displacement $d\xi$ is $\left[k(\xi)\,\xi\right]d\xi$, and the potential energy developed in the spring stretched to some displacement Δy is then obtained from the integral

$$U_{NL} = \int_0^{\Delta y} \left[k(\xi)\,\xi\right] d\xi \tag{B7}$$

The displacement Δy is a function of the degrees of freedom of the system, and in this investigation, Δy is given by equations (15). Thus, the potential energy due to the nonlinear lateral bolster springs is

$$U_{NL} = \int_0^{\Delta y_r} \left[k_{lcr}(\xi)\,\xi\right] d\xi + \int_0^{\Delta y_f} \left[k_{lcf}(\xi)\,\xi\right] d\xi \tag{B8}$$

which replaces the second and third terms in equation (B6).

Dissipation energy.- The dissipation energy of the lateral model in terms of both viscous and structural damping constants is written as follows:

$$\begin{aligned}
D_L = {} & \frac{c_{lc}}{2}\left\{\left[\dot{y}_{Ar} - \dot{b}(t)\,W(d) - \dot{y}_c(t) + \left(\frac{L}{2} - d\right)\dot{\eta}(t) - h_{2r}\dot{\theta}_{Ar}(t) - h_3\left(\dot{\theta}_{c0}(t) + \dot{\theta}_{c1}(t)\cos\frac{\pi d}{L}\right)\right]^2\right. \\
& \left. + \left[\dot{y}_{Af}(t) - \dot{b}(t)\,W(L-d) - \dot{y}_c(t) - \left(\frac{L}{2} - d\right)\dot{\eta}(t) - h_{2f}\dot{\theta}_{Af}(t) - h_3\left(\dot{\theta}_{c0}(t) + \dot{\theta}_{c1}(t)\cos\frac{\pi(L-d)}{L}\right)\right]^2\right\} \\
& + \frac{c_{lg}}{2}\left[\dot{y}_g(t) - \dot{b}(t)\,W\left(\frac{L}{2}\right) - \dot{y}_c(t) - h_T\dot{\theta}_{c0}(t)\right]^2 \\
& + \frac{c_s B^2}{8}\left\{\left[\dot{\theta}_{c0}(t) + \dot{\theta}_{c1}\cos\frac{\pi d}{L} - \dot{\theta}_{Ar}(t)\right]^2 + \left[\dot{\theta}_{c0}(t) + \dot{\theta}_{c1}\cos\frac{\pi(L-d)}{L} - \dot{\theta}_{Af}(t)\right]^2\right\} \\
& + \frac{c_{Ar}}{4}\left\{\left[\frac{R}{2}\dot{\theta}_{Ar}(t) - \dot{S}_r(t) - \dot{\delta}_r(t)\right]^2 + \left[\frac{R}{2}\dot{\theta}_{Ar}(t) + \dot{S}_r(t)\right]^2\right\} \\
& + \frac{c_{Af}}{4}\left\{\left[\frac{R}{2}\dot{\theta}_{Af}(t) - \dot{S}_f(t) - \dot{\delta}_f(t)\right]^2 + \left[\frac{R}{2}\dot{\theta}_{Af}(t) + \dot{S}_f(t)\right]^2\right\} \\
& + \frac{c_{lr}}{2}\left[\dot{y}_{Ar}(t) + h_{1r}\dot{\theta}_{Ar}(t) - \dot{Y}_r(t)\right]^2 + \frac{c_{lf}}{2}\left[\dot{y}_{Af}(t) + h_{1f}\dot{\theta}_{Af}(t) - \dot{Y}_f(t)\right]^2 \\
& + \frac{c_{\alpha r}}{2}\dot{\theta}_{Ar}(t) + \frac{c_{\alpha f}}{2}\dot{\theta}_{Af}(t) + \frac{1}{2}\frac{g_{cl}}{\omega}(EI)_L\int_0^L\left[\dot{b}(t)\frac{d^2W(x)}{dx^2}\right]^2 dx \\
& + \frac{1}{2}\frac{g_{cT}}{\omega}GJ\int_0^L\left[-\dot{\theta}_{c1}(t)\frac{\pi}{L}\sin\frac{\pi x}{L}\right]^2 dx
\end{aligned} \tag{B9}$$

where g_{cl} is the structural damping coefficient of the car in lateral bending, and g_{cT} is the structural damping coefficient of the car in torsion. These coefficients have been introduced in the same manner as the bending structural damping coefficient of the car in the vertical model. (See appendix A.)

Matrix Elements of Mathematical Lateral Model

The elements of the square matrices of equations (1) and (4) were obtained by carrying out the indicated operations in Lagrange's equation for each degree of freedom in the lateral model in the same manner as for the vertical model in appendix A. For the nonlinear springs, the Lagrange operation $\frac{\partial U_{NL}}{\partial q_j}$ reduces the integrals in equation (B7) to functions of Δy; that is,

$$\frac{\partial U_{NL}}{\partial q_j} = \frac{\partial}{\partial q_j}\left\{\int_0^{\Delta y}\left[k(\xi)\ \xi\right]d\xi\right\} = \left[k(\Delta y)\ \Delta y\right]\frac{\partial(\Delta y)}{\partial q_j} \tag{B10}$$

Thus, the integrals in equation (B8) reduce to

$$\frac{\partial U_{NL}}{\partial q_j} = \left[k_{lcr}(\Delta y_r)\right](\Delta y_r)\frac{\partial(\Delta y_r)}{\partial q_j} + \left[k_{lcf}(\Delta y_f)\right](\Delta y_f)\frac{\partial(\Delta y_f)}{\partial q_j} \tag{B11}$$

where $q_j = b(t), y_c(t), \ldots \theta_{Af}(t)$. The elements of the stiffness matrix obtained from this operation for equation (1) are identical in form with those obtained for the linear springs on the basis of equation (B6).

Matrix elements for the lateral model are given in tables X to XII. Each matrix is symmetric about its principal diagonal. The mass matrices are given in table X, the upper matrix being for the general form of equation (1) and the lower matrix, for the frequency-domain form of equations (4). The stiffness and damping matrices are given in table XI for equation (1) and in table XII for equations (4), the upper matrices being the stiffness (K) matrices and the lower matrices the damping (C) matrices. The moment of inertia of the car per unit length about the car elastic axis is given by $I_{EA} = I_c + mh_4^2$. The matrix elements corresponding to equations (4) were obtained by dividing each equation by the car mass M_c (or mL) and sinusoidal input amplitude Q_o in a manner similar to that done for the vertical model in appendix A.

The rearward and forward lateral bolster spring constants (k_{lcr} and k_{lcf} in table XI) were kept equal throughout the investigation. However, the distinction between them is necessary when these springs are nonlinear, in order to relate the nonlinear

deflections properly to the motion throughout the system in accordance with equations (15) during the numerical integration of equation (1). Since there is no nonlinear damping in the system, $c_{lcr} = c_{lcf} = c_{lc}$ in the damping matrix of table XI.

The input matrices of equation (1) for the lateral model are

$$\{Q\} = \begin{Bmatrix} 0 \\ \cdot \\ \cdot \\ \cdot \\ 0 \\ k_{lr}Y_r(t) \\ k_{lf}Y_f(t) \\ k_{lr}h_{1r}Y_r(t) + \frac{k_{Ar}R}{4}\delta_r(t) \\ k_{lf}h_{1f}Y_f(t) + \frac{k_{Af}R}{4}\delta_f(t) \end{Bmatrix} \qquad \{\dot{Q}\} = \begin{Bmatrix} 0 \\ \cdot \\ \cdot \\ \cdot \\ 0 \\ c_{lr}\dot{Y}_r(t) \\ c_{lf}\dot{Y}_f(t) \\ c_{lr}h_{1r}\dot{Y}_r(t) + \frac{c_{Ar}R}{4}\dot{\delta}_r(t) \\ c_{lf}h_{1f}\dot{Y}_f(t) + \frac{c_{Af}R}{4}\dot{\delta}_f(t) \end{Bmatrix} \tag{B12}$$

Equations (4) were programed for either lateral or cross-level rail inputs, and the input amplitudes Y_{of} and δ_{of} to the forward trucks were chosen as reference displacements in defining the dimensionless degrees of freedom for the $\{\bar{q}_1\}$ and $\{\bar{q}_2\}$ matrices. The complete sinusoidal relations involving these input amplitudes are

$$\left.\begin{aligned} Y_f(t) &= Y_{of} \sin \omega t \\ \delta_f(t) &= \delta_{of} \sin \omega t \\ Y_r(t) &= Y_{of} \sin (\omega t + \kappa_1) \\ Y_f(t) &= \delta_{of} \sin (\omega t + \kappa_2) \end{aligned}\right\} \tag{B13}$$

where κ_1 and κ_2 are phase angles which, in this study, were each an integral multiple of π. Even multiples imply in-phase inputs to front and rear trucks, whereas odd multiples imply out-of-phase inputs. The quantity $\delta_r(t)$ or $\delta_f(t)$ represents the difference in vertical inputs to left and right rails under each set of trucks (see again fig. 13(b)) and completely defines the cross-level input. The quantities $S_r(t)$ and $S_f(t)$ disappear in the derivation of the equations of motion. The matrix elements for $\{\bar{q}_1\}$, $\{\bar{q}_2\}$, $\{Q_1\}$, and $\{Q_2\}$ for these inputs are as follows:

$$\left\{\bar{q}_1\right\} = \begin{Bmatrix} \frac{b_1}{Y_{of}} \\ \frac{y_{c1}}{Y_{of}} \\ \frac{\theta_{c01}{}^B}{Y_{of}} \\ \frac{\theta_{c11}{}^B}{Y_{of}} \\ \frac{\eta_1 L}{Y_{of}} \\ \frac{y_{g1}}{Y_{of}} \\ \frac{y_{Ar1}}{Y_{of}} \\ \vdots \\ \frac{\theta_{Af1}{}^R}{Y_{of}} \end{Bmatrix} \qquad \left\{\bar{q}_2\right\} = \begin{Bmatrix} \frac{b_2}{Y_{of}} \\ \frac{y_{c2}}{Y_{of}} \\ \frac{\theta_{c02}{}^B}{Y_{of}} \\ \frac{\theta_{c12}{}^B}{Y_{of}} \\ \frac{\eta_2 L}{Y_{of}} \\ \frac{y_{g2}}{Y_{of}} \\ \frac{y_{Ar2}}{Y_{of}} \\ \vdots \\ \frac{\theta_{Af2}{}^R}{Y_{of}} \end{Bmatrix} \qquad \text{(B14)}$$

$$\left\{Q_1\right\} = \begin{Bmatrix} 0 \\ \vdots \\ 0 \\ \omega_{lr}^2 \frac{M_{Ar}}{M_c} \frac{\sin(\omega t + \kappa_1)}{\sin \omega t} \\ \omega_{lf}^2 \frac{M_{Af}}{M_c} \\ \omega_{lr}^2 \frac{M_{Ar}}{M_c} \frac{h_{1r}}{R} \frac{\sin(\omega t + \kappa_1)}{\sin \omega t} \\ \omega_{lf}^2 \frac{M_{Af}}{M_c} \frac{h_{1f}}{R} \end{Bmatrix} \qquad \left\{Q_2\right\} = \begin{Bmatrix} 0 \\ \vdots \\ 0 \\ 2n_{lr}\omega_{lr} \frac{M_{Ar}}{M_c} \frac{\cos(\omega t + \kappa_2)}{\cos \omega t} \\ 2n_{lf}\omega_{lf} \frac{M_{Af}}{M_c} \\ 2n_{lr}\omega_{lr} \frac{M_{Ar}}{M_c} \frac{h_{1r}}{R} \frac{\cos(\omega t + \kappa_2)}{\cos \omega t} \\ 2n_{lf}\omega_{lf} \frac{M_{Af}}{M_c} \frac{h_{1f}}{R} \end{Bmatrix}$$

for the lateral rail input. The $\{\bar{q}_1\}$ and $\{\bar{q}_2\}$ matrices for the cross-level input are of the same form as those for the lateral input except that δ_{of} replaces Y_{of}. The cross-level input matrices are

$$\{Q_1\} = \begin{Bmatrix} 0 \\ \cdot \\ \cdot \\ \cdot \\ 0 \\ \omega_{Ar}^2 \dfrac{I_{Ar}}{M_c R^2} \dfrac{\sin(\omega t + \kappa_1)}{\sin \omega t} \\ \omega_{Af}^2 \dfrac{I_{Af}}{M_c R^2} \end{Bmatrix} \qquad \{Q_2\} = \begin{Bmatrix} 0 \\ \cdot \\ \cdot \\ \cdot \\ 0 \\ 2n_{Ar}\omega_{Ar} \dfrac{I_{Ar}}{M_c R^2} \dfrac{\cos(\omega t + \kappa_2)}{\cos \omega t} \\ 2n_{Af}\omega_{Af} \dfrac{I_{Af}}{M_c R^2} \end{Bmatrix} \tag{B15}$$

As in the case of the vertical model, the natural frequencies and viscous damping coefficients of the lateral model appearing throughout the matrix elements in tables X to XII and equations (B14) and (B15) are related to the spring and damping constants by the following expressions:

First lateral car bending frequency:

$$\omega_{lB} = (\beta_1 L)^2 \sqrt{\frac{(EI)_L}{M_c L^3}} \tag{B16a}$$

Lateral shear bolster rigid-body translation frequency:

$$\omega_{lc} = \sqrt{\frac{k_{lcr} + k_{lcf}}{M_c}} \tag{B16b}$$

Bolster rigid-body rolling frequency:

$$\omega_{oT} = B\sqrt{\frac{k_s}{2I_{EA}L}} \tag{B16c}$$

First torsional frequency of car:

$$\omega_T = \frac{\pi}{L}\sqrt{\frac{GJ}{I_{EA}}} \tag{B16d}$$

Lateral transformer frequency:

$$\omega_{lg} = \sqrt{\frac{k_{lg}}{M_g}} \tag{B16e}$$

Lateral equalizer frequency:

$$\omega_{l} = \sqrt{\frac{k_{l}}{M_A}} \tag{B16f}$$

Rear equalizer rolling frequency:

$$\omega_{Ar} = \frac{R}{2}\sqrt{\frac{k_{Ar}}{M_{Ar}}} \tag{B16g}$$

Front equalizer rolling frequency:

$$\omega_{Af} = \frac{R}{2}\sqrt{\frac{k_{Af}}{M_{Af}}} \tag{B16h}$$

Roll frequency of rear traction motor:

$$\omega_{\alpha r} = \sqrt{\frac{k_{\alpha r}}{I_{Ar}}} \tag{B16i}$$

Roll frequency of front traction motor:

$$\omega_{\alpha f} = \sqrt{\frac{k_{\alpha f}}{I_{Af}}} \tag{B16j}$$

Bolster lateral damping coefficient (for both sets of trucks):

$$n_{lc} = \frac{c_{lc}}{\omega_{lc} M_c} \tag{B16k}$$

Lateral transformer damping coefficient:

$$n_{lg} = \frac{c_{lg}}{2\omega_{lg} M_g} \tag{B16l}$$

Bolster rigid-body roll damping coefficient:

$$n_{oT} = \frac{c_s B^2}{4\omega_{oT} I_{EA} L} \tag{B16m}$$

Lateral shear equalizer damping coefficient:

$$n_l = \frac{c_l}{2\omega_l M_A} \tag{B16n}$$

Rear equalizer roll damping coefficient:

$$n_{Ar} = \frac{c_{Ar} R^2}{8\omega_{Ar} I_{Ar}} \tag{B16o}$$

Front equalizer roll damping coefficient:

$$n_{Af} = \frac{c_{Af} R^2}{8\omega_{Af} I_{Af}} \tag{B16p}$$

Roll damping coefficient of rear traction motor:

$$n_{\alpha r} = \frac{c_{\alpha r}}{2\omega_{\alpha r} I_{Ar}} \tag{B16q}$$

Roll damping coefficient of front traction motor:

$$n_{\alpha f} = \frac{c_{\alpha f}}{2\omega_{\alpha f} I_{Af}} \tag{B16r}$$

REFERENCES

1. Kaplan, A.; Koval, L. R.; and Choy, F., Jr.: Rail Vehicle Dynamics Analysis for High Speed Ground Transportation Roadbed Study. EM-17-22 (Contract C-353), TRW Systems, Sept. 1967.

2. Robinson, R. R.: Dynamic Simulation of Auto and Passenger Rail Transports (Dart Code). IITRI Project M6167, IIT Res. Inst., Jan. 1968.

3. Nelson, J. A.; and Hapemann, M. J.: A New Transit Propulsion Unit Suspension – Proved on Northeast Corridor High-Speed Test Cars. Trans. ASME, Ser. B.: J. Eng. Ind., vol. 91, no. 3, Aug. 1969, pp. 897-907.

4. Mixson, John S.; and Steiner, Roy: Optimization of a Simple Dynamic Model of a Railroad Car Under Random and Sinusoidal Inputs. Paper presented at ASME Annual Meeting "Symposium on Random Processes in Dynamical Problems" (Los Angeles, Calif.), Nov. 1969.

5. Sewall, John L.; Parrish, Russell V.; and Durling, Barbara J.; Rail Vehicle Dynamic Studies. Shock Vib. Bull., Bull. 40, Pt. 6, U.S. Dep. Def., Dec. 1969, pp. 109-126.

6. White, Ellis: Eastern Simulation Council Meeting. Simulation, vol. 12, no. 2, Feb. 1969, pp. 53-56.

7. Bendat, Julius S.; and Piersol, Allan G.: Measurement and Analysis of Random Data. John Wiley & Sons, Inc., c.1966.

8. Scanlan, Robert H.; and Rosenbaum, Robert: Introduction to the Study of Aircraft Vibration and Flutter. Macmillan Co., 1951.

9. Young, Dana; and Felgar, Robert P., Jr.: Tables of Characteristic Functions Representing Normal Modes of Vibration of a Beam. Publ. No. 4913, Eng. Res. Ser. No. 44, Bur. Eng. Res., Univ. of Texas, July 1, 1949.

10. Felgar, Robert P., Jr.: Formulas for Integrals Containing Characteristic Functions of a Vibrating Beam. Circ. No. 14, Bur. of Eng. Res., Univ. of Texas, 1950.

TABLE I.- PROPERTIES AND INPUTS FOR VERTICAL MODEL

(a) Fixed properties

Property	Value
Car length, L, m (in. or ft)	25.9 (1020 or 85)
Truck attachment distance, d, m (in. or ft)	3.81 (150 or 12.5)
Transformer weight, $M_g g$, N (lb)	57 800 (13 000)
Traction motor weight, $M_A g$, N (lb)	53 000 (11 908)
Bolster (car) rigid-body frequency, f_S, Hz	1.0

(b) Variable properties

Figure	Car weight, $M_c g$		Car bending frequency, f_B, Hz	Transformer frequency, f_g, Hz	Equalizer frequency, f_A, Hz	Car damping coefficient, g_{cv}	Bolster damping coefficient, n_S	Transformer damping coefficient, n_g	Equalizer damping coefficient, n_A	Input
	kN	lb								
3	574	129 000	8.0	6.0	4.12	0	0.11	0.25	0.10	Sinusoidal
4	574	129 000	8.0	Variable	4.12	0	.11	.18	.10	Sinusoidal
5	574	129 000	8.0	6.0	4.12	0	.11	Variable	.10	Sinusoidal
6	574	129 000	8.0	6.0	4.12	0	Variable	.25	.10	Sinusoidal
7	574	129 000	8.0	6.0	4.12	0	.11	.25	Variable	Sinusoidal
8	574	129 000	8.0	6.0	4.12	0	Variable	.25	.10	Random*
9	574	129 000	8.0	6.0	4.12	0	.30	.25	Variable	Random*
10	574	129 000	8.0	6.0	4.12	0	.30	.25	.30	Random*
11	574	129 000	Variable	5.0	4.12	Variable	.057	.18	.03	Sinusoidal
12	Variable	Variable	Variable	5.0	4.12	0	.057	.18	.03	Sinusoidal

*Spectral density given by equation (3).

TABLE II.- OPTIMUM PARAMETER VALUES

FOR TWO EQUALIZER FREQUENCIES

Parameter	Values for equalizer frequency, f_A, of –	
	4.12 Hz	5.53 Hz
Transformer frequency, f_g, Hz . .	6 (or 6.5)	6
Transformer damping, n_g.	0.25	0.18
Bolster damping, n_s.	0.11	0.057
Equalizer damping, n_A	0.10	0.10

TABLE III.- TRANSFER FUNCTIONS FOR LATERAL MODEL

Location	Acceleration transfer function
Car	$\frac{A_{cl}(x)}{gQ_o} = \frac{\omega^2}{g}\left\{\left[\bar{b}_1 W(x) + \bar{y}_{c1} - \frac{h_4}{B}\left(\bar{\theta}_{c01} + \bar{\theta}_{c11}\cos\frac{\pi x}{L}\right) - \frac{\frac{L}{2} - x}{L}\bar{\eta}_1\right]^2 + \left[\bar{b}_2 W(x) + \bar{y}_{c2} - \frac{h_4}{B}\left(\bar{\theta}_{c02} + \bar{\theta}_{c12}\cos\frac{\pi x}{L}\right) - \frac{\frac{L}{2} - x}{L}\bar{\eta}_2\right]^2\right\}^{1/2}$
Transformer	$\frac{A_{gl}}{gQ_o} = \frac{\omega^2}{g}\sqrt{\bar{y}_{g1}^2 + \bar{y}_{g2}^2}$
Traction motors	$\frac{A_{Af}}{gQ_o} = \frac{\omega^2}{g}\sqrt{\bar{y}_{Af1}^2 + \bar{y}_{Af2}^2}$ $\qquad$ $\frac{A_{Ar}}{gQ_o} = \frac{\omega^2}{g}\sqrt{\bar{y}_{Ar1}^2 + \bar{y}_{Ar}^2}$
In car over bolsters (vertical)	$\frac{A_{Bf}}{gQ_o} = \frac{\omega^2}{2g}\left\{\left[\bar{\theta}_{c01} + \bar{\theta}_{c11}\cos\frac{\pi(L-d)}{L}\right]^2 + \left[\bar{\theta}_{c02} + \bar{\theta}_{c12}\cos\frac{\pi(L-d)}{L}\right]^2\right\}^{1/2}$ $\frac{A_{Br}}{gQ_o} = \frac{\omega^2}{2g}\left[\left(\bar{\theta}_{c01} + \bar{\theta}_{c11}\cos\frac{\pi d}{L}\right)^2 + \left(\bar{\theta}_{c02} + \bar{\theta}_{c12}\cos\frac{\pi d}{L}\right)^2\right]^{1/2}$
Equalizers (vertical)	$\frac{A_{Ef}}{gQ_o} = \frac{\omega^2}{2g}\sqrt{\bar{\theta}_{Af1}^2 + \bar{\theta}_{Af2}^2}$ $\qquad$ $\frac{A_{Er}}{gQ_o} = \frac{\omega^2}{2g}\sqrt{\bar{\theta}_{Ar1}^2 + \bar{\theta}_{Ar2}^2}$

TABLE IV.- FIXED PROPERTIES FOR LATERAL MODEL

Property	Value
Car length, L, m (in. or ft)	25.9 (1 020 or 85)
Truck attachment distance, d, m (in. or ft)	3.81 (150 or 12.5)
Lateral distance between bolster springs, B, m (in.)	2.34 (92)
Lateral distance between equalizer springs, R, m (in.)	2.01 (79)
Distance of traction motor to lateral equalizer, h_{1r} and h_{1f}, m (in.)	0.534 (21)
Distance of traction motor to lateral bolster, h_{2r} and h_{2f}, m (in.)	0.305 (12)
Distance of lateral bolster to car elastic axis, h_3, m (in.)	0.305 (12)
Distance of lateral transformer to car elastic axis, h_T, m (in.)	0.305 (12)
Distance of car elastic axis to center of gravity, h_4, m (in.)	0.610 (24)
Center-to-center distance between truck axles, $(\Delta l)_t$, m (in.)	2.595 (102)
Transformer weight, $M_g g$, kN (lb)	57.8 (13 000)
Traction-motor weight, $M_{Ar}g$ and $M_{Af}g$, kN (lb)	53.0 (11 908)
Traction-motor mass moment of inertia, I_{Ar} and I_{Af}, kg-m^2 (in.-lb-sec^2)	2100 (18 600)
Lateral bolster spring constant, k_{lcr} and k_{lcf}, N/cm (lb/in.)	5 250 (3 000)
Vertical bolster spring constant, k_s, N/cm (lb/in.)	11 520 (6 570)
Lateral equalizer spring constant, k_{lr} and k_{lf}, N/cm (lb/in.)	7 000 (4 000)
Vertical equalizer spring constant*, k_{Ar} and k_{Af}, N/cm (lb/in.)	36 300 (20 680)
Lateral bolster frequency, f_{lc}, Hz	0.674
Bolster rolling frequency, f_{oT}, Hz	0.997
Lateral equalizer frequency, f_{lr} and f_{lf}, Hz	1.81
Equalizer rolling frequency, f_{Ar} and f_{Af}, Hz	6.62
Equalizer roll damping coefficient, n_{Ar} and n_{Af}	0.10
Traction-motor roll damping coefficient, $n_{\alpha r} = n_{\alpha f}$	0.60

*Total of four springs per truck at 9070 N/cm (5 170 lb/in.) each.

TABLE V.- VARIABLE PROPERTIES

Figure	Traction-motor rolling frequency, $f_{\alpha r} = f_{\alpha f}$, Hz	Car lateral bending frequency, $f_{\ell B}$, Hz	Car torsional frequency, f_T, Hz	Lateral transformer frequency, $f_{\ell g}$, Hz	Car weight, $M_c g$		Car mass moment of inertia per unit length, I_{EA}		Car structural damping coefficient in lateral bending, $g_{c\ell}$	Car structural damping coefficient in torsion, g_{cT}
					kN	lb	kg-m	lb-sec^2		
19	18.0	8.0	15.0	6.0	574	129000	3090	695	0	0
20, 21	Variable	8.0	15.0	6.0	574	129000	3090	695	0	0
22	18.0	Variable	15.0	6.0	574	129000	3090	695	Variable	0
23	18.0	8.0	Variable	6.0	574	129000	3090	695	0	Variable
24	18.0	Variable	Variable	6.0	Variable	Variable	Variable	Variable	0	0
25	18.0	8.0	15.0	Variable	574	129000	3090	695	0	0
26	18.0	8.0	15.0	6.0	574	129000	3090	695	0	0
27	18.0	8.0	15.0	6.0	574	129000	3090	695	Variable	Variable
28	18.0	8.0	15.0	6.0	574	129000	3090	695	0	0
29	18.0	8.0	15.0	6.0	574	129000	3090	695	0	Variable
30	18.0	8.0	15.0	6.0	574	129000	3090	695	0	0
31, 36	18.0	8.0	15.0	6.0	574	129000	3090	695	0	0
32	18.0	8.0	15.0	6.0	574	129000	3090	695	0	0
33	18.0	8.0	15.0	6.0	574	129000	3090	695	0	0
34	18.0	8.0	15.0	6.0	574	129000	3090	695	0	0
35	18.0	8.0	15.0	6.0	574	129000	3090	695	0	0
37	18.0	8.0	15.0	6.0	574	129000	3090	695	0	0
38	18.0	8.0	15.0	6.0	574	129000	3090	695	0	0
39	18.0	8.0	15.0	6.0	574	129000	3090	695	0	0

AND INPUTS FOR LATERAL MODEL

Lateral transformer damping coefficient, n_{lg}	Lateral bolster damping coefficient, n_{lc}	Bolster roll damping coefficient, n_{oT}	Lateral equalizer damping coefficient, $n_{lr} = n_{ll}$	Sinusoidal lateral input (fig. 15(a)) in-phase, out-of-phase: $\kappa_1 = 0$ or π	Sinusoidal cross-level input (fig. 15(a)) in-phase, out-of-phase: $\kappa_2 = 0$ or π	Transient and random inputs (figs. 15(b) to 15(g))
0.25	0.057	0.20	0.10	0	---	--------
.25	.057	.20	.10	0, --	--, π	--------
.25	.057	.20	.10	0	---	--------
.25	.057	.20	.10	π	π	--------
.25	.057	.20	.10	π	π	--------
.25	.057	.20	.10	0	---	--------
Variable	.057	.20	.10	0	---	--------
.25	Variable	.20	.10	0, π	---	--------
.25	.20	.20	Variable	0, π	---	--------
.25	.057	Variable	.10	---	0, π	--------
.25	Variable	Variable	.10	---	---	fig. 15(b)
.25	Variable	.20	.10	---	---	fig. 15(c)
.25	Variable	.20	.10	---	---	fig. 15(d)
.25	.057	.20	.10	---	---	fig. 15(d)
.25	.057	.20	.10	---	---	fig. 15(c), fig. 15(f)
.25	Variable	.20	.10	---	---	fig. 15(g)
.25	Variable	.20	.10	---	---	fig. 15(e)
.25	Variable	.20	.10	---	---	fig. 15(e)
.25	Variable	.20	.10	---	---	fig. 15(d)

TABLE VI.- ROOT-MEAN-SQUARE ACCELERATIONS FOR TWO DIFFERENT LATERAL RANDOM INPUTS TO LATERAL MODEL

Car location	RMS accelerations, g, for –	
	No. 3 Eastern U.S. railroad test track (fig. 37)	Combined input (fig. 35)
Rear trucks	0.0416	0.0342
Forward trucks	.0416	.0342
Middle of car	.0465	.0334

TABLE VII.- CAR BENDING MODE SHAPE

$\frac{x}{L}$	$W_1\left(\frac{x}{L}\right)$
0	2.000
.1	1.0743
.147	.6509
.2	.1954
.3	-.5440
.4	-1.040
.5	-1.2156
.6	-1.040
.7	-.5440
.8	.1954
.853	.6509
.9	1.0743
1.0	2.000

TABLE VIII.- MASS MATRIX FOR VERTICAL MODEL

	1	2	3	4
1	1	0	0	0
2	0	1	0	0
3	0	0	$\frac{M_g}{M_c}$	0
4	0	0	0	$2\frac{M_A}{M_c}$

TABLE IX.- STIFFNESS AND DAMPING MATRICES FOR VERTICAL MODEL, $\begin{bmatrix} K \\ C \end{bmatrix}$

[From table VII, $W(d) = W(L - d)$]

	1	2	3	4	
	$\omega_B^2 + \frac{\omega_s^2}{2}\left[W^2(d) + W^2(L-d)\right] + \omega_g^2 \frac{M_g}{M_c} W^2\left(\frac{L}{2}\right)$	$\frac{\omega_s^2}{2}\left[W(d) + W(L-d)\right] + \omega_g^2 \frac{M_g}{M_c} W\left(\frac{L}{2}\right)$	$-\omega_g^2 \frac{M_g}{M_c} W\left(\frac{L}{2}\right)$	$-\frac{\omega_s^2}{2}\left[W(d) + W(L-d)\right]$	1
		$\omega_s^2 + \omega_g^2 \frac{M_g}{M_c}$	$-\omega_g^2 \frac{M_g}{M_c}$	$-\omega_s^2$	2
			$\omega_g^2 \frac{M_g}{M_c}$	0	3
1	$n_s\omega_s\left[W^2(d) + W^2(L-d)\right] + 2n_g \frac{M_g}{M_c}\omega_g W^2\left(\frac{L}{2}\right) + g_{cv}\frac{\omega_B^2}{\omega}$				
				$\omega_s^2 + 2\frac{M_A}{M_c}\omega_A^2$	4
2	$n_s\omega_s\left[W(d) + W(L-d)\right] + 2n_g \frac{M_g}{M_c}\omega_g W\left(\frac{L}{2}\right)$	$2\left(n_s\omega_s + n_g \frac{M_g}{M_c}\omega_g\right)$			
3	$-2n_g \frac{M_g}{M_c}\omega_g W\left(\frac{L}{2}\right)$	$-2n_g \frac{M_g}{M_c}\omega_g$	$2n_g \frac{M_g}{M_c}\omega_g$		
4	$-n_s\omega_s\left[W(d) + W(L-d)\right]$	$-2n_s\omega_s$	0	$2\left(n_s\omega_s + 2n_A \frac{M_A}{M_c}\omega_A\right)$	

TABLE X.- MASS MATRICES FOR LATERAL MODEL, Eq. (1) / Eqs. (4)

$$\{*\} = -\left[\frac{\sinh \beta_1 L}{\beta_1^2 + \left(\frac{\pi}{L}\right)^2} + \frac{\sin \beta_1 L}{\beta_1^2 - \left(\frac{\pi}{L}\right)^2}\right] + \alpha_1 \left[\frac{\cosh \beta_1 L + 1}{\beta_1^2 + \left(\frac{\pi}{L}\right)^2} - \frac{\cos \beta_1 L + 1}{\beta_1^2 - \left(\frac{\pi}{L}\right)^2}\right]$$

	1	2	3	4	5	6	7	8	9	10	
	M_c	0	0	$-mh_4\beta_1\{*\}$	0—	—	—	—	—	→0	1
		M_c	$-M_c h_4$	0—	—	—	—	—	—	→	2
			$I_{EA}L$	0—	—	—	—	—	—	→	3
1	1			$I_{EA}\frac{L}{2}$	$2mh_4\left(\frac{L}{\pi}\right)^2$	0—	—	—	—	→	4
2	0	1			$\frac{M_c L^2}{12}$	0—	—	—	—	→	5
3	0	$-\frac{h_4}{B}$	$\frac{I_{EA}}{mB^2}$			M_g	0—	—	—	→	6
4	$-\frac{h_4\beta_1}{BL}\{*\}$	0	0	$\frac{I_{EA}}{2mB^2}$			M_{Ar}	0—	—	→	7
5	0			$2\frac{h_4}{B}\left(\frac{1}{\pi}\right)^2$	$\frac{1}{12}$			M_{Af}	0—	→	8
6				0	0	$\frac{M_g}{M_c}$			I_{Ar}	↓0	9
7						0	$\frac{M_{Ar}}{M_c}$			I_{Af}	10
8							0	$\frac{M_{Af}}{M_c}$			
9								0	$\frac{I_{Ar}}{M_c R^2}$		
10	↓0	↓	↓	↓	↓	↓	↓	↓	→0	$\frac{I_{Af}}{M_c R^2}$	

	1	2	3	4	5
	$(EI)_L \beta_1^4 L + k_{lcr} W^2(d) + k_{lcf} W^2(L-d) + k_{lg} W^2\left(\frac{L}{2}\right)$	$k_{lcr} W(d) + k_{lcf} W(L-d) + k_{lg} W\left(\frac{L}{2}\right)$	$h_3\left[k_{lcr} W(d) + k_{lcf} W(L-d)\right] + k_{lg} h_T W\left(\frac{L}{2}\right)$	$h_3\left[k_{lcr} W(d) \cos\frac{\pi d}{L} + k_{lcf} W(L-d) \cos\frac{\pi(L-d)}{L}\right]$	$\left(\frac{L}{2}-d\right)\left[-k_{lcr} W(d) + k_{lcf} W(L-d)\right]$
		$k_{lcr} + k_{lcf} + k_{lg}$	$h_3\left(k_{lcr} + k_{lcf}\right) + k_{lg} h_T$	$h_3\left[k_{lcr} \cos\frac{\pi d}{L} + k_{lcf} \cos\frac{\pi(L-d)}{L}\right]$	$\left(\frac{L}{2}-d\right)\left(-k_{lcr} + k_{lcf}\right)$
			$\frac{k_s B^2}{2} + h_3^2\left(k_{lcr} + k_{lcf}\right) + k_{lg} h_T^2$	$\frac{k_s B^2}{4}\left[\cos\frac{\pi d}{L} + \cos\frac{\pi(L-d)}{L}\right] + h_3^2\left[k_{lcr} \cos\frac{\pi d}{L} + k_{lcf} \cos\frac{\pi(L-d)}{L}\right]$	$h_3\left(\frac{L}{2}-d\right)\left(-k_{lcr} + k_{lcf}\right)$
1	$c_{lc}\left[W^2(d) + W^2(L-d)\right] + c_{lg} W^2\left(\frac{L}{2}\right)$			$\frac{k_s B^2}{4}\left[\cos^2\frac{\pi d}{L} + \cos^2\frac{\pi(L-d)}{L}\right] + h_3^2\left[k_{lcr}\cos^2\frac{\pi d}{L} + k_{lcf}\cos^2\frac{\pi(L-d)}{L}\right] + \frac{GJL}{2}\left(\frac{\pi}{L}\right)^2$	$h_3\left(\frac{L}{2}-d\right)\left[-k_{lcr}\cos\frac{\pi d}{L} + k_{lcf}\cos\frac{\pi(L-d)}{L}\right]$
2	$c_{lc}\left[W(d) + W(L-d)\right] + c_{lg} W\left(\frac{L}{2}\right)$	$2c_{lc} + c_{lg}$			$\left(\frac{L}{2}-d\right)^2\left(k_{lcr} + k_{lcf}\right)$
3	$h_3 c_{lc}\left[W(d) + W(L-d)\right] + h_T c_{lg} W\left(\frac{L}{2}\right)$	$2h_3 c_{lc} + h_T c_{lg}$	$\frac{c_s B^2}{2} + 2h_3^2 c_{lc} + h_T^2 c_{lg}$		
4	$h_3 c_{lc}\left[W(d)\cos\frac{\pi d}{L} + W(L-d)\cos\frac{\pi(L-d)}{L}\right]$	$h_3 c_{lc}\left[\cos\frac{\pi d}{L} + \cos\frac{\pi(L-d)}{L}\right]$	$\left(\frac{c_s B^2}{4} + h_3^2 c_{lc}\right)\left[\cos\frac{\pi d}{L} + \cos\frac{\pi(L-d)}{L}\right]$	$\left(\frac{c_s B^2}{4} + c_{lc} h_3^2\right)\left[\cos^2\frac{\pi d}{L} + \cos^2\frac{\pi(L-d)}{L}\right]$	
5	$c_{lc}\left(\frac{L}{2}-d\right)\left[-W(d) + W(L-d)\right]$	0	0	$h_3 c_{lc}\left(\frac{L}{2}-d\right)\left[-\cos\frac{\pi d}{L} + \cos\frac{\pi(L-d)}{L}\right]$	$2c_{lc}\left(\frac{L}{2}-d\right)^2$
6	$-c_{lg} W\left(\frac{L}{2}\right)$	$-c_{lg}$	$-c_{lg} h_T$	0	0
7	$-c_{lc} W(d)$	$-c_{lc}$	$-h_3 c_{lc}$	$-h_3 c_{lc}\cos\frac{\pi d}{L}$	$c_{lc}\left(\frac{L}{2}-d\right)$
8	$-c_{lcf} W(L-d)$	$-c_{lc}$	$-h_3 c_{lc}$	$-h_3 c_{lc}\cos\frac{\pi(L-d)}{L}$	$-c_{lc}\left(\frac{L}{2}-d\right)$
9	$h_{2r} c_{lc} W(d)$	$h_{2r} c_{lc}$	$-\left(\frac{c_s B^2}{4} - c_{lc} h_{2r} h_3\right)$	$-\left(\frac{c_s B^2}{4} - c_{lc} h_{2r} h_3\right)\cos\frac{\pi d}{L}$	$-c_{lc} h_{2r}\left(\frac{L}{2}-d\right)$
10	$h_{2f} c_{lc} W(L-d)$	$h_{2f} c_{lc}$	$-\left(\frac{c_s B^2}{4} - c_{lc} h_{2f} h_3\right)$	$-\left(\frac{c_s B^2}{4} - c_{lc} h_{2f} h_3\right)\cos\frac{\pi(L-d)}{L}$	$c_{lc} h_{2f}\left(\frac{L}{2}-d\right)$

MATRICES FOR LATERAL MODEL (EQ. (1)), $\begin{bmatrix} K \\ C \end{bmatrix}$

6	7	8	9	10	
$-k_{lg}W\left(\frac{L}{2}\right)$	$-k_{lcr}W(d)$	$-k_{lcf}W(L-d)$	$k_{lcr}h_{2r}W(d)$	$k_{lcf}h_{2f}W(L-d)$	1
$-k_{lg}$	$-k_{lcr}$	$-k_{lcf}$	$k_{lcr}h_{2r}$	$k_{lcf}h_{2f}$	2
$-k_{lg}h_T$	$-k_{lcr}h_3$	$-k_{lcf}h_3$	$-\left(\frac{k_sB^2}{4}-k_{lcr}h_{2r}h_3\right)$	$-\left(\frac{k_sB^2}{4}-k_{lcf}h_{2f}h_3\right)$	3
0	$-k_{lcr}h_3\cos\frac{\pi d}{L}$	$-k_{lcf}h_3\cos\frac{\pi(L-d)}{L}$	$-\left(\frac{k_sB^2}{4}-k_{lcr}h_{2r}h_3\right)\cos\frac{\pi d}{L}$	$-\left(\frac{k_sB^2}{4}-k_{lcf}h_{2f}h_3\right)\cos\frac{\pi(L-d)}{L}$	4
0	$k_{lcr}\left(\frac{L}{2}-d\right)$	$-k_{lcf}\left(\frac{L}{2}-d\right)$	$-k_{lcr}h_{2r}\left(\frac{L}{2}-d\right)$	$k_{lcf}h_{2f}\left(\frac{L}{2}-d\right)$	5
k_{lg}	0	0	0	0	6
	$k_{lr}+k_{lcr}$	0	$k_{lr}h_{1r}-k_{lcr}h_{2r}$	0	7
		$k_{lf}+k_{lcf}$	0	$k_{lf}h_{1f}-k_{lcf}h_{2f}$	8
c_{lg}			$\frac{k_sB^2}{4}+\frac{k_{Ar}R^2}{4}+k_{\alpha r}$ $+k_{lr}h_{1r}^2+k_{lcr}h_{2r}^2$	0	9
0	$c_{lr}+c_{lc}$			$\frac{k_sB^2}{4}+\frac{k_{Af}R^2}{4}+k_{\alpha f}$ $+k_{lf}h_{1f}^2+k_{lcf}h_{2f}^2$	10
0	0	$c_{lf}+c_{lc}$			
0	$c_{lr}h_{1r}-c_{lc}h_{2r}$	0	$\frac{c_sB^2}{4}+\frac{c_{Ar}R^2}{4}+c_{\alpha r}$ $+c_{lr}h_{1r}^2+c_{lc}h_{2r}^2$		
0	0	$c_{lf}h_{1f}-c_{lc}h_{2f}$	0	$\frac{c_sB^2}{4}+\frac{c_{Af}R^2}{4}+c_{\alpha f}$ $+c_{lf}h_{1f}^2+c_{lc}h_{2f}^2$	

	1	2	3	4	5
	$\omega_{lB}^2+\frac{\omega_{lc}^2}{2}\left[W^2(d)+W^2(L-d)\right]$ $+\omega_{lg}^2\frac{M_g}{M_c}W^2\left(\frac{L}{2}\right)$	$\frac{\omega_{lc}^2}{2}\left[W(d)+W(L-d)\right]$ $+\omega_{lg}^2\frac{M_g}{M_c}W\left(\frac{L}{2}\right)$	$\frac{\omega_{lc}^2 h_3}{2B}\left[W(d)+W(L-d)\right]$ $+\omega_{lg}^2\frac{M_g}{M_c}\frac{h_T}{B}W\left(\frac{L}{2}\right)$	$\frac{\omega_{lc}^2 h_3}{2B}\left[W(d)\cos\frac{\pi d}{L}$ $+W(L-d)\cos\frac{\pi(L-d)}{L}\right]$	$\frac{\omega_{lc}^2}{2}\left(\frac{\frac{L}{2}-d}{L}\right)\left[-W(d)+W(L-d)\right]$
		$\omega_{lc}^2+\omega_{lg}^2\frac{M_g}{M_c}$	$\omega_{lc}^2\frac{h_3}{B}+\omega_{lg}^2\frac{M_g}{M_c}\frac{h_T}{B}$	$\frac{\omega_{lc}^2}{2}\frac{h_3}{B}\left[\cos\frac{\pi d}{L}+\cos\frac{\pi(L-d)}{L}\right]$	0
			$\omega_{oT}^2\frac{I_{EA}}{mB^2}+\omega_{lc}^2\left(\frac{h_3}{B}\right)^2$ $+\omega_{lg}^2\left(\frac{h_T}{B}\right)^2\frac{M_g}{M_c}$	$\frac{1}{2}\left(\omega_{oT}^2\frac{I_{EA}}{mB^2}+\omega_{lc}^2\frac{h_3^2}{B^2}\right)\left[\cos\frac{\pi d}{L}$ $+\cos\frac{\pi(L-d)}{L}\right]$	0
1	$n_{lc}\omega_{lc}\left[W^2(d)+W^2(L-d)\right]$ $+2n_{lg}\omega_{lg}\frac{M_g}{M_c}W^2\left(\frac{L}{2}\right)+g_c l\frac{\omega_{lB}^2}{\omega}$			$\frac{\omega_T^2 I_{EA}}{2mB^2}+\frac{1}{2}\left(\omega_{oT}^2\frac{I_{EA}}{mB^2}\right.$ $\left.+\omega_{lc}^2\frac{h_3^2}{B^2}\right)\left[\cos^2\frac{\pi d}{L}+\cos^2\frac{\pi(L-d)}{L}\right]$	$\frac{\omega_{lc}^2}{2}\frac{h_3}{B}\left(\frac{\frac{L}{2}-d}{L}\right)\left[-\cos\frac{\pi d}{L}\right.$ $\left.+\cos\frac{\pi(L-d)}{L}\right]$
2	$n_{lc}\omega_{lc}\left[W(d)+W(L-d)\right]$ $+2n_{lg}\omega_{lg}\frac{M_g}{M_c}W\left(\frac{L}{2}\right)$	$2\left(n_{lc}\omega_{lc}+n_{lg}\omega_{lg}\frac{M_g}{M_c}\right)$			$\omega_{lc}^2\left(\frac{\frac{L}{2}-d}{L}\right)^2$
3	$n_{lc}\omega_{lc}\frac{h_3}{B}\left[W(d)+W(L-d)\right]$ $+2n_{lg}\omega_{lg}\frac{M_g}{M_c}\frac{h_T}{B}W\left(\frac{L}{2}\right)$	$2\left(n_{lc}\omega_{lc}\frac{h_3}{B}+n_{lg}\omega_{lg}\frac{M_g}{M_c}\frac{h_T}{B}\right)$	$2\left(n_{oT}\omega_{oT}\frac{I_{EA}}{mB^2}+n_{lc}\omega_{lc}\frac{h_3^2}{B^2}\right.$ $\left.+n_{lg}\omega_{lg}\frac{M_g}{M_c}\frac{h_T^2}{B^2}\right)$		
4	$n_{lc}\omega_{lc}\frac{h_3}{B}\left[W(d)\cos\frac{\pi d}{L}\right.$ $\left.+W(L-d)\cos\frac{\pi(L-d)}{L}\right]$	$n_{lc}\omega_{lc}\frac{h_3}{B}\left[\cos\frac{\pi d}{L}+\cos\frac{\pi(L-d)}{L}\right]$	$\left(n_{oT}\omega_{oT}\frac{I_{EA}}{mB^2}+n_{lc}\omega_{lc}\frac{h_3^2}{B^2}\right)\left[\cos\frac{\pi d}{L}\right.$ $\left.+\cos\frac{\pi(L-d)}{L}\right]$	$\left(n_{oT}\omega_{oT}\frac{I_{EA}}{mB^2}+n_{lc}\omega_{lc}\frac{h_3^2}{B^2}\right)\left[\cos^2\frac{\pi d}{L}\right.$ $\left.+\cos^2\frac{\pi(L-d)}{L}\right]+g_{cT}\frac{\omega_T^2}{\omega}\frac{I_{EA}}{2mB^2}$	
5	$n_{lc}\omega_{lc}\frac{\frac{L}{2}-d}{L}\left[-W(d)+W(L-d)\right]$	0	0	$n_{lc}\omega_{lc}\frac{h_3}{B}\left(\frac{\frac{L}{2}-d}{L}\right)\left[-\cos\frac{\pi d}{L}\right.$ $\left.+\cos\frac{\pi(L-d)}{L}\right]$	$2n_{lc}\omega_{lc}\left(\frac{\frac{L}{2}-d}{L}\right)^2$
6	$-2n_{lg}\omega_{lg}\frac{M_g}{M_c}W\left(\frac{L}{2}\right)$	$-2n_{lg}\omega_{lg}\frac{M_g}{M_c}$	$-2n_{lg}\omega_{lg}\frac{M_g}{M_c}\frac{h_T}{B}$	0	0
7	$-n_{lc}\omega_{lc}W(d)$	$-n_{lc}\omega_{lc}$	$-n_{lc}\omega_{lc}\frac{h_3}{B}$	$-n_{lc}\omega_{lc}\frac{h_3}{B}\cos\frac{\pi d}{L}$	$n_{lc}\omega_{lc}\left(\frac{\frac{L}{2}-d}{L}\right)$
8	$-n_{lc}\omega_{lc}W(L-d)$	$-n_{lc}\omega_{lc}$	$-n_{lc}\omega_{lc}\frac{h_3}{B}$	$-n_{lc}\omega_{lc}\frac{h_3}{B}\cos\frac{\pi(L-d)}{L}$	$-n_{lc}\omega_{lc}\left(\frac{\frac{L}{2}-d}{L}\right)$
9	$n_{lc}\omega_{lc}\frac{h_{2r}}{R}W(d)$	$n_{lc}\omega_{lc}\frac{h_{2r}}{R}$	$-\left(n_{oT}\omega_{oT}\frac{I_{EA}}{mBR}-n_{lc}\omega_{lc}\frac{h_{2r}h_3}{BR}\right)$	$-\left(n_{oT}\omega_{oT}\frac{I_{EA}}{mBR}\right.$ $\left.-n_{lc}\omega_{lc}\frac{h_{2r}h_3}{BR}\right)\cos\frac{\pi d}{L}$	$-n_{lc}\omega_{lc}\frac{h_{2r}}{R}\left(\frac{\frac{L}{2}-d}{L}\right)$
10	$n_{lc}\omega_{lc}\frac{h_{2f}}{R}W(L-d)$	$n_{lc}\omega_{lc}\frac{h_{2f}}{R}$	$-\left(n_{oT}\omega_{oT}\frac{I_{EA}}{mBR}-n_{lc}\omega_{lc}\frac{h_{2f}h_3}{BR}\right)$	$-\left(n_{oT}\omega_{oT}\frac{I_{EA}}{mBR}\right.$ $\left.-n_{lc}\omega_{lc}\frac{h_{2f}h_3}{BR}\right)\cos\frac{\pi(L-d)}{L}$	$n_{lc}\omega_{lc}\frac{h_{2f}}{R}\left(\frac{\frac{L}{2}-d}{L}\right)$

MODEL UNDERGOING SINUSOIDAL MOTION (EQS. (4)), $\frac{K}{C}$

6	7	8	9	10	
$-\omega_{lg}^2 \frac{M_g}{M_c} W\left(\frac{L}{2}\right)$	$-\frac{\omega_{lc}^2}{2} W(d)$	$-\frac{\omega_{lc}^2}{2} W(L-d)$	$\frac{\omega_{lc}^2}{2} \frac{h_{2r}}{R} W(d)$	$\frac{\omega_{lc}^2}{2} \frac{h_{2f}}{R} W(L-d)$	1
$-\omega_{lg}^2 \frac{M_g}{M_c}$	$-\frac{\omega_{lc}^2}{2}$	$-\frac{\omega_{lc}^2}{2}$	$\frac{\omega_{lc}^2 h_{2r}}{2R}$	$\frac{\omega_{lc}^2 h_{2f}}{2R}$	2
$-\omega_{lg}^2 \frac{M_g}{M_c} \frac{h_T}{B}$	$-\frac{\omega_{lc}^2 h_3}{2B}$	$-\frac{\omega_{lc}^2 h_3}{2B}$	$-\frac{1}{2}\left(\omega_{oT}^2 \frac{I_{EA}}{mBR} - \omega_{lc}^2 \frac{h_{2r} h_3}{BR}\right)$	$-\frac{1}{2}\left(\omega_{oT}^2 \frac{I_{EA}}{mBR} - \omega_{lc}^2 \frac{h_{2f} h_3}{BR}\right)$	3
0	$-\frac{\omega_{lc}^2}{2} \frac{h_3}{B} \cos \frac{\pi d}{L}$	$-\frac{\omega_{lc}^2}{2} \frac{h_3}{B} \cos \frac{\pi(L-d)}{L}$	$-\frac{1}{2}\left(\omega_{oT}^2 \frac{I_{EA}}{mBR} - \omega_{lc}^2 \frac{h_{2r} h_3}{BR}\right) \cos \frac{\pi d}{L}$	$-\frac{1}{2}\left(\omega_{oT}^2 \frac{I_{EA}}{mBR} - \omega_{lc}^2 \frac{h_{2f} h_3}{BR}\right) \cos \frac{\pi(L-d)}{L}$	4
0	$\frac{\omega_{lc}^2}{2}\left(\frac{\frac{L}{2}-d}{L}\right)$	$-\frac{\omega_{lc}^2}{2}\left(\frac{\frac{L}{2}-d}{L}\right)$	$-\frac{\omega_{lc}^2 h_{2r}}{2R}\left(\frac{\frac{L}{2}-d}{L}\right)$	$\frac{\omega_{lc}^2 h_{2f}}{2R}\left(\frac{\frac{L}{2}-d}{L}\right)$	5
$\omega_{lg}^2 \frac{M_g}{M_c}$	0	0	0	0	6
	$\omega_{lr}^2 \frac{M_{Ar}}{M_c} + \frac{\omega_{lc}^2}{2}$	0	$\omega_{lr}^2 \frac{M_{Ar}}{M_c} \frac{h_{1r}}{R} - \frac{\omega_{lc}^2 h_{2r}}{2R}$	0	7
		$\omega_{lf}^2 \frac{M_{Af}}{M_c} + \frac{\omega_{lc}^2}{2}$	0	$\omega_{lf}^2 \frac{M_{Af}}{M_c} \frac{h_{1f}}{R} - \frac{\omega_{lc}^2 h_{2f}}{2R}$	8
$2n_{lg}\omega_{lg}\frac{M_g}{M_c}$			$\frac{\omega_{oT}^2 I_{EA}}{2mR^2} + \left(\omega_{Ar}^2 + \omega_{\sigma r}^2\right)\frac{I_{Ar}}{M_c R^2}$ $+\omega_{lr}^2 \frac{M_{Ar}}{M_c}\left(\frac{h_{1r}}{R}\right)^2 + \frac{\omega_{lc}^2}{2}\left(\frac{h_{2r}}{R}\right)^2$	0	9
0	$2n_{lr}\omega_{lr}\frac{M_{Ar}}{M_c} + n_{lc}\omega_{lc}$			$\frac{\omega_{oT}^2 I_{EA}}{2mR^2} + \left(\omega_{Af}^2 + \omega_{\sigma f}^2\right)\frac{I_{Af}}{M_c R^2}$ $+\omega_{lf}^2 \frac{M_{Af}}{M_c}\left(\frac{h_{1f}}{R}\right)^2 + \frac{\omega_{lc}^2}{2}\left(\frac{h_{2f}}{R}\right)^2$	10
0	0	$2n_{lf}\omega_{lf}\frac{M_{Af}}{M_c} + n_{lc}\omega_{lc}$			
0	$2n_{lr}\omega_{lr}\frac{M_{Ar}}{M_c}\frac{h_{1r}}{R} - n_{lc}\omega_{lc}\frac{h_{2r}}{R}$	0	$n_{oT}\omega_{oT}\frac{I_{EA}}{mR^2} + 2\left(n_{Ar}\omega_{Ar}\right.$ $\left.+ n_{\sigma r}\omega_{\sigma r}\right)\frac{I_{Ar}}{M_c R^2} + 2n_{lr}\omega_{lr}\frac{M_{Ar}}{M_c}\left(\frac{h_{1r}}{R}\right)^2$ $+ n_{lc}\omega_{lc}\left(\frac{h_{2r}}{R}\right)^2$		
0	0	$2n_{lf}\omega_{lf}\frac{M_{Af}}{M_c}\frac{h_{1f}}{R} - n_{lc}\omega_{lc}\frac{h_{2f}}{R}$	0	$n_{oT}\omega_{oT}\frac{I_{EA}}{mR^2} + 2\left(n_{Af}\omega_{Af}\right.$ $\left.+ n_{\sigma f}\omega_{\sigma f}\right)\frac{I_{Af}}{M_c R^2} + 2n_{lf}\omega_{lf}\frac{M_{Af}}{M_c}\left(\frac{h_{1f}}{R}\right)^2$ $+ n_{lc}\omega_{lc}\left(\frac{h_{2f}}{R}\right)^2$	

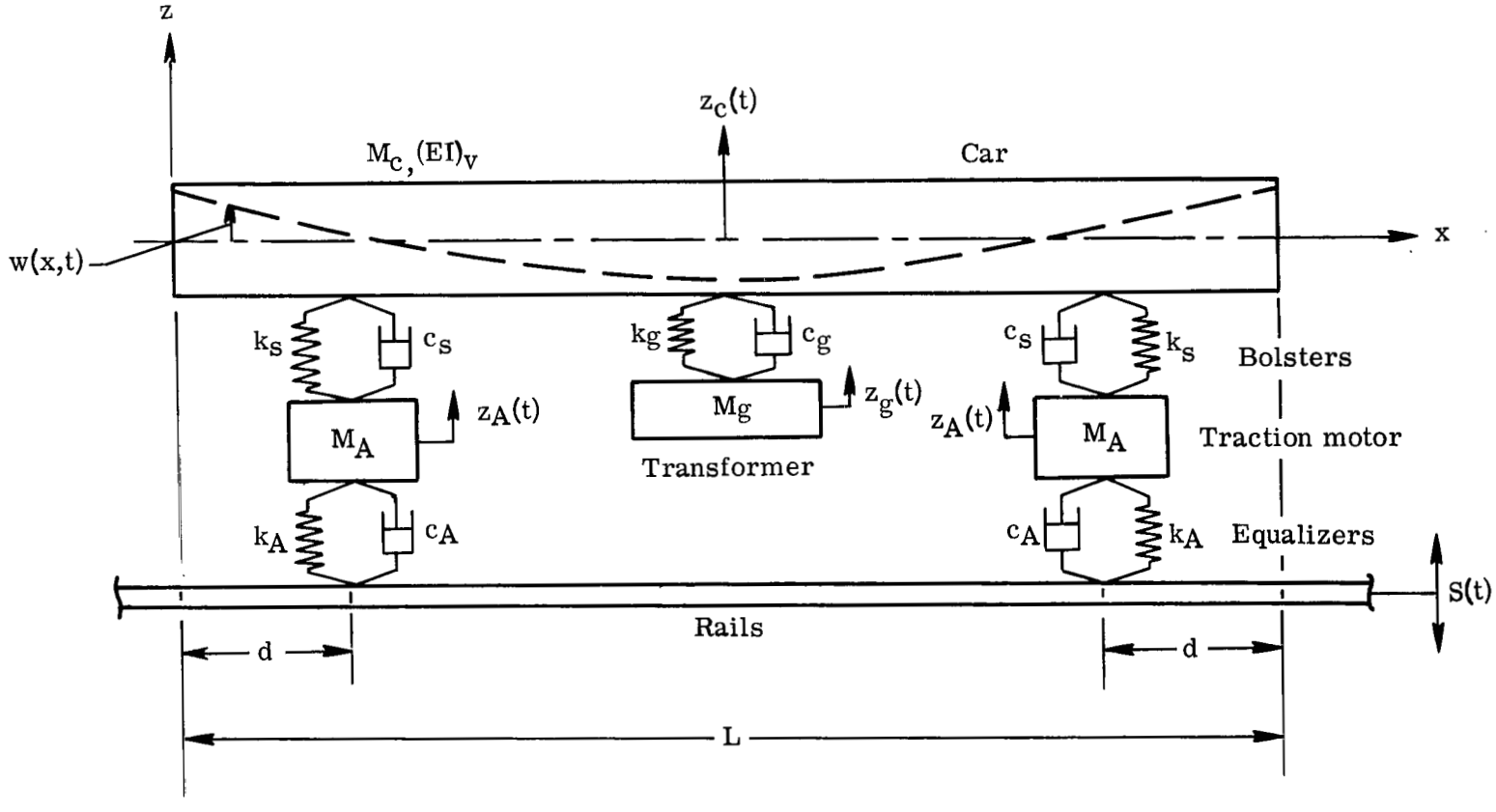

Figure 1.- Mathematical vertical model of railroad car and truck suspension.

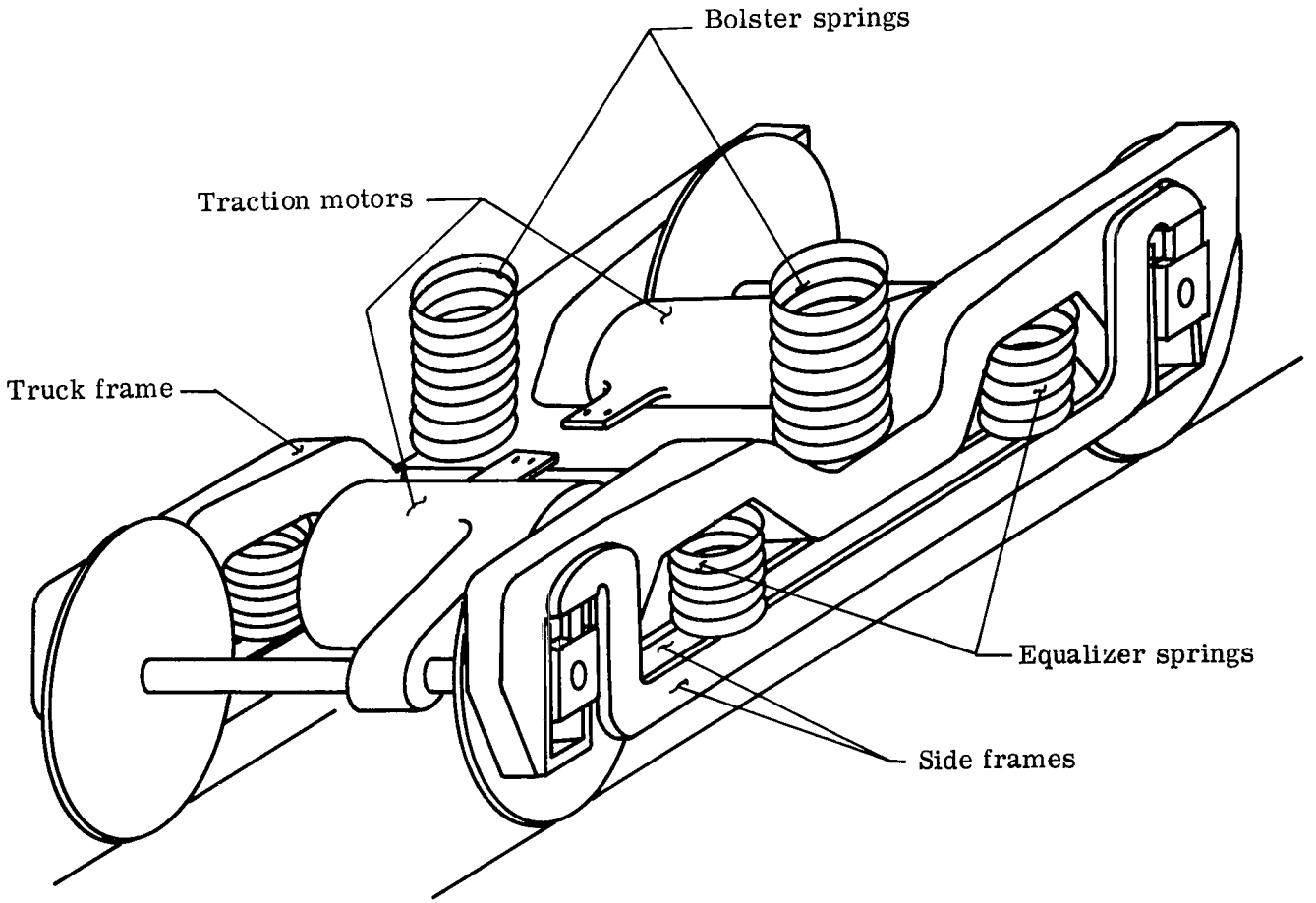

Figure 2.- Schematic view of truck suspension system.

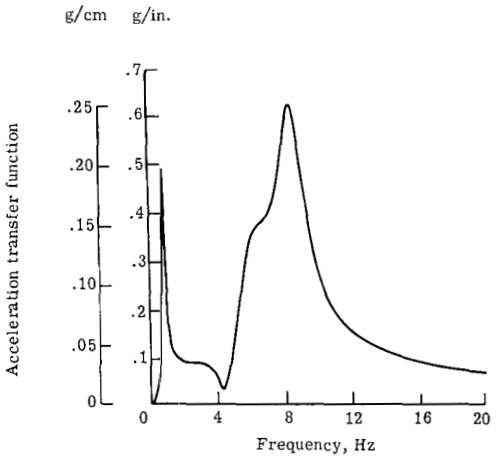

(a) End of car.

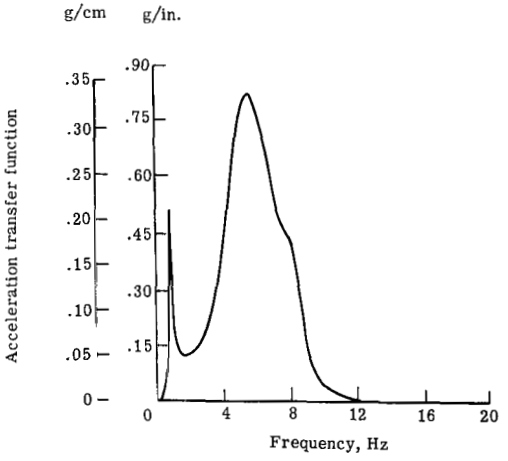

(c) Transformer.

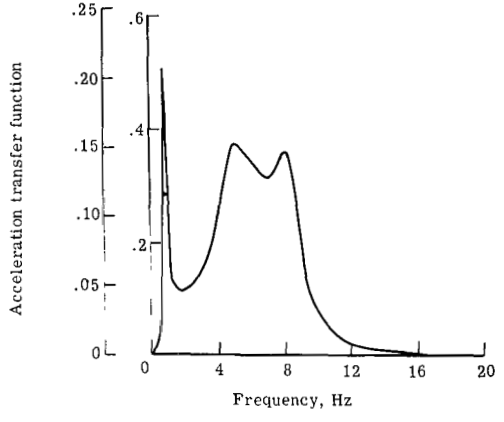

(b) Middle of car.

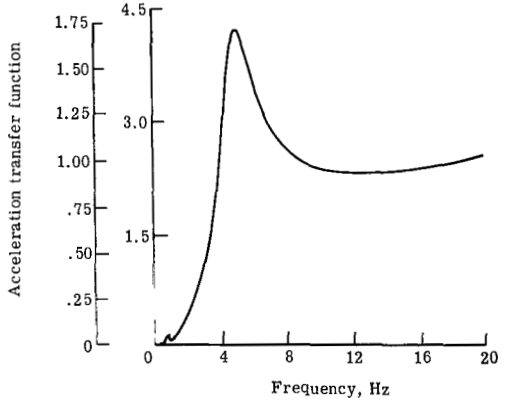

(d) Traction motors.

Figure 3.- Acceleration transfer functions for optimized vertical model.

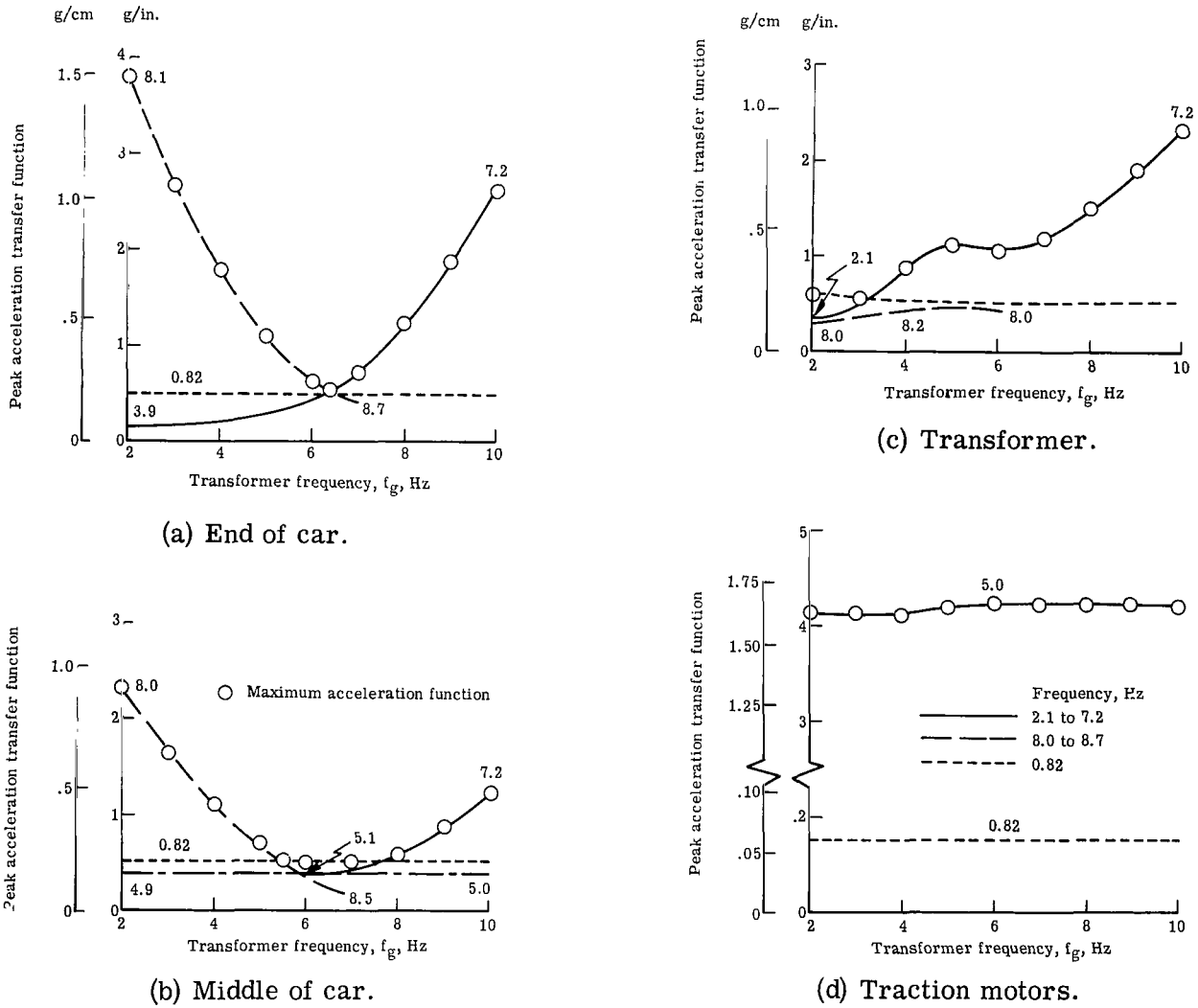

Figure 4.- Effects of vertical transformer frequency on acceleration transfer functions for vertical model with first equalizer spring $(f_A = 4.12$ Hz$)$. Numbers beside curves are frequencies of peak acceleration transfer functions.

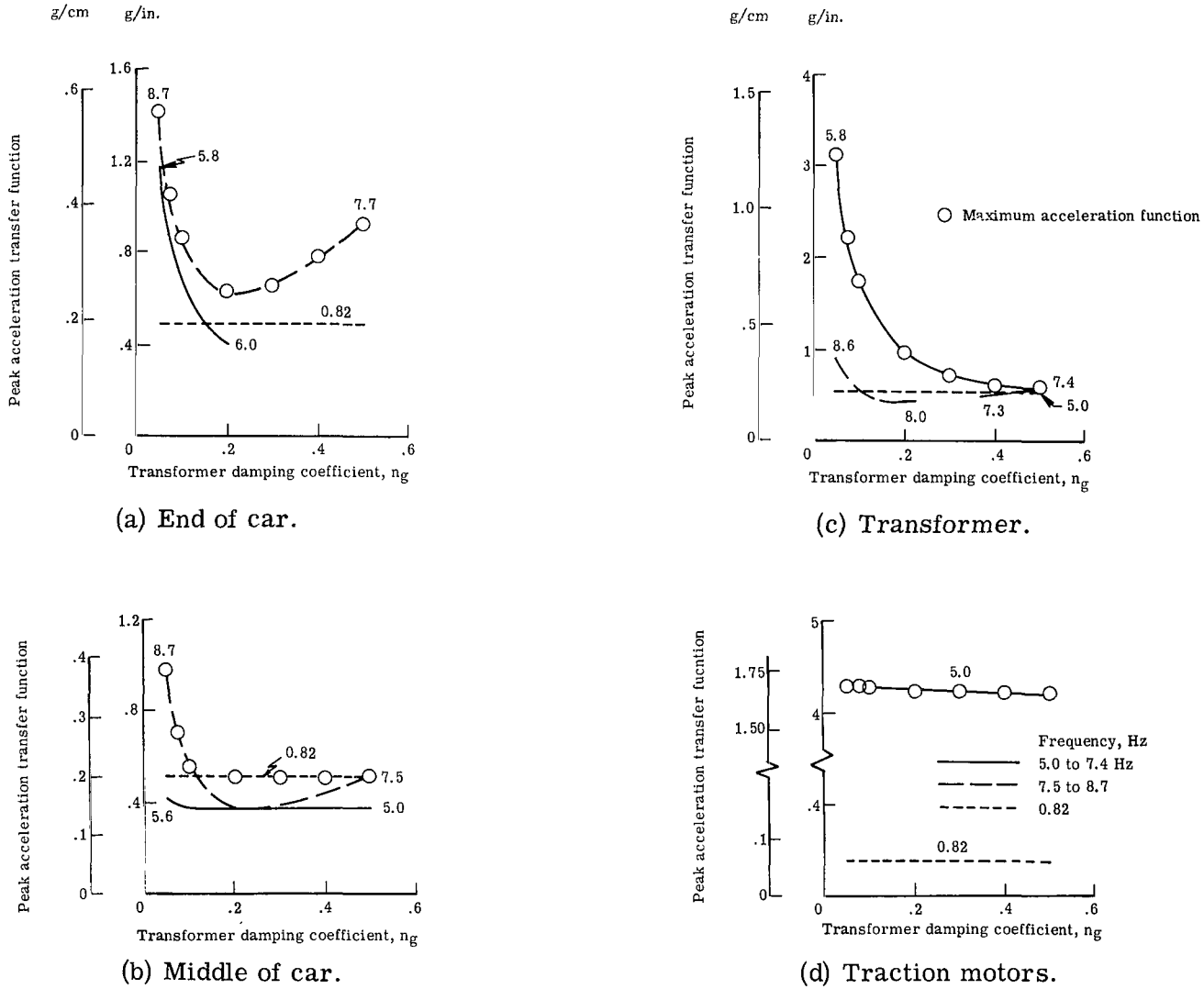

Figure 5.- Effects of vertical transformer damping coefficient on acceleration transfer functions for vertical model with first equalizer spring (f_A = 4.12 Hz). Numbers beside curves are frequencies of peak acceleration transfer functions.

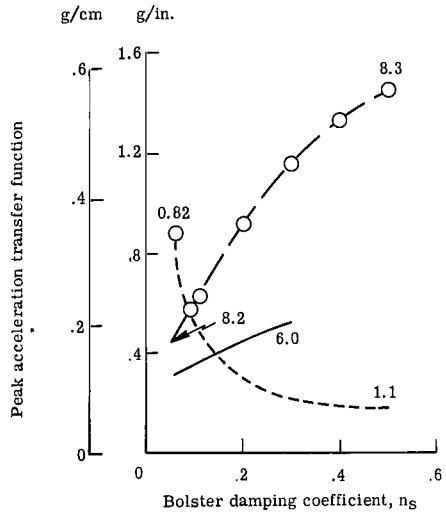

(a) End of car.

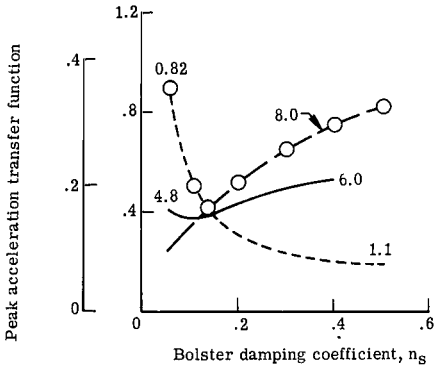

(b) Middle of car.

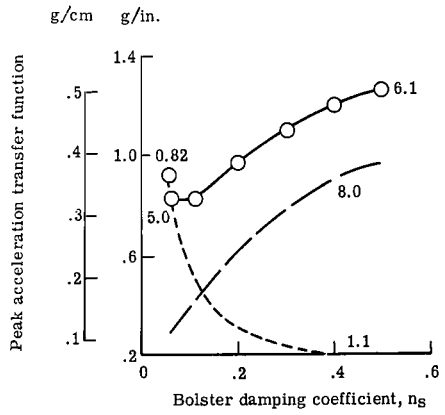

(c) Transformer.

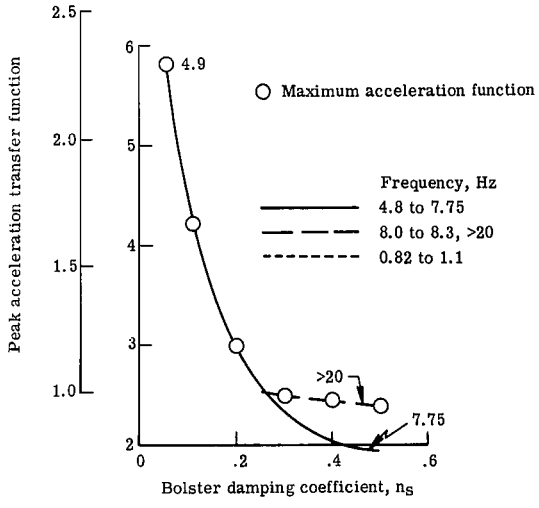

(d) Traction motors.

Figure 6.- Effects of vertical bolster damping coefficient on acceleration transfer functions for vertical model with first equalizer spring $(f_A = 4.12$ Hz$)$. Numbers beside curves are frequencies of peak acceleration transfer functions.

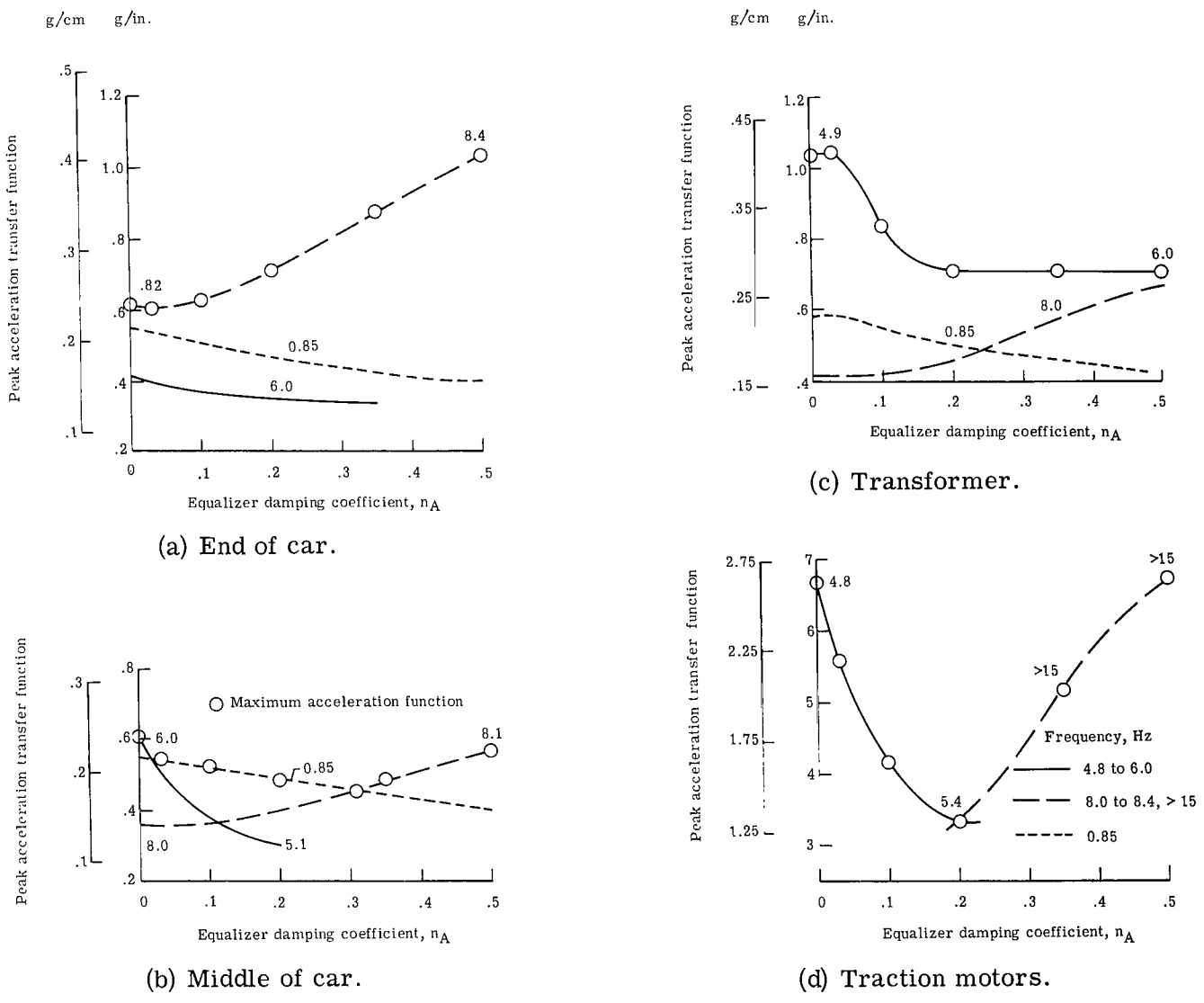

Figure 7.- Effects of vertical equalizer damping coefficient on acceleration transfer functions for vertical model with first equalizer spring (f_A = 4.12 Hz). Numbers beside curves are frequencies of peak acceleration transfer functions.

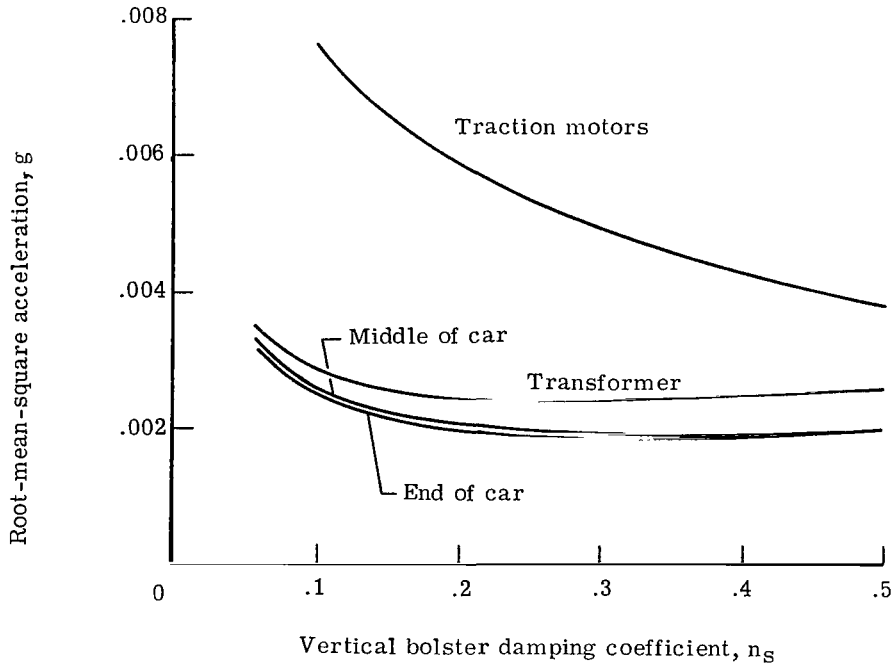

Figure 8.- Effects of vertical bolster damping coefficient acceleration root-mean-square values for vertical model with first equalizer spring $\left(f_A = 4.12 \text{ Hz}\right)$.

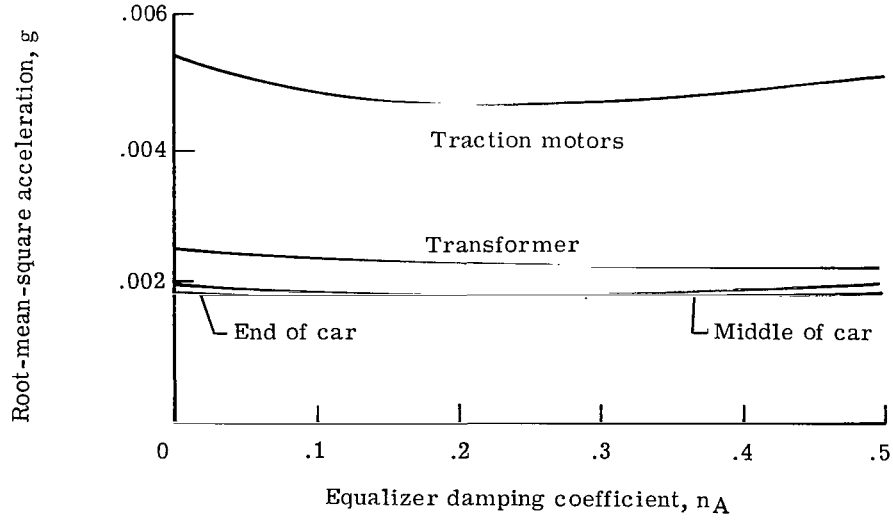

Figure 9.- Effects of vertical equalizer damping coefficient on acceleration root-mean-square values for vertical model with first equalizer spring $\left(f_A = 4.12 \text{ Hz}\right)$.

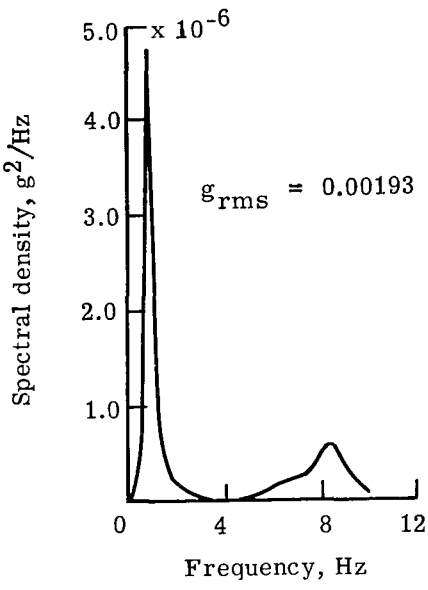

(a) End of car

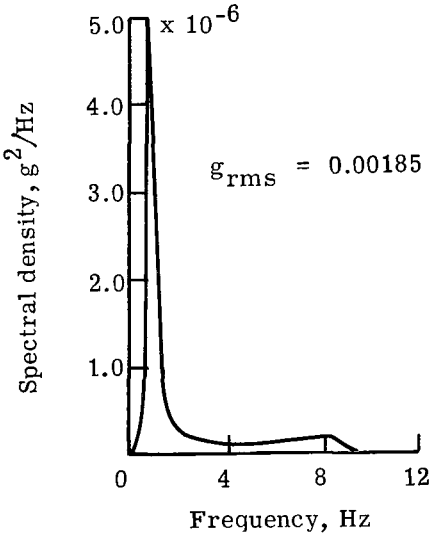

(b) Middle of car.

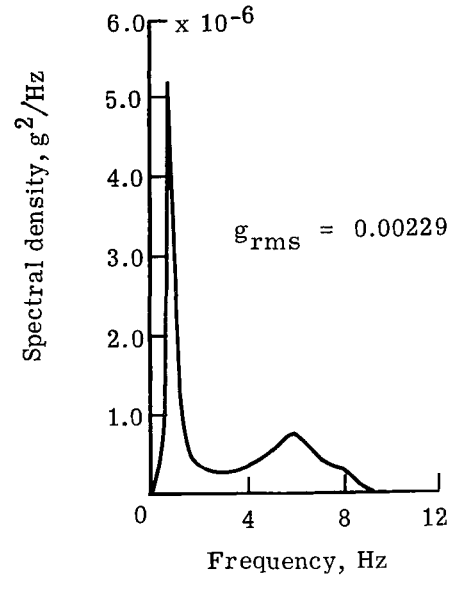

(c) Transformer.

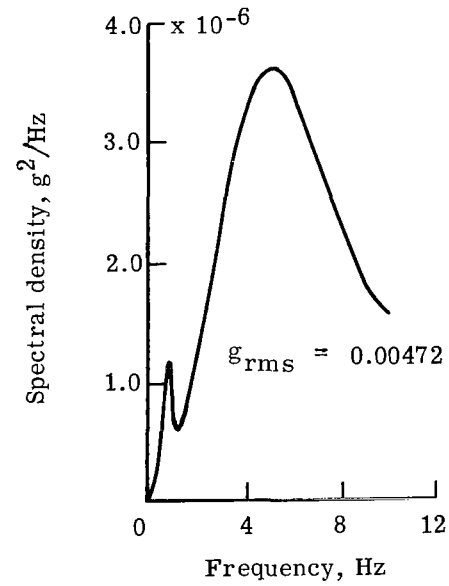

(d) Traction motors.

Figure 10.- Optimum root-mean-square accelerations due to random input for vertical model.

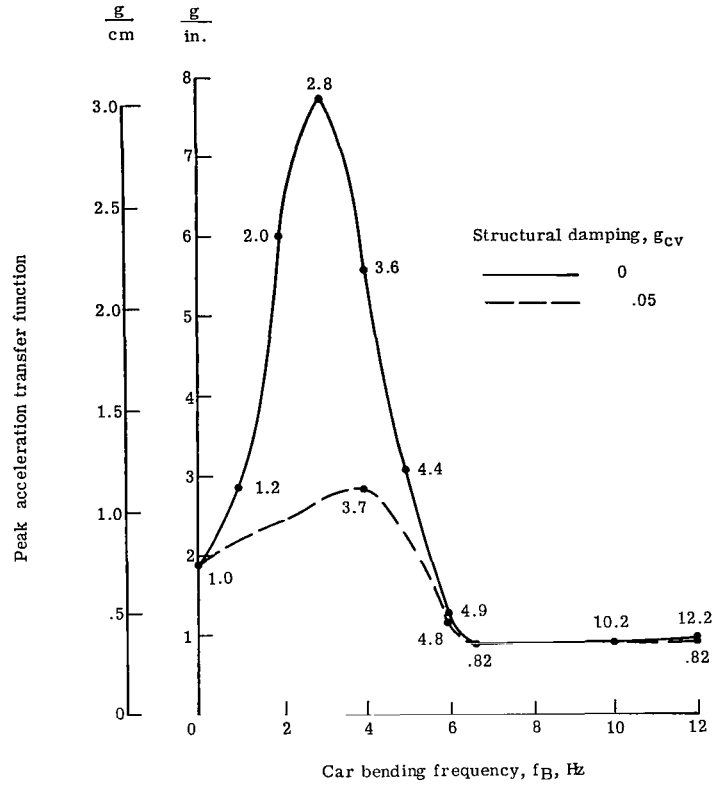

(a) End of car.

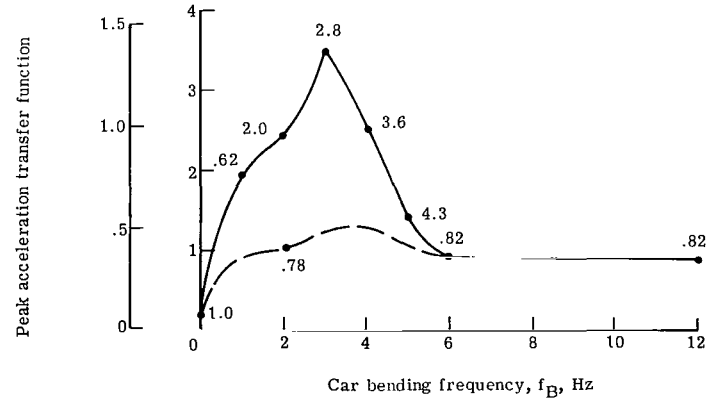

(b) Middle of car.

Figure 11.- Effect of car vertical bending frequency and structural damping on car vertical peak acceleration transfer functions for first equalizer spring (f_A = 4.12 Hz). Numbers beside curves are frequencies of peak acceleration transfer functions.

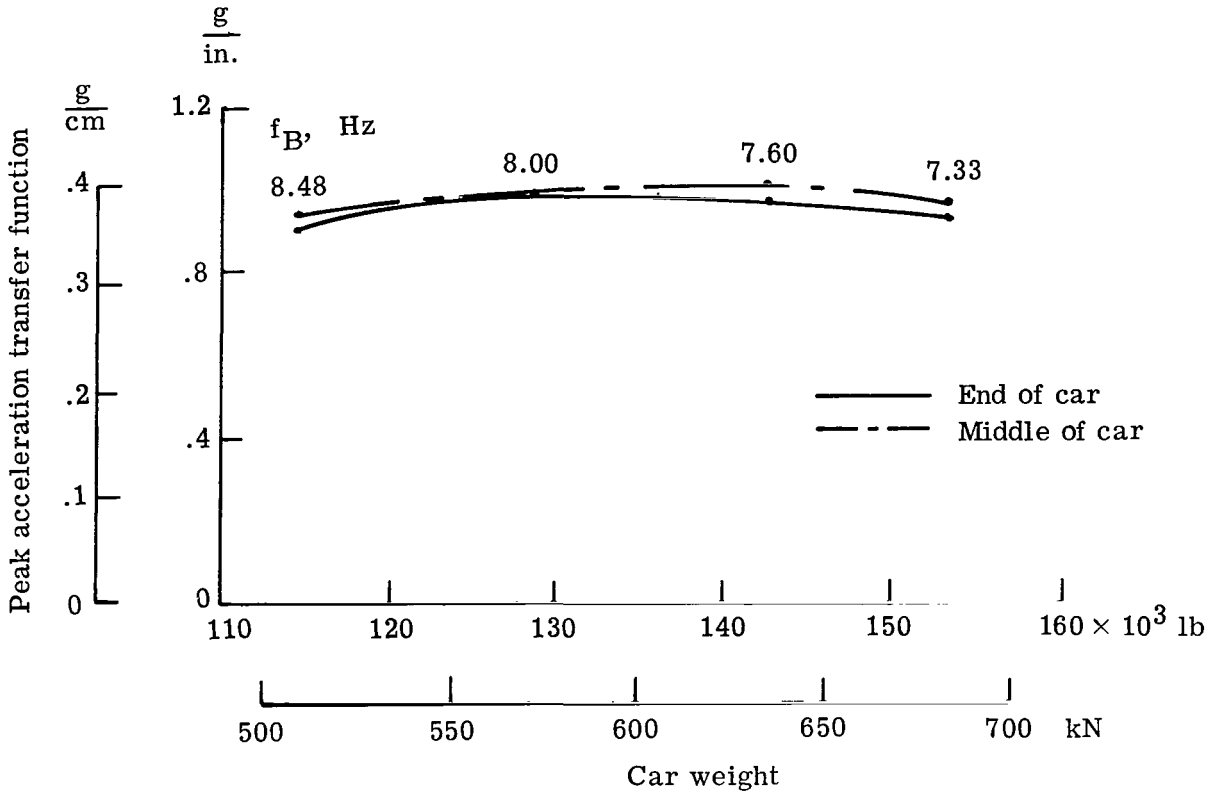

Figure 12.- Effects of car weight on vertical peak acceleration transfer function for first equalizer spring $(f_A = 4.12$ Hz$)$ at peak frequencies of about 0.8 Hz.

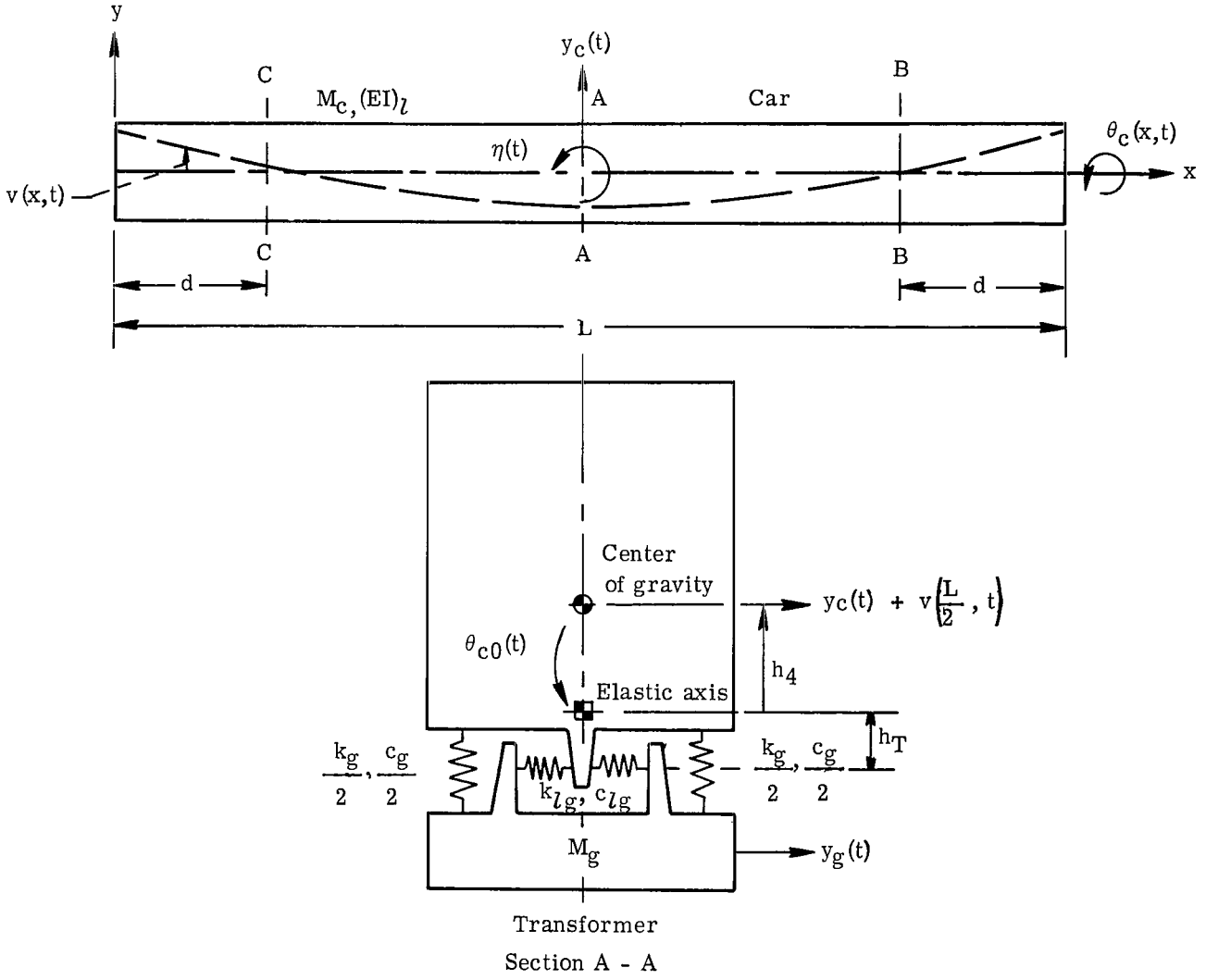

(a) Top and mid-section views.

Figure 13.- Mathematical lateral model of railroad car and truck suspension, with sections A-A, B-B, and C-C viewed from front of car (x = L).

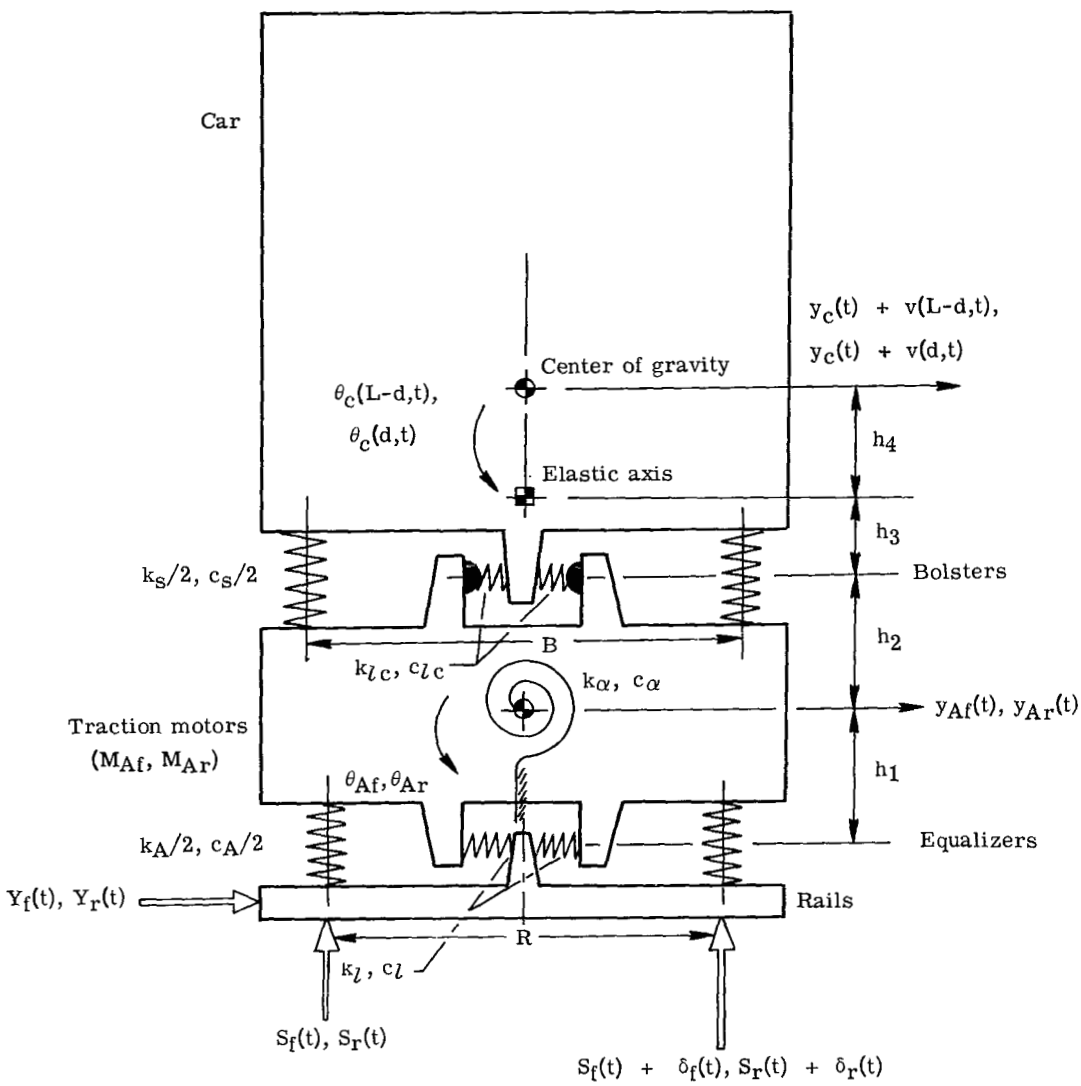

(b) Truck suspension (sections B-B, C-C).

Figure 13.- Concluded.

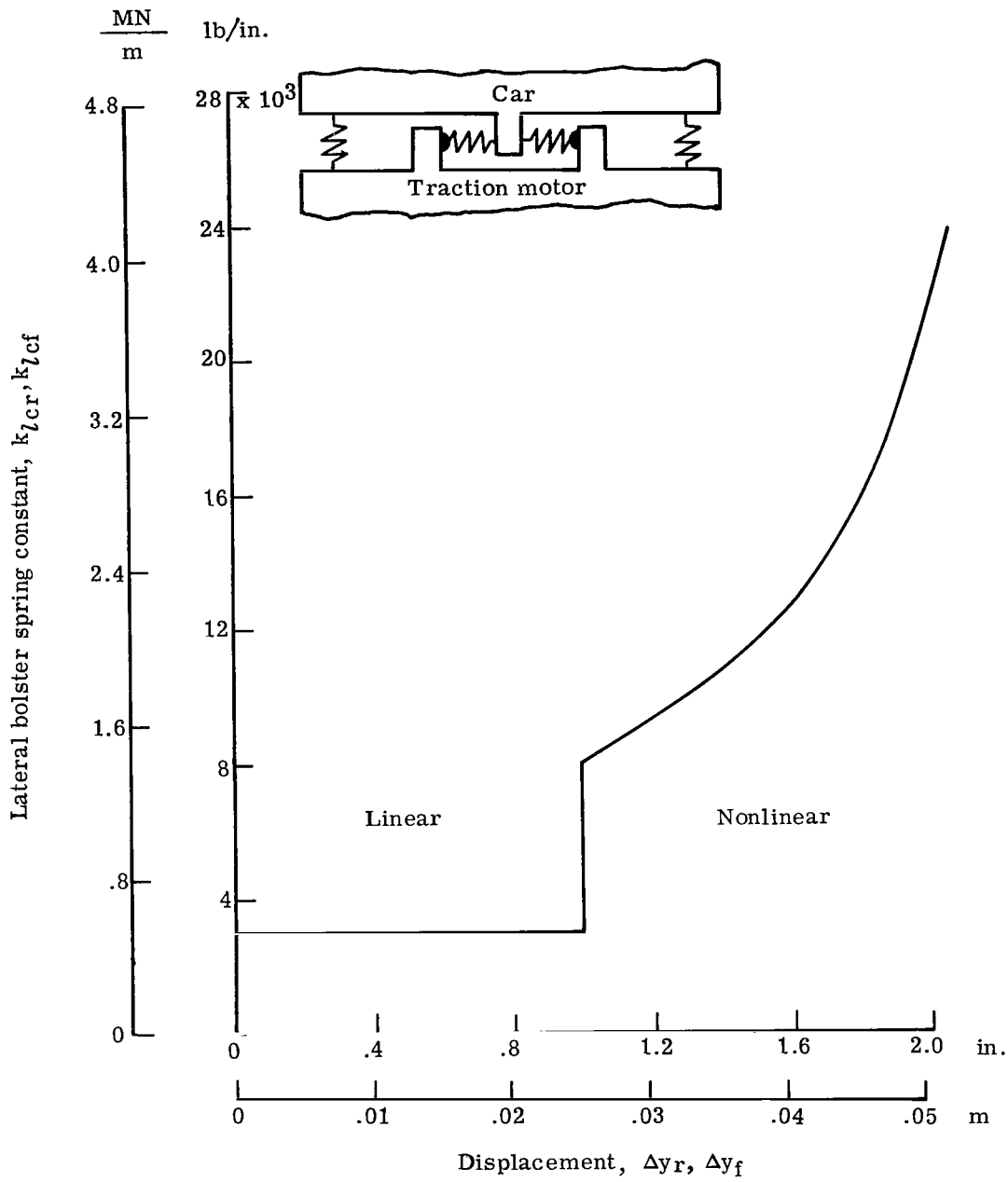

Figure 14.- Nonlinear lateral spring functions. k is an even function of Δy.

Deterministic

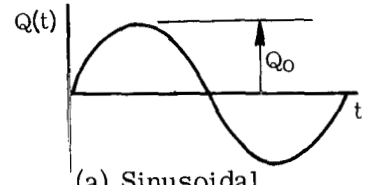

(a) Sinusoidal.

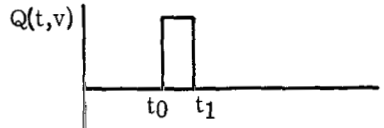

(b) Square pulse.

(c) Square pulse train.

(d) Wave pulse.

Random

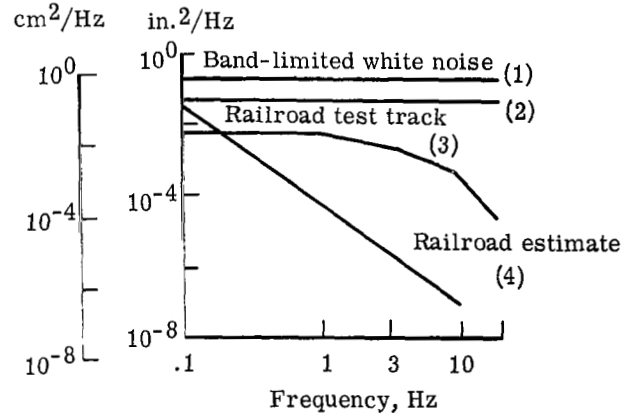

(e) Input spectral densities.

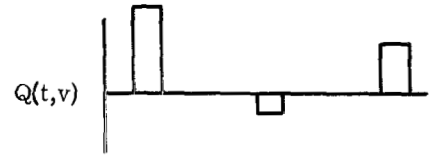

(f) Random pulse train.

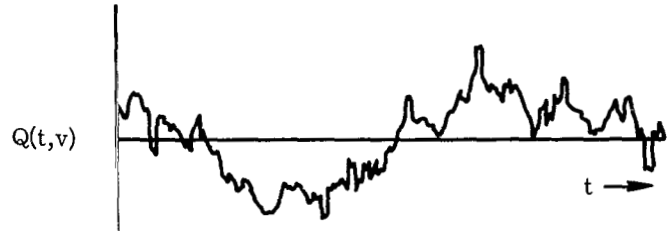

(g) Combined railroad estimate (4) and random pulse train.

Figure 15.- Forward truck inputs.

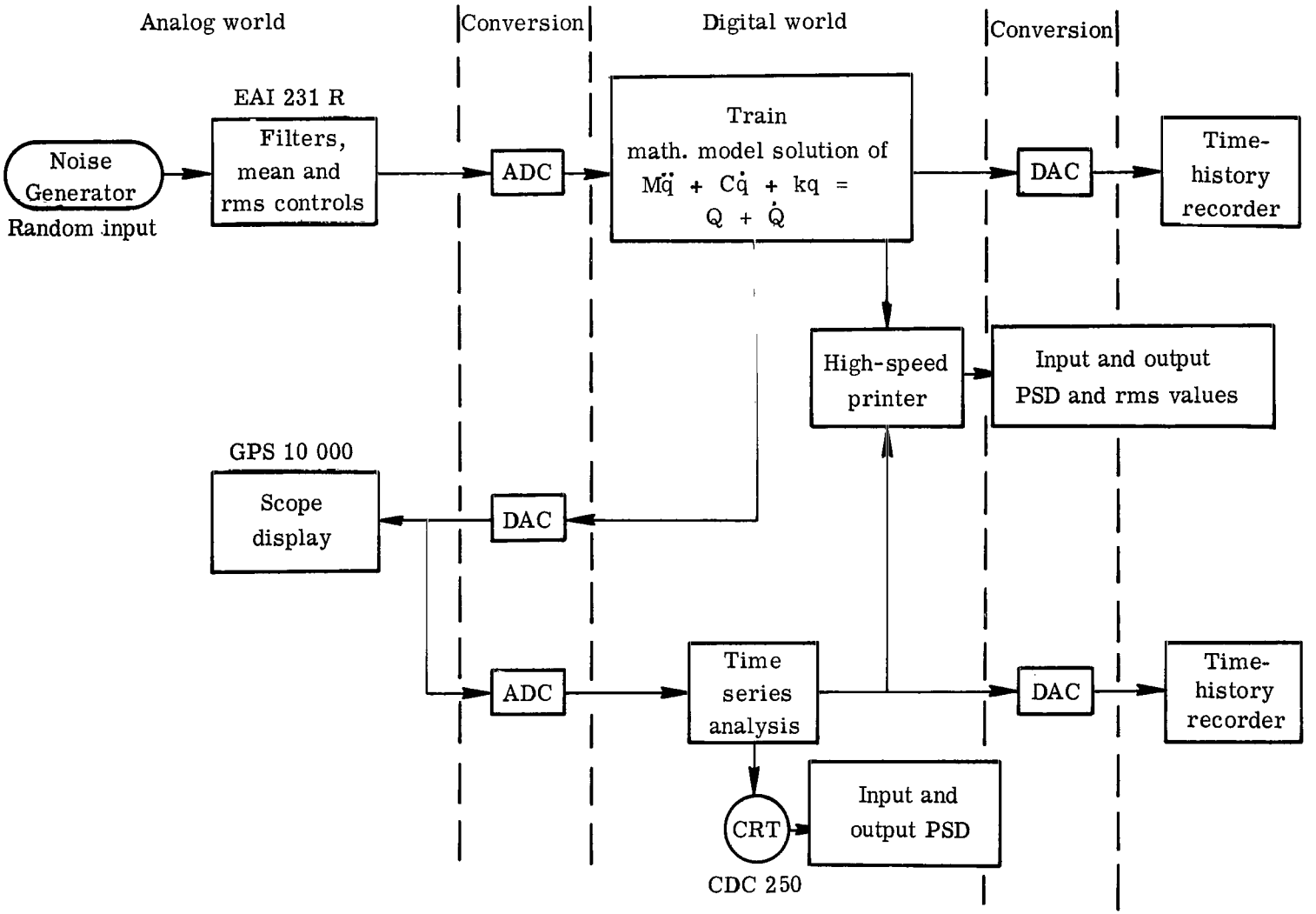

Figure 16.- Flow chart for RTS on-line random input capability. DAC denotes digital-to-analog converters; ADC denotes analog-to-digital converters; and CRT denotes cathode ray tube.

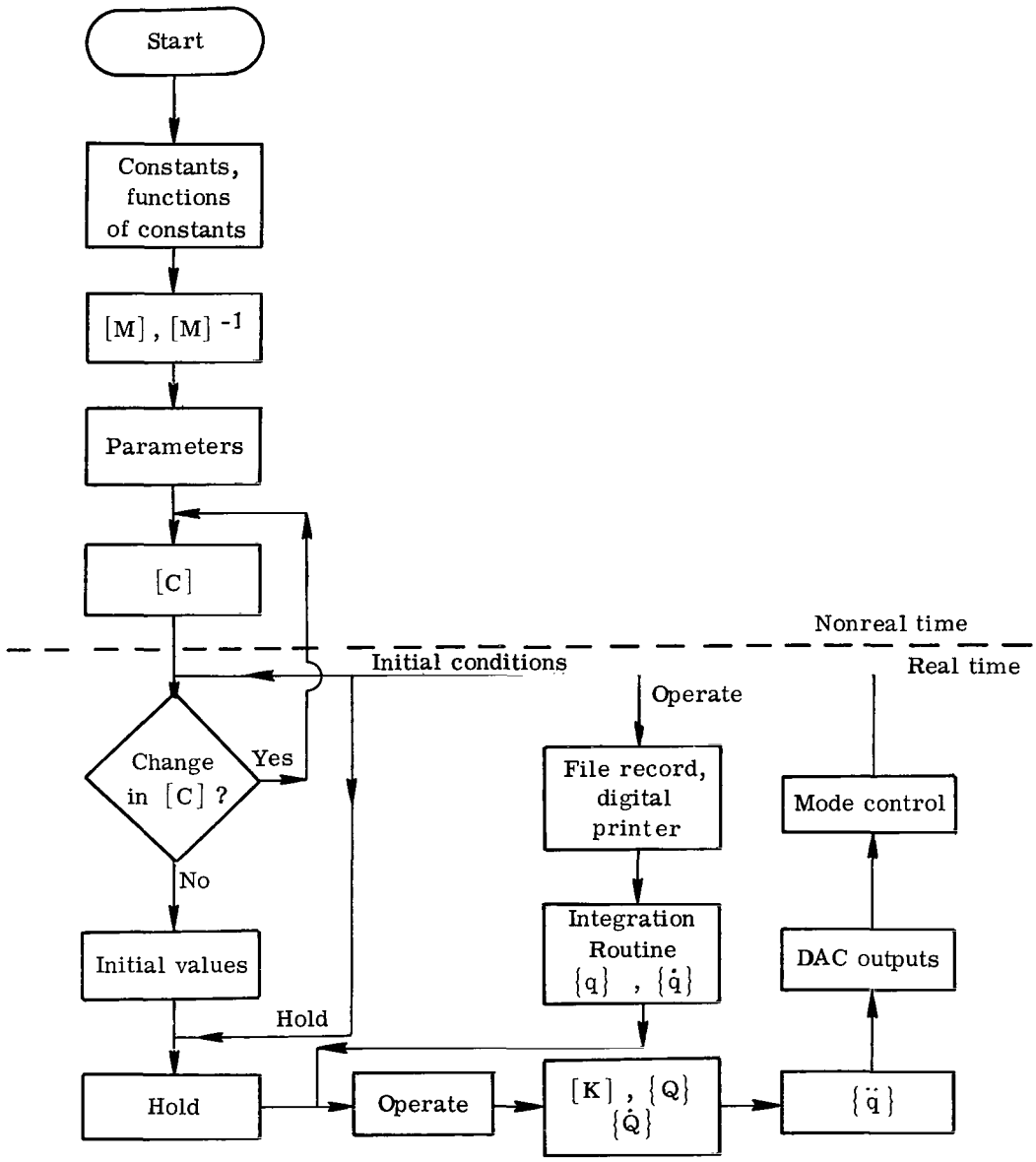

Figure 17.- RTS flow chart for solution of equations of motion for lateral model. $\{\ddot{q}\} = [M]^{-1}\left(\{Q\} + \{\dot{Q}\} - [C]\{\dot{q}\} - [K]\{q\}\right)$.

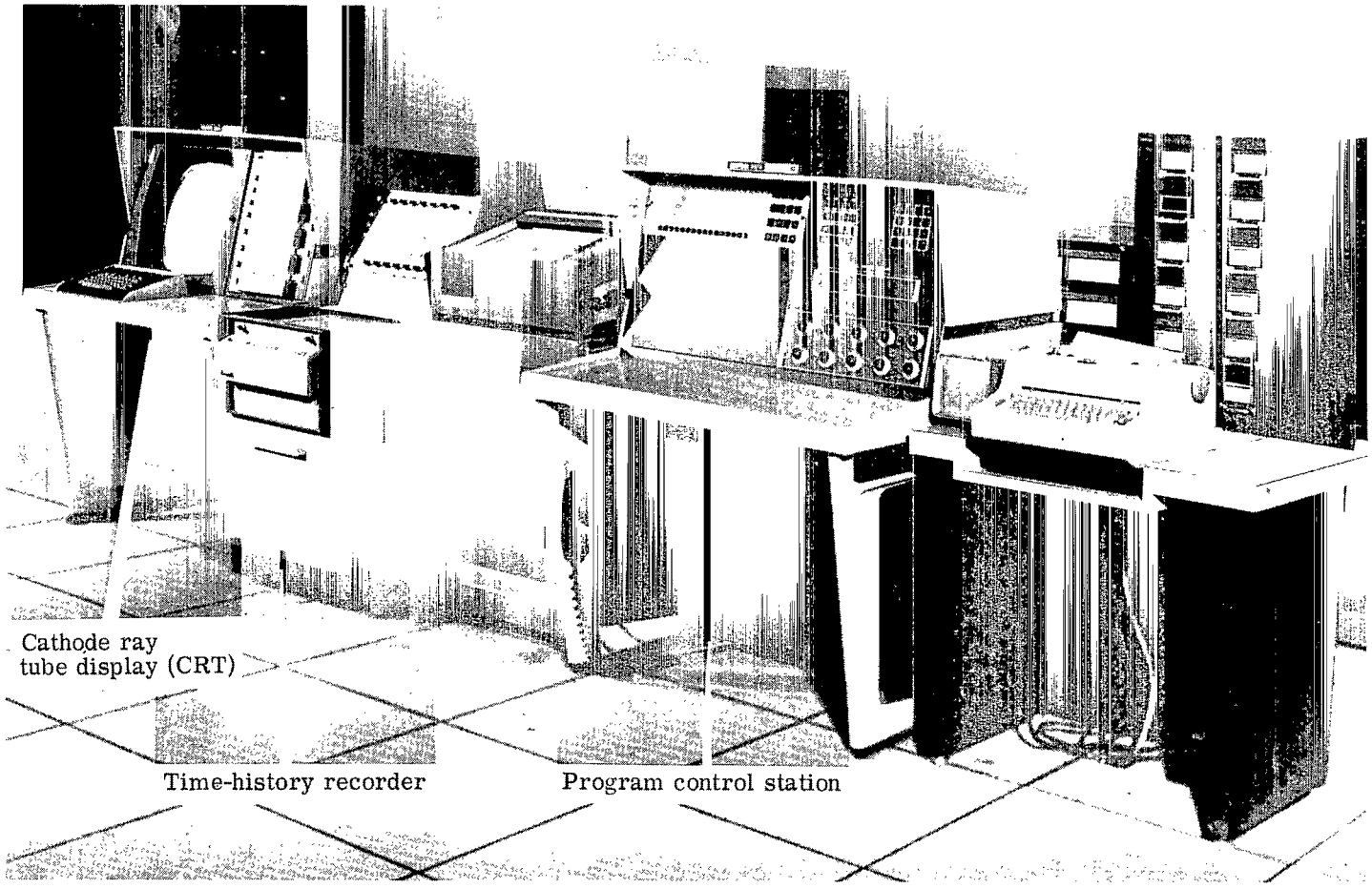

Figure 18.- Views of basic items of real-time simulation (RTS) facilities.

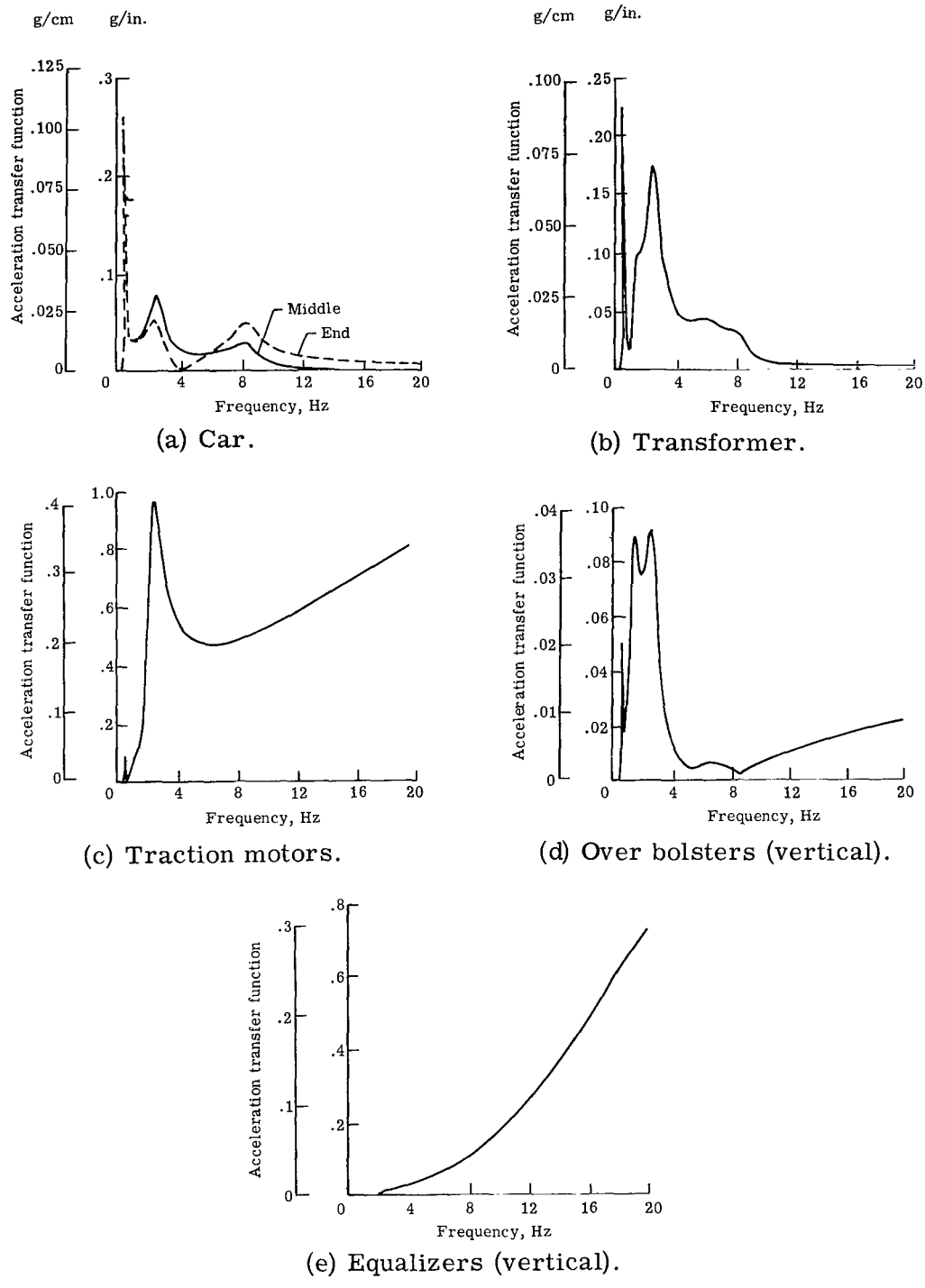

Figure 19.- Acceleration transfer functions for lateral model with lateral in-phase inputs $(\kappa_1 = 0)$.

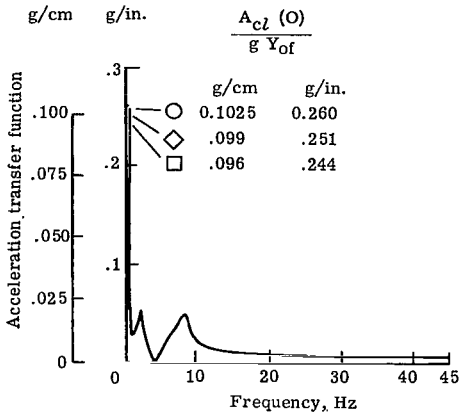

(a) End of car.

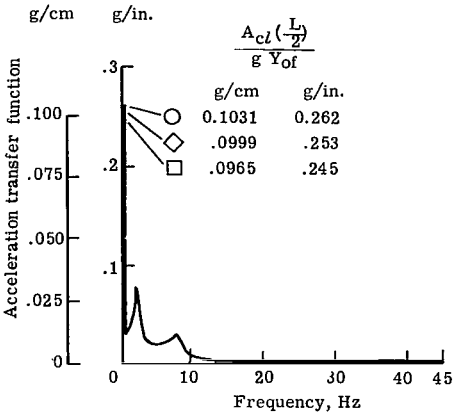

(b) Middle of car.

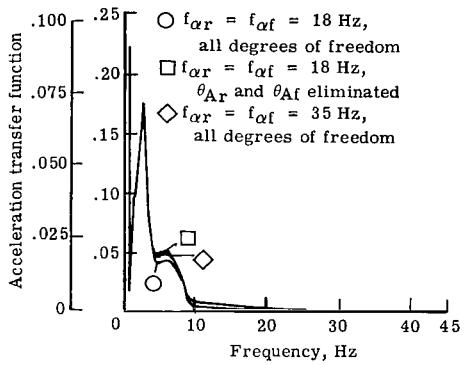

(c) Transformer.

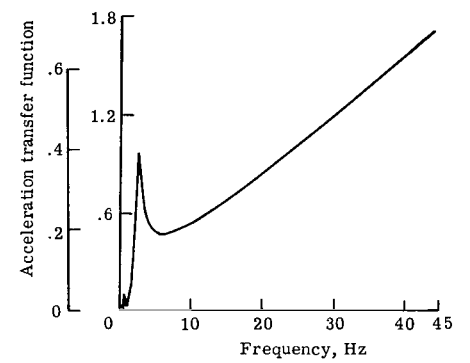

(d) Traction motor (rear).

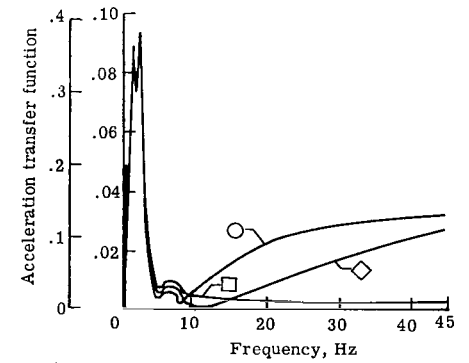

(e) Over bolsters, vertical acceleration (rear).

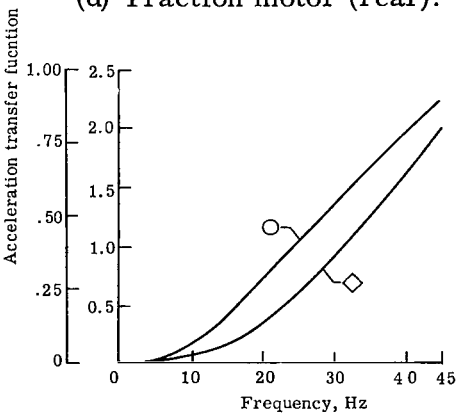

(f) Equalizers (vertical).

Figure 20.- Effects of traction-motor rolling degrees of freedom and rolling stiffnesses on acceleration transfer functions for lateral model with lateral in-phase inputs $(\kappa_1 = 0)$.

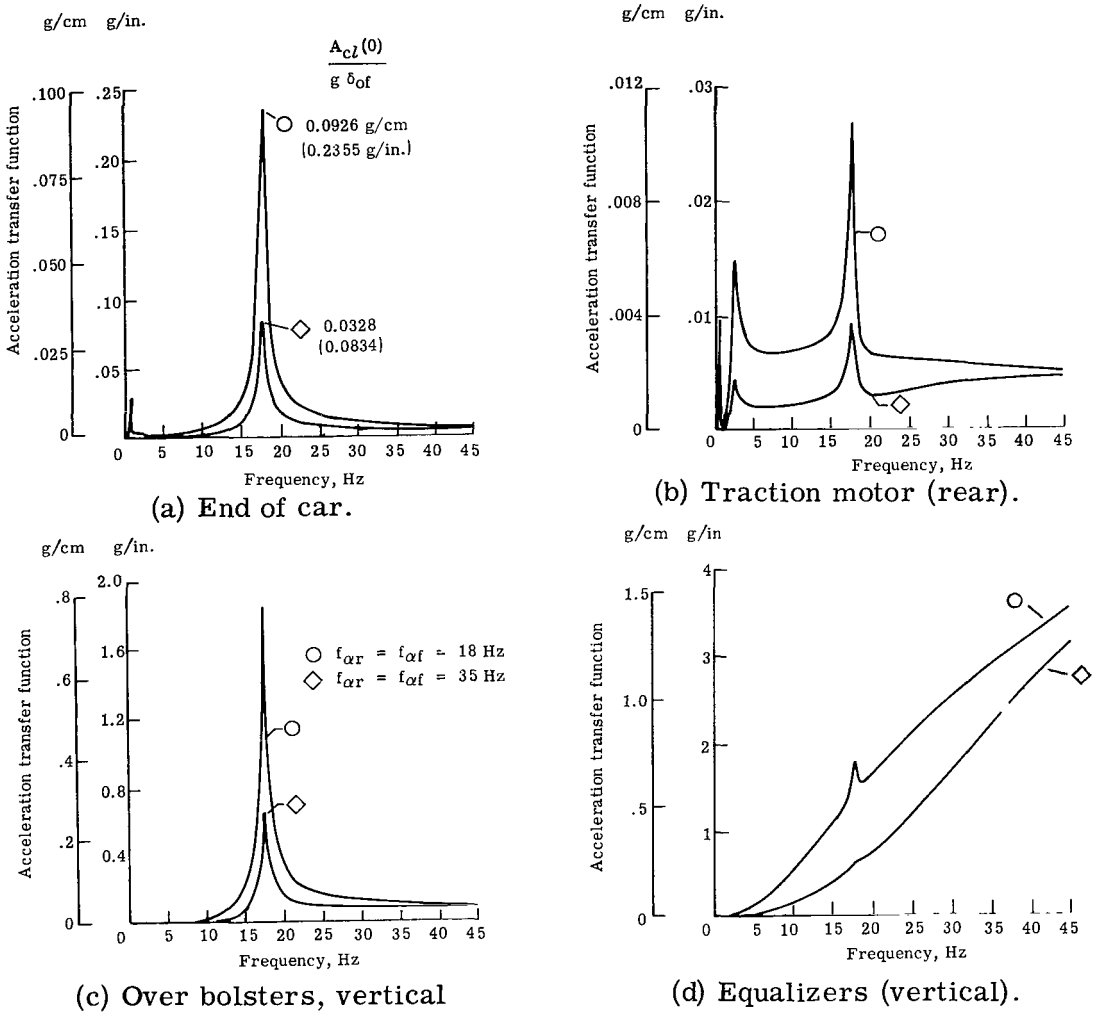

Figure 21.- Effects of varying traction-motor rolling stiffnesses on acceleration transfer functions for lateral model with cross-level out-of-phase inputs $(\kappa_2 = \pi)$.

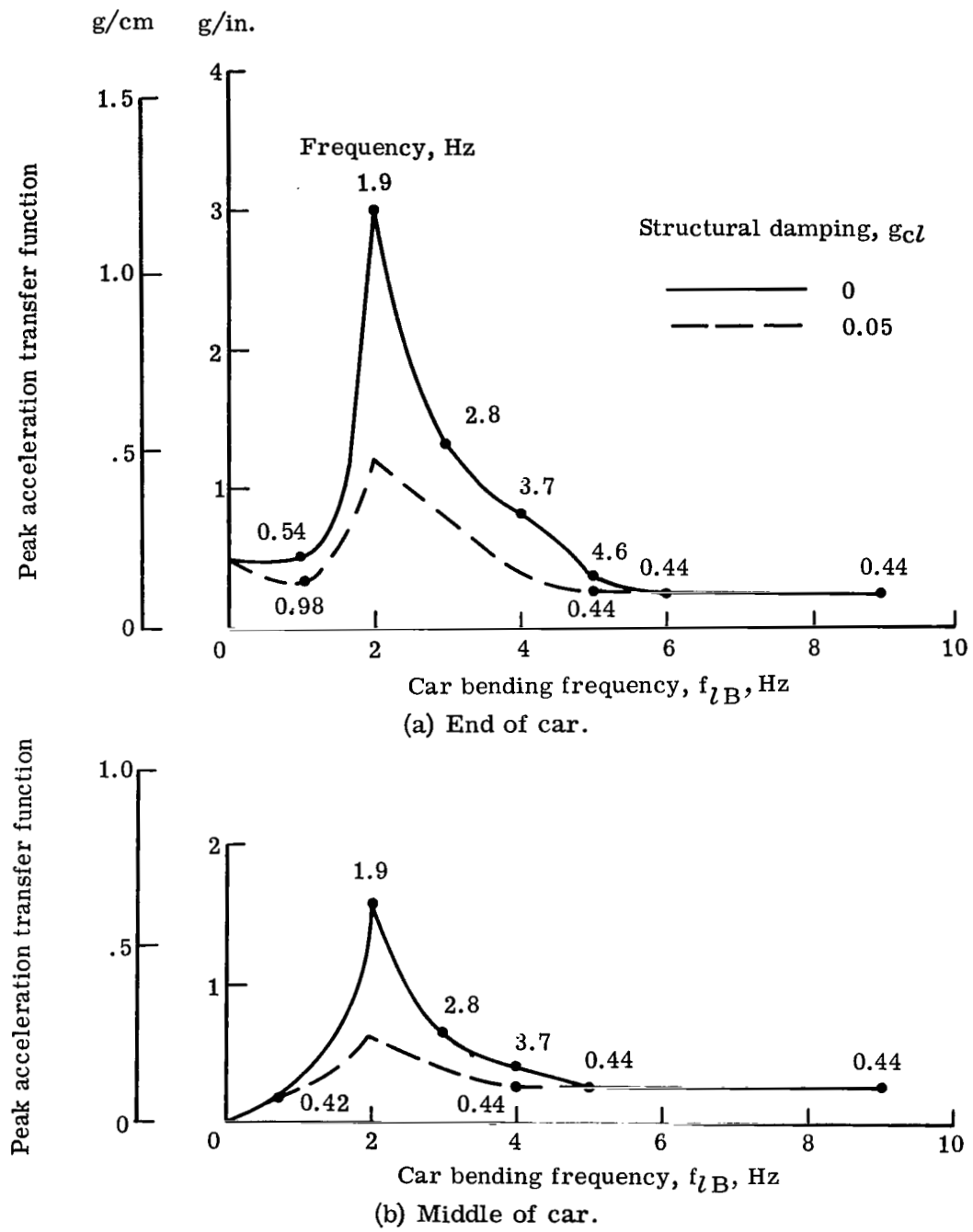

Figure 22.- Effect of car lateral bending frequency and structural damping on car lateral peak acceleration transfer functions. Numbers beside curves are frequencies of peak acceleration transfer functions.

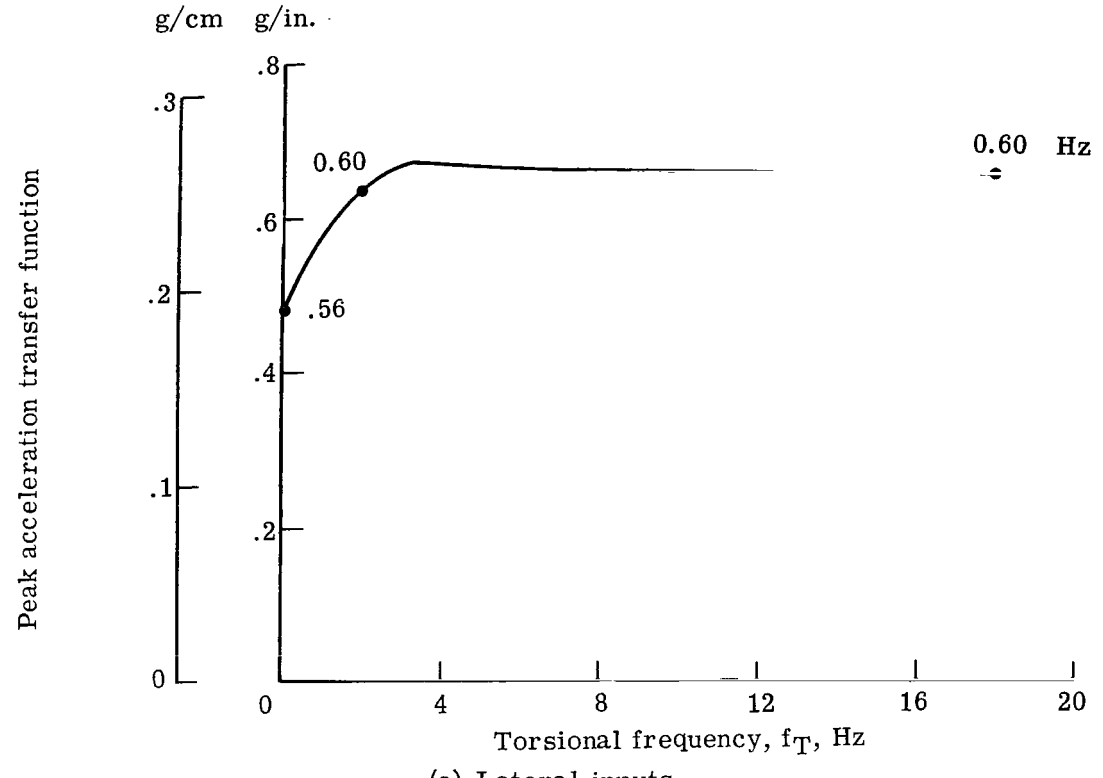

(a) Lateral inputs.

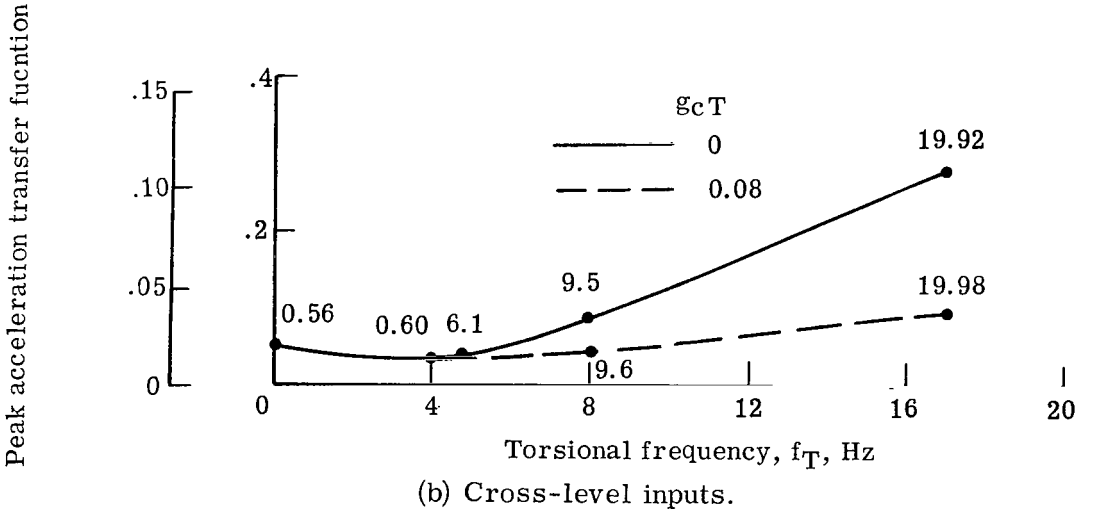

(b) Cross-level inputs.

Figure 23.- Effects of car torsional frequency and structural damping on car lateral peak acceleration transfer functions for out-of-phase inputs at end of car. Numbers beside curves are frequencies of peak acceleration transfer functions.

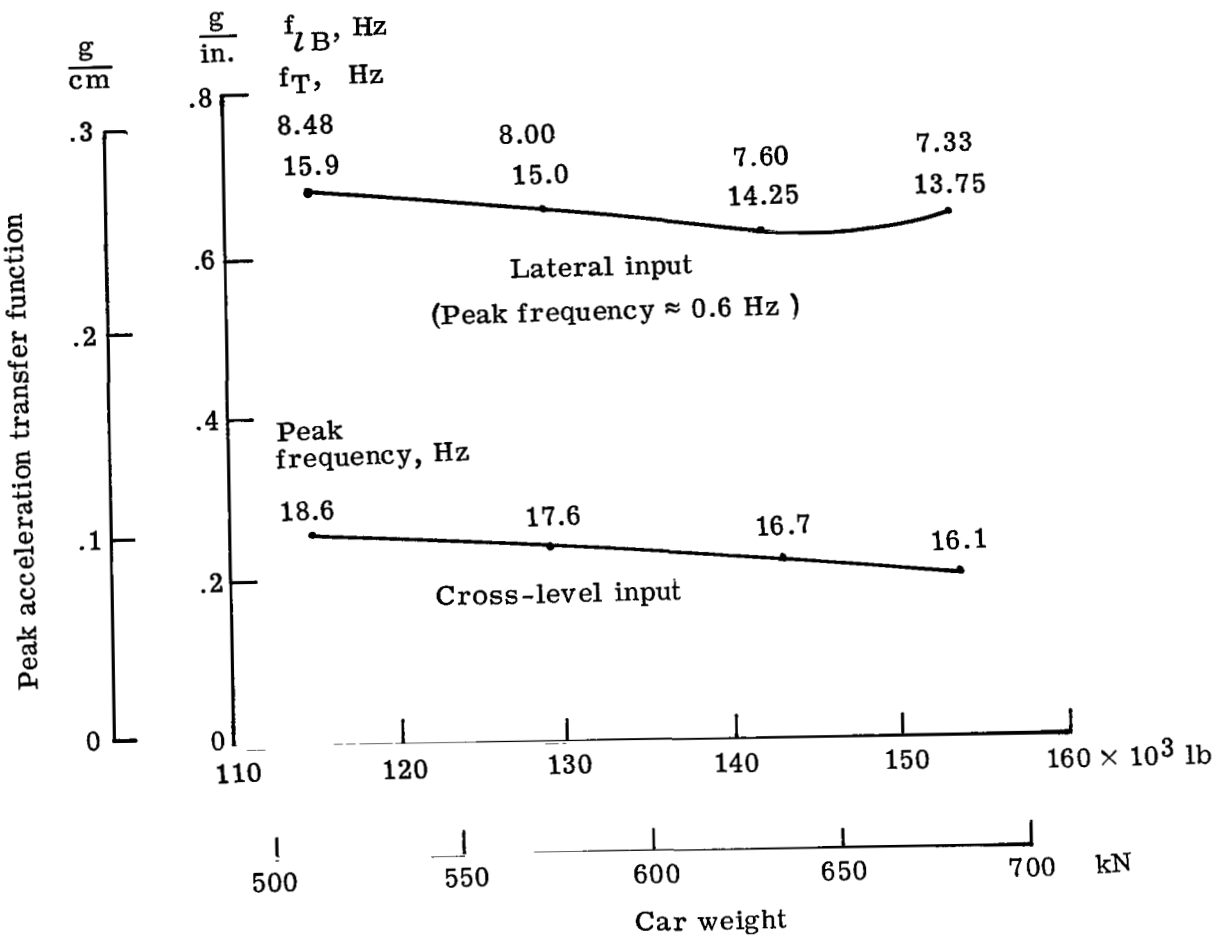

Figure 24.- Effect of car weight on lateral peak acceleration transfer functions at end of car for out-of-phase inputs $(\kappa_1, \kappa_2 = \pi)$.

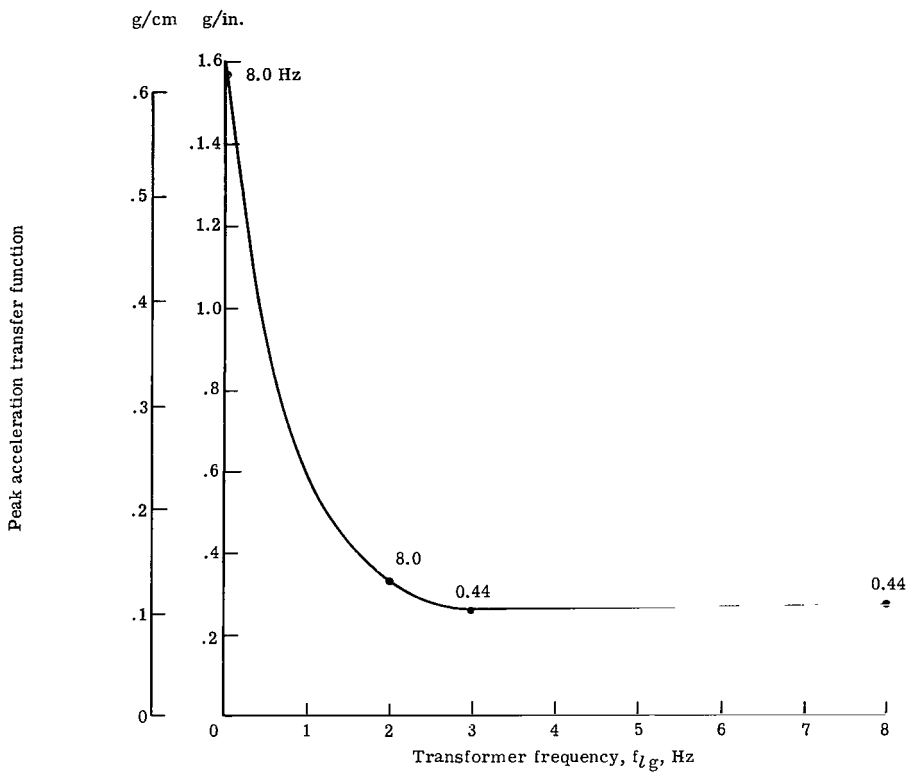

(a) End of car.

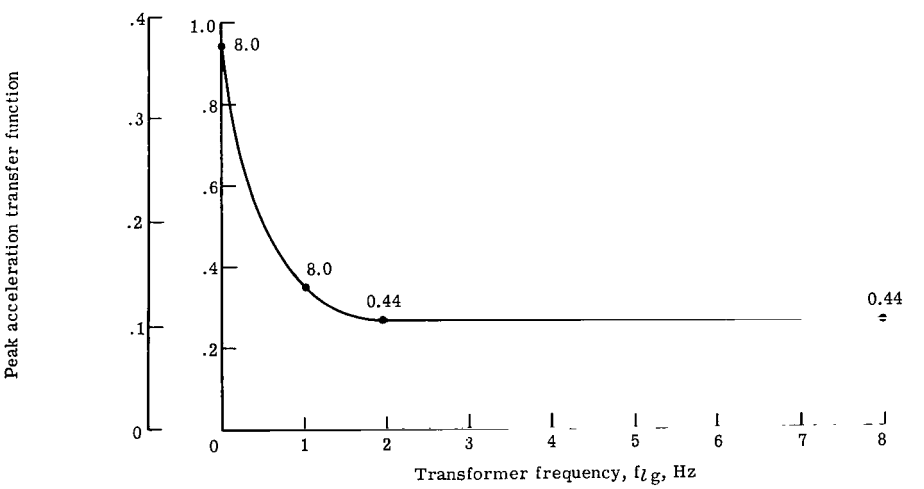

(b) Middle of car.

Figure 25.- Variation of car lateral peak acceleration transfer functions with lateral transformer frequency. Numbers beside curves are frequencies of peak acceleration transfer functions.

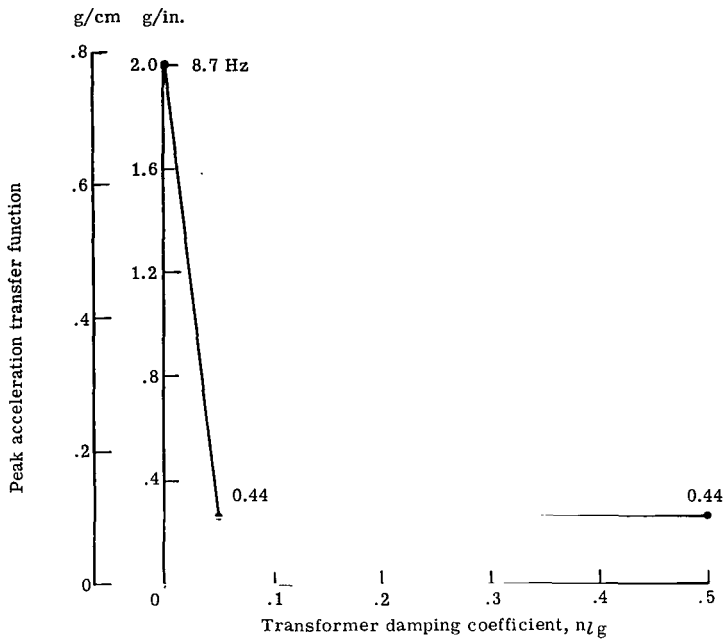

(a) End of car.

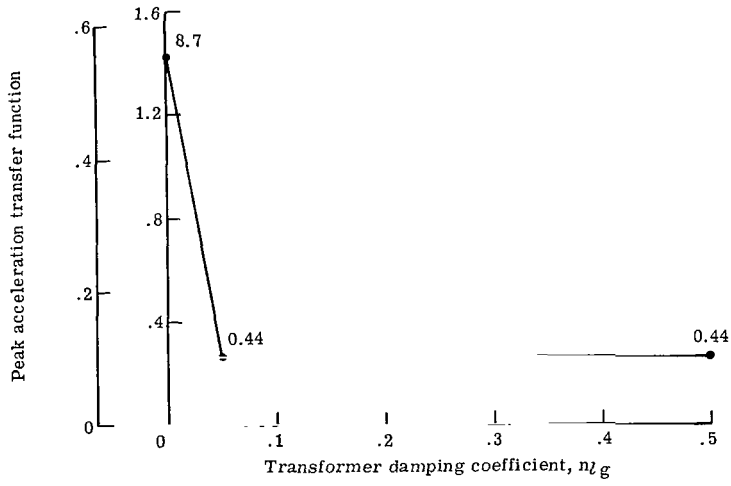

(b) Middle of car.

Figure 26.- Variation of car lateral peak acceleration transfer functions with lateral transformer damping coefficient. Numbers beside curves are frequencies of peak acceleration transfer functions.

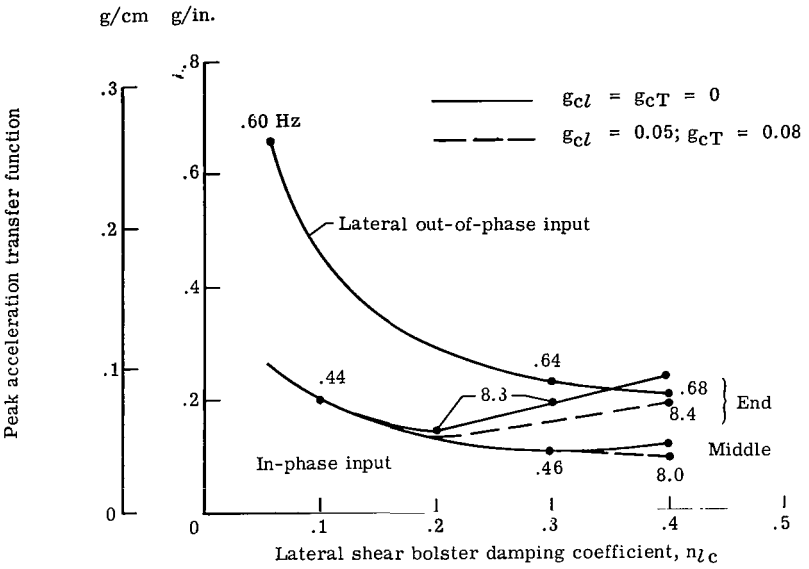

Figure 27.- Variation of peak acceleration transfer functions with lateral bolster damping. Numbers beside curves are frequencies of peak acceleration transfer functions.

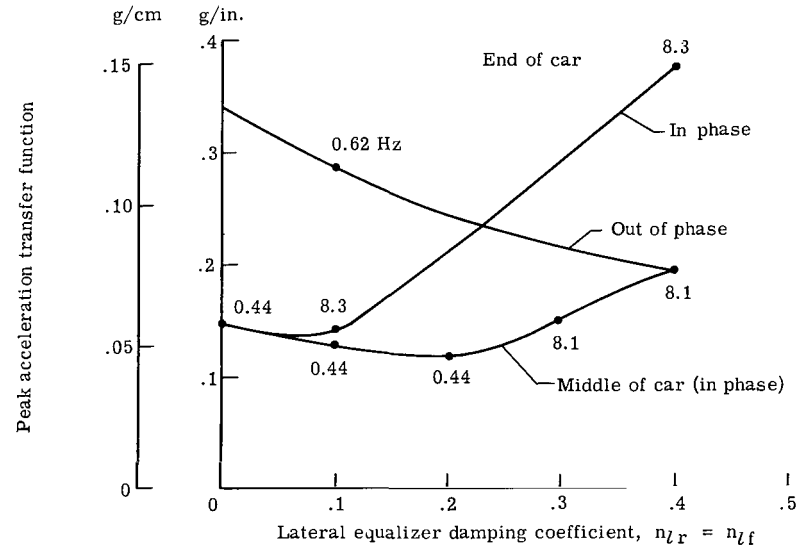

Figure 28.- Variation of car lateral peak acceleration transfer functions with lateral equalizer damping coefficient. Numbers beside curves are frequencies of peak acceleration transfer functions.

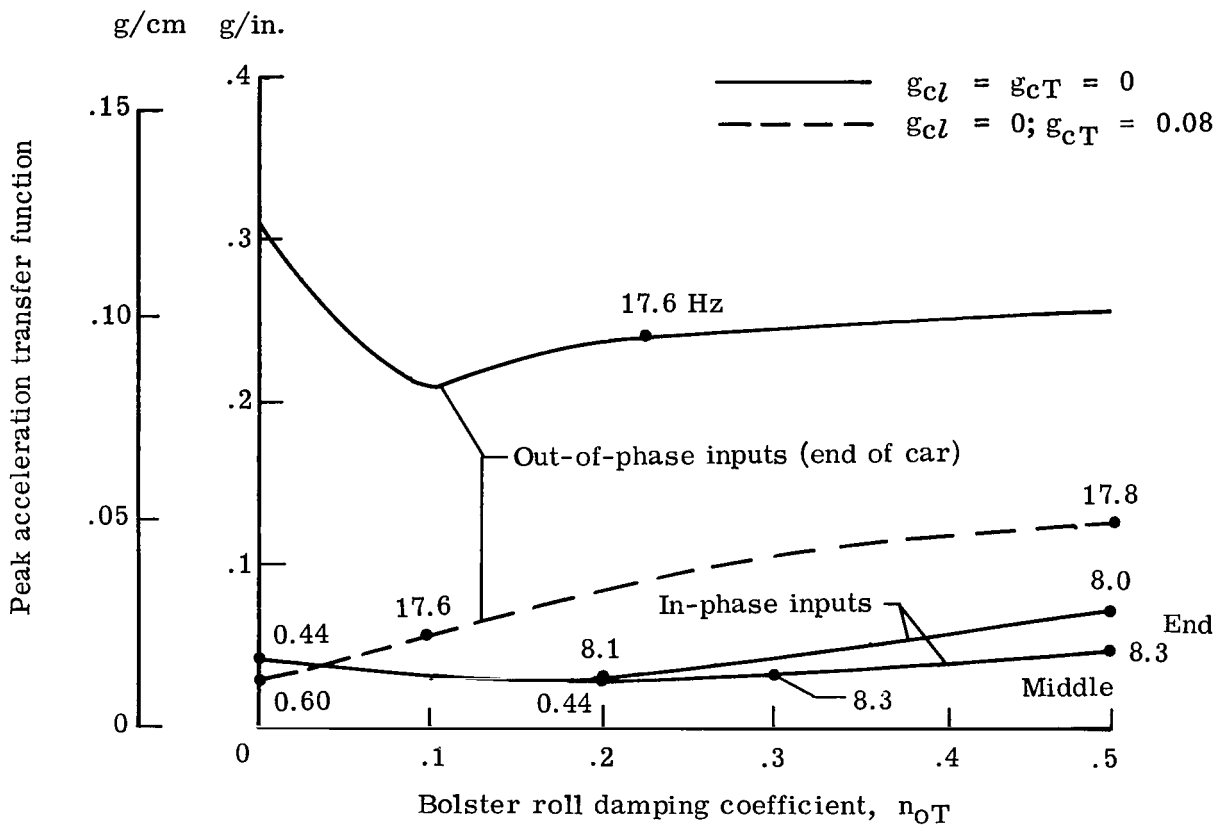

Figure 29.- Variation of peak acceleration transfer function with bolster roll damping for cross-level inputs. Numbers beside curves are frequencies of peak acceleration transfer functions.

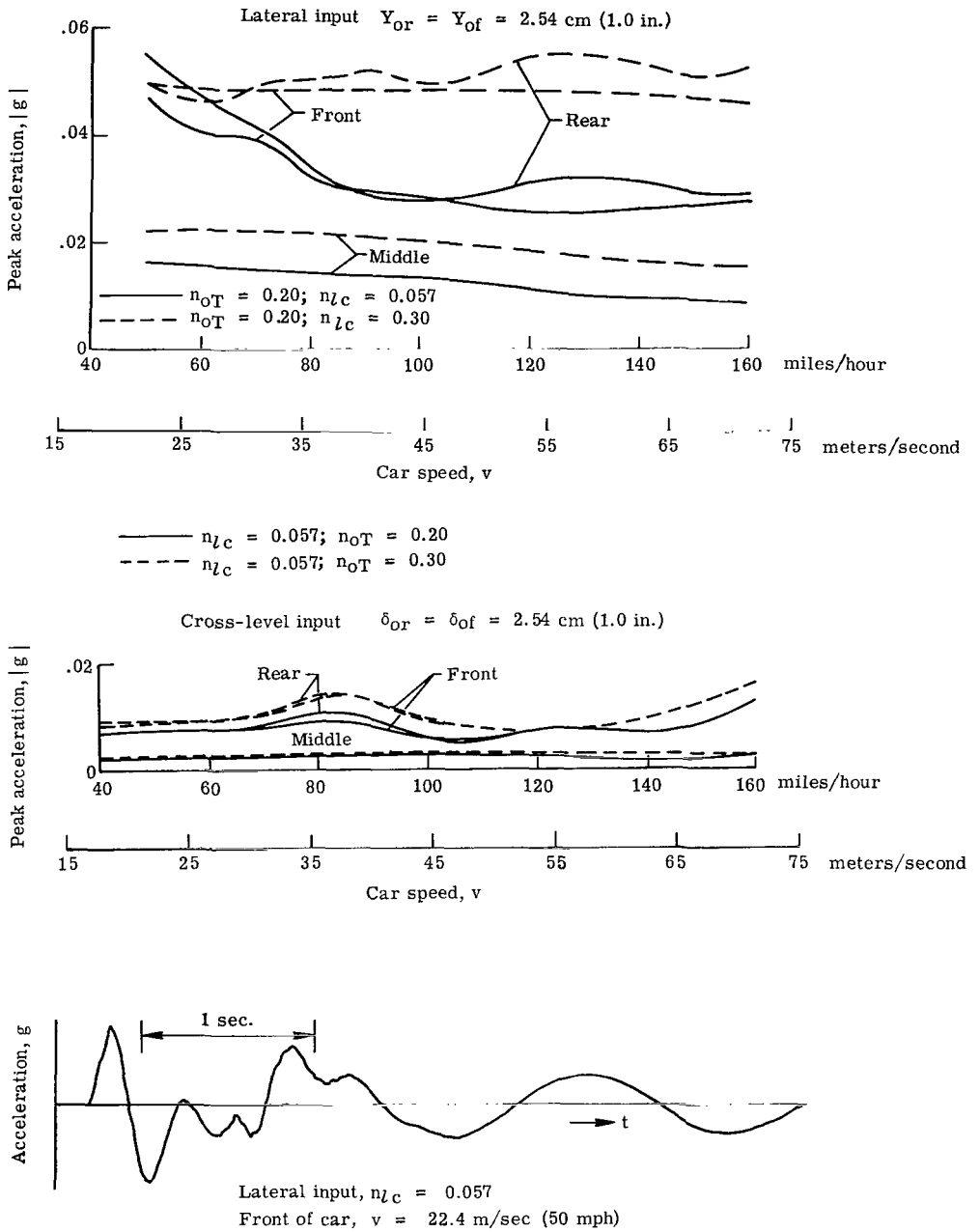

Figure 30.- Lateral car peak acceleration responses to square-pulse inputs for $\lambda = 0.305$ m (12.0 in.).

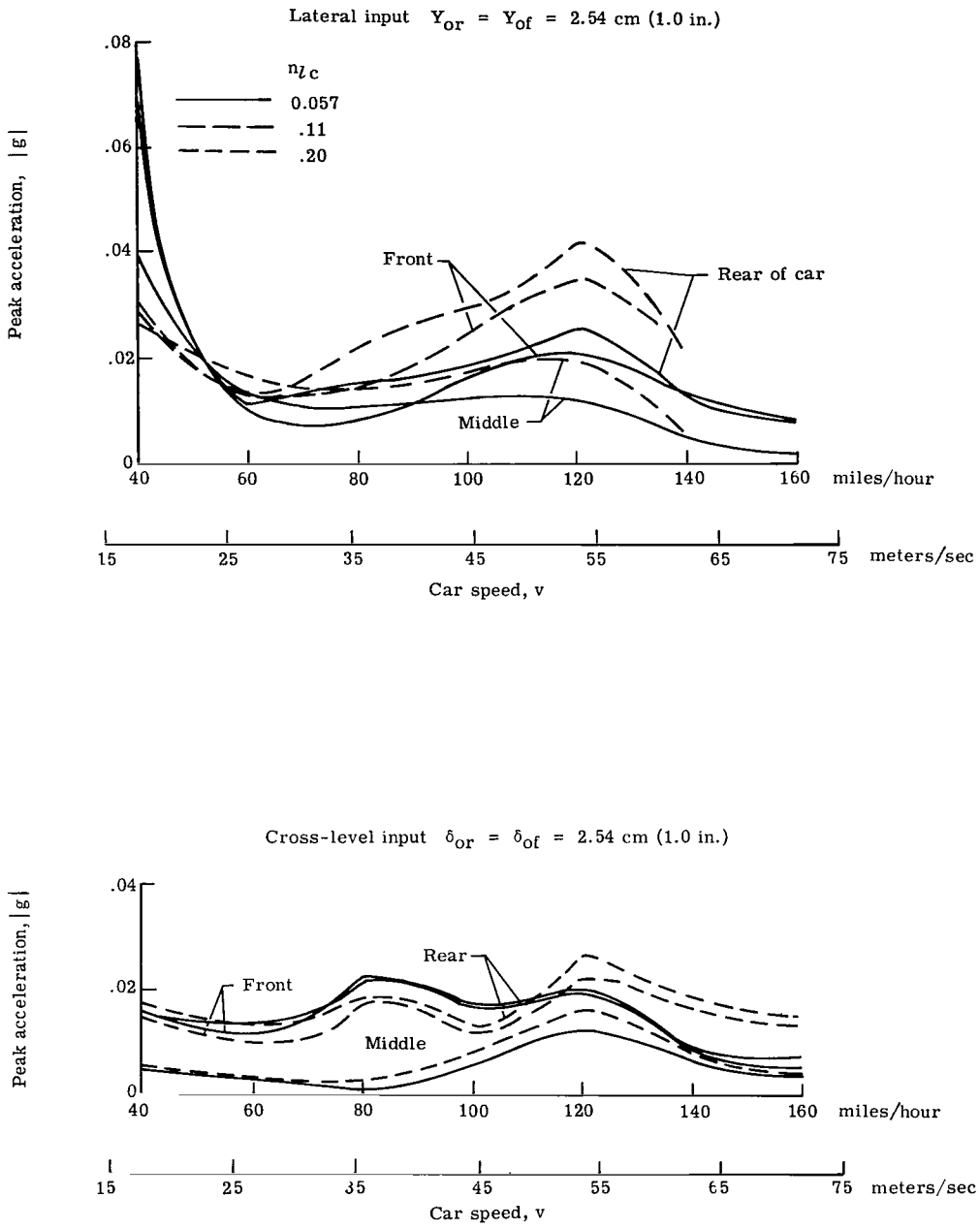

Figure 31.- Lateral car peak acceleration responses to deterministic square-pulse train inputs.

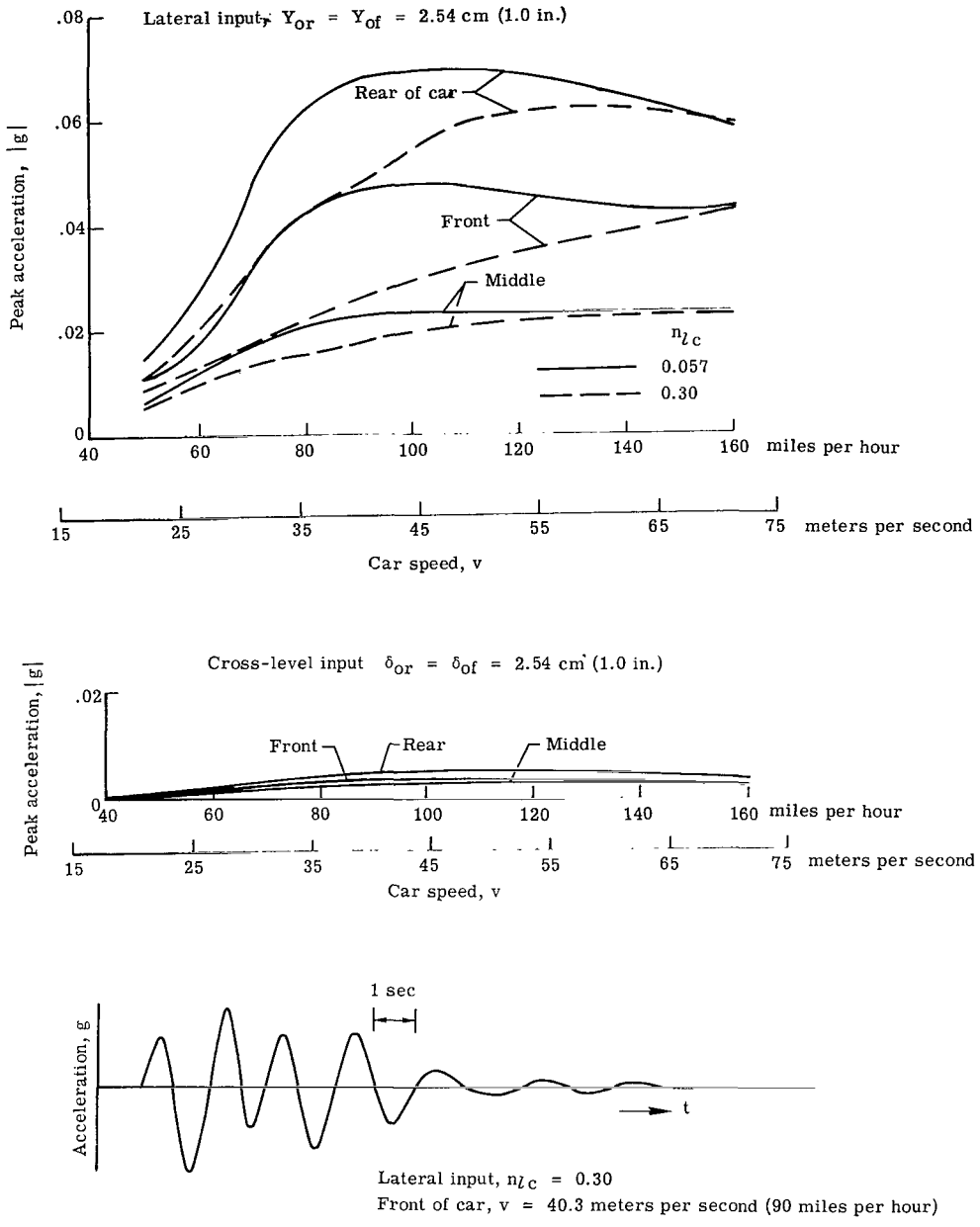

Figure 32.- Lateral car peak acceleration responses to wave-pulse input for λ = 76.2 m (3000 in.).

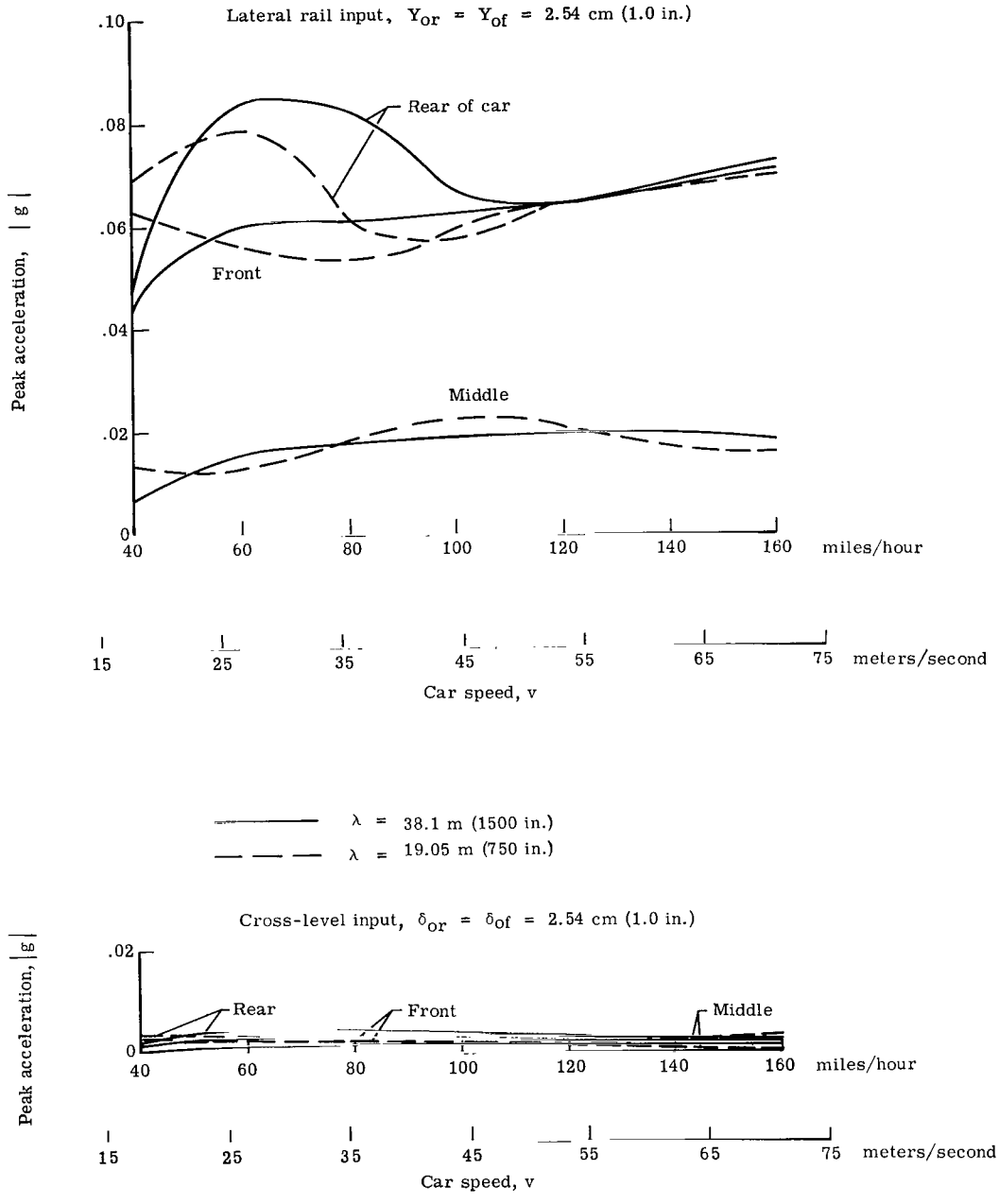

Figure 33.- Effects of input wave length on lateral car peak acceleration responses to wave inputs.

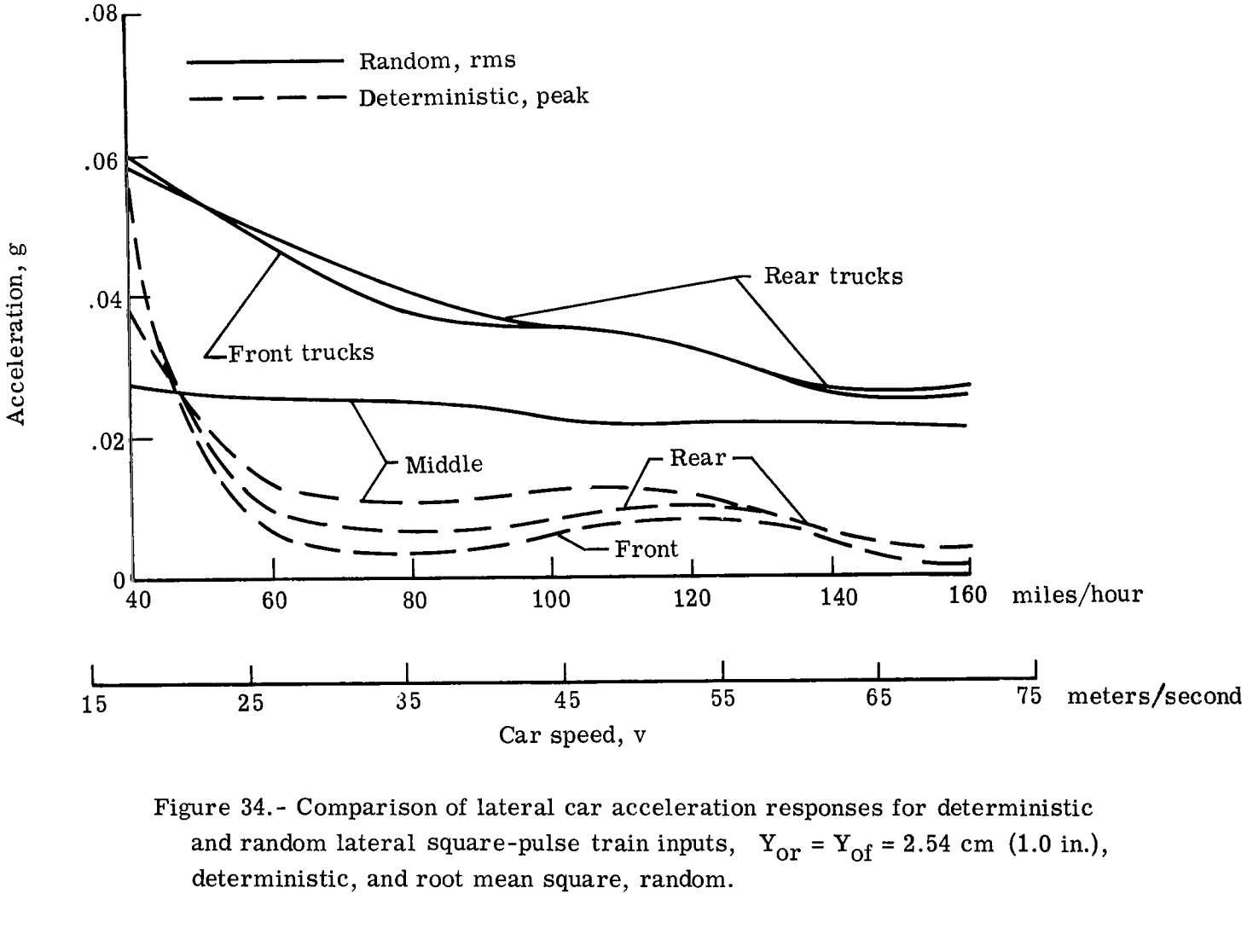

Figure 34.- Comparison of lateral car acceleration responses for deterministic and random lateral square-pulse train inputs, $Y_{or} = Y_{of} = 2.54$ cm (1.0 in.), deterministic, and root mean square, random.

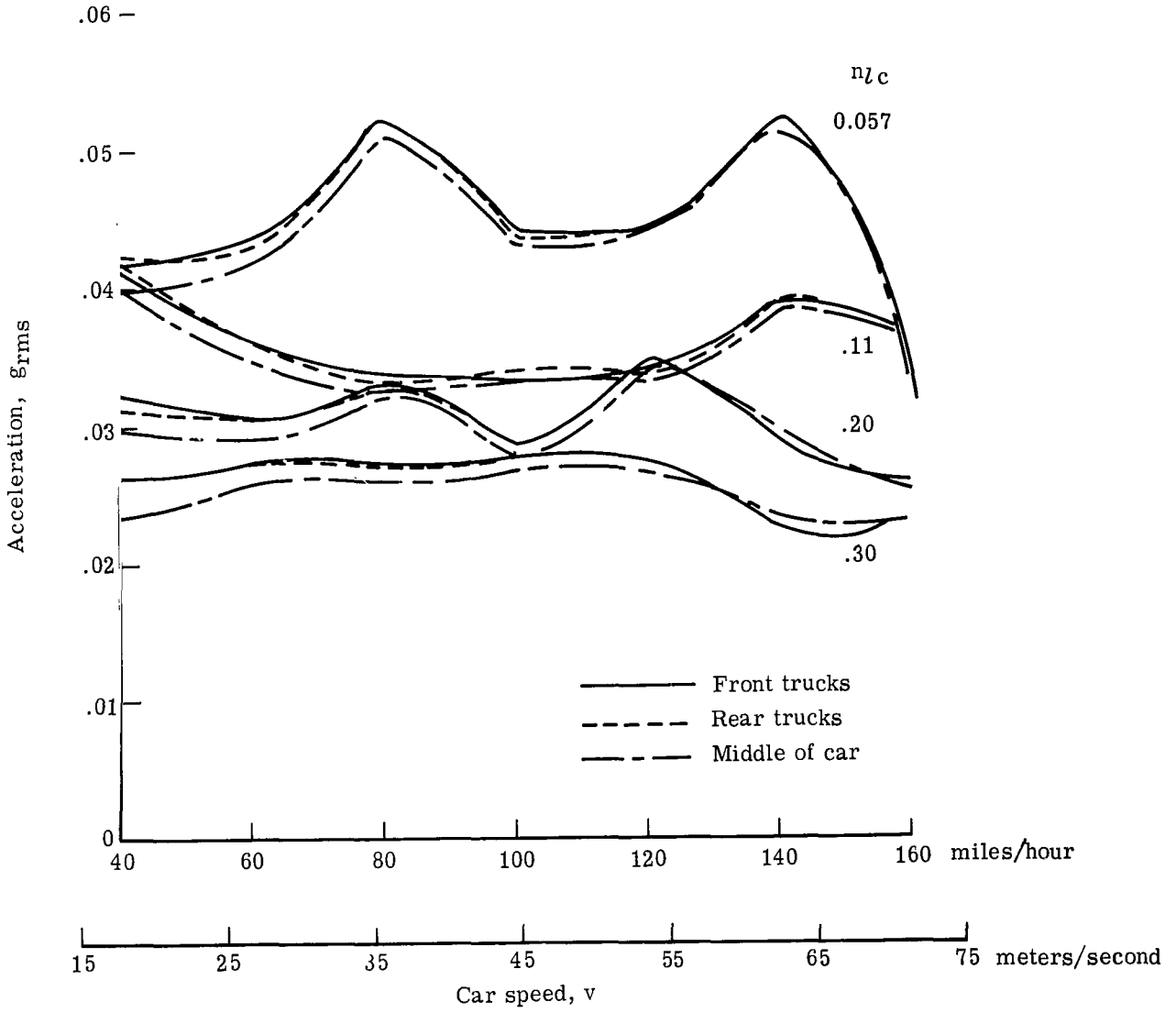

Figure 35.- Lateral responses to combined random pulse train and railroad estimate (fig. 15(g)).

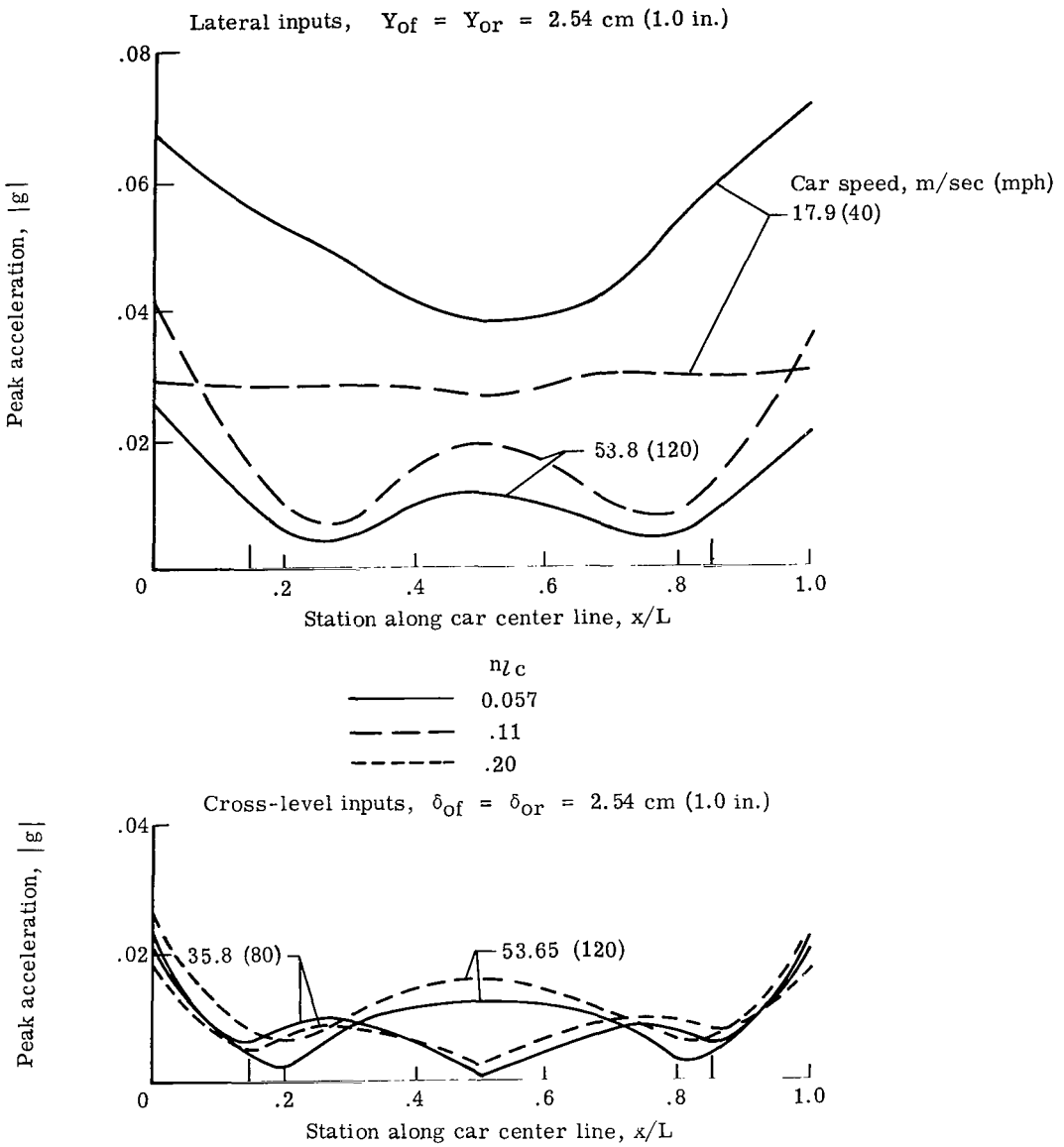

Figure 36.- Variation of lateral car peak acceleration responses with car length for deterministic square-pulse train inputs.

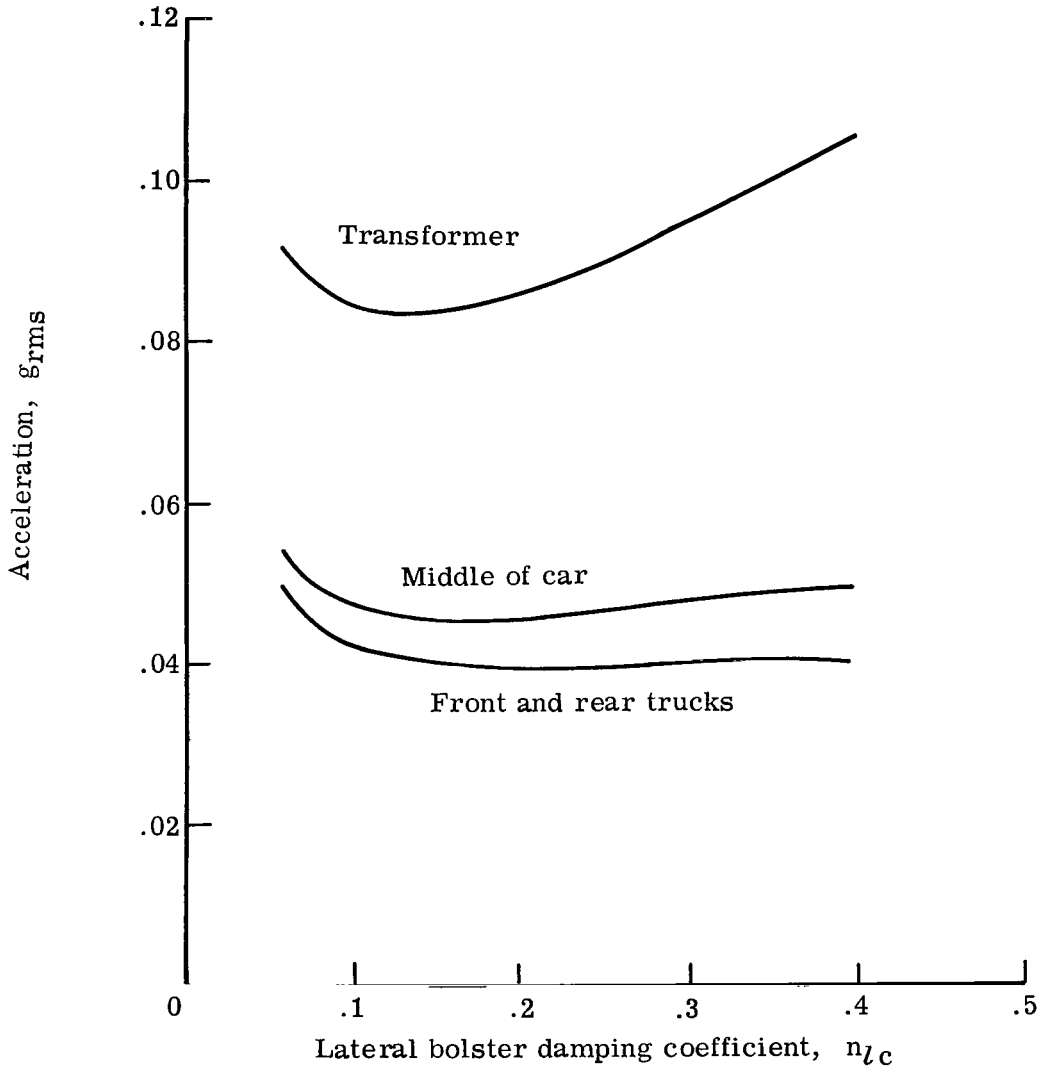

Figure 37.- Lateral car root-mean-square acceleration responses to lateral railroad test track input (no. 3 in fig. 15(e) with $Y_{or} = Y_{of} = 2.54$ cm (1.0 in.) rms).

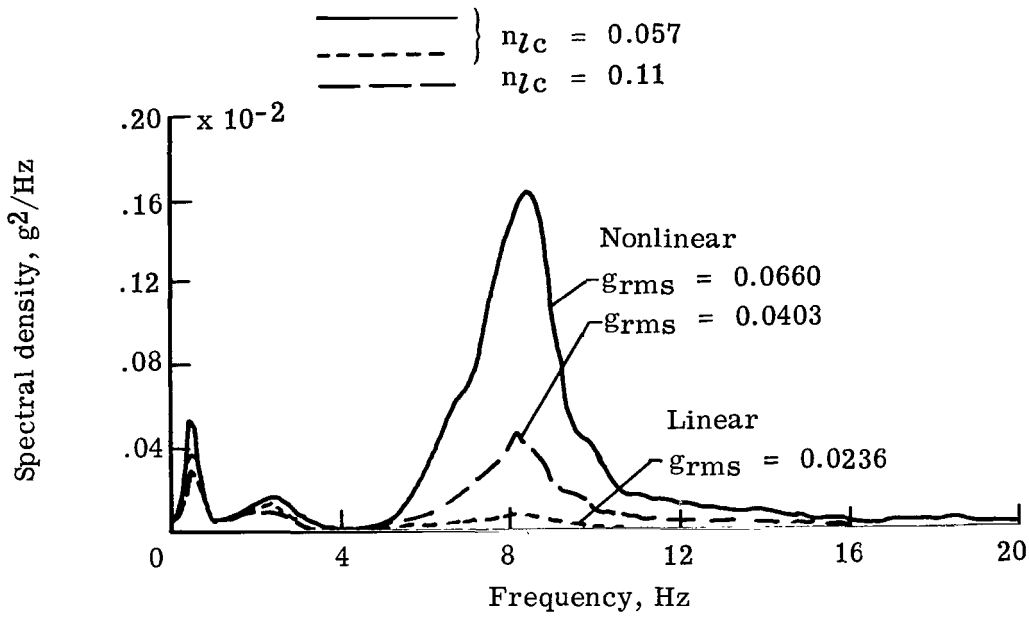

(a) End of car (rear).

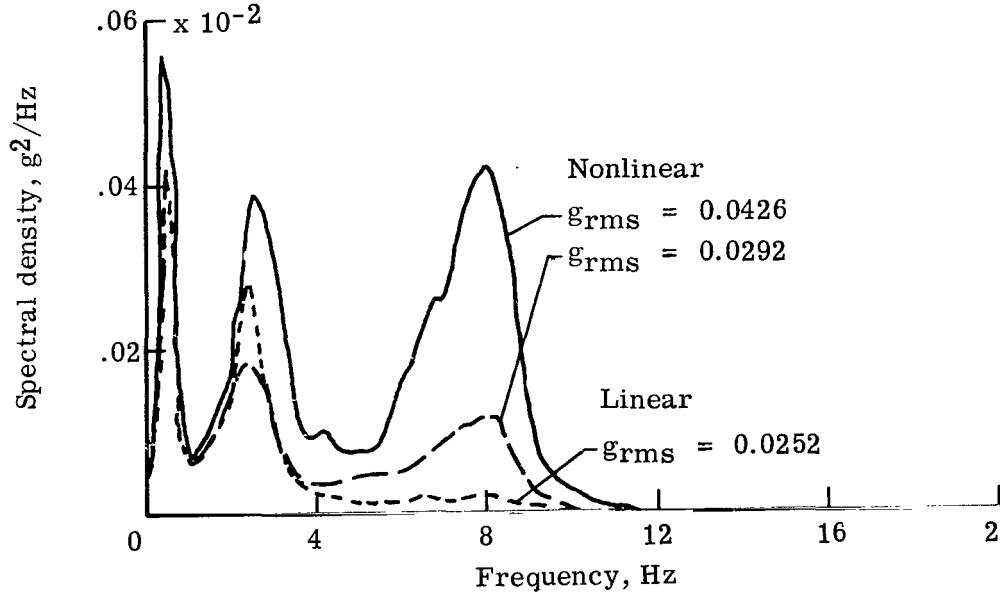

(b) Middle of car.

Figure 38.- Comparisons of linear with nonlinear lateral car acceleration spectral densities for lateral band-limited white-noise input (no. 2 in fig. 15(e)).

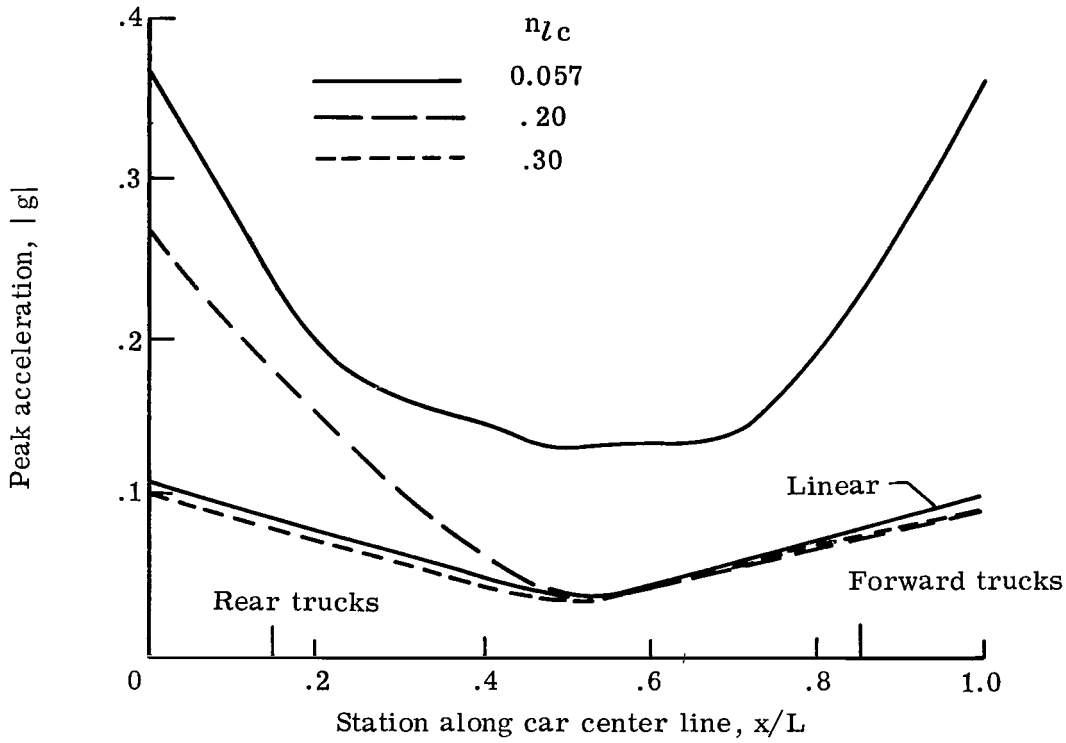

Figure 39.- Nonlinear lateral responses to lateral wave input for $Y_{or} = Y_{of} = 5.08$ cm (2.0 in.). $\lambda = 9.52$ m (375 in.); v = 35.8 m/sec (80 mph).

"The aeronautical and space activities of the United States shall be conducted so as to contribute . . . to the expansion of human knowledge of phenomena in the atmosphere and space. The Administration shall provide for the widest practicable and appropriate dissemination of information concerning its activities and the results thereof."

—NATIONAL AERONAUTICS AND SPACE ACT OF 1958

NASA SCIENTIFIC AND TECHNICAL PUBLICATIONS

TECHNICAL REPORTS: Scientific and technical information considered important, complete, and a lasting contribution to existing knowledge.

TECHNICAL NOTES: Information less broad in scope but nevertheless of importance as a contribution to existing knowledge.

TECHNICAL MEMORANDUMS: Information receiving limited distribution because of preliminary data, security classification, or other reasons.

CONTRACTOR REPORTS: Scientific and technical information generated under a NASA contract or grant and considered an important contribution to existing knowledge.

TECHNICAL TRANSLATIONS: Information published in a foreign language considered to merit NASA distribution in English.

SPECIAL PUBLICATIONS: Information derived from or of value to NASA activities. Publications include conference proceedings, monographs, data compilations, handbooks, sourcebooks, and special bibliographies.

TECHNOLOGY UTILIZATION PUBLICATIONS: Information on technology used by NASA that may be of particular interest in commercial and other non-aerospace applications. Publications include Tech Briefs, Technology Utilization Reports and Technology Surveys.

Details on the availability of these publications may be obtained from:

SCIENTIFIC AND TECHNICAL INFORMATION OFFICE

NATIONAL AERONAUTICS AND SPACE ADMINISTRATION

Washington, D.C. 20546